Chapter 2

A combinatorial library of Memantine based Salts – Crystallography, Hirshfeld surfaces and dissolution studies

Published in *Journal of Molecular Structure*, 1206 (2020) 127672.

2.1 INTRODUCTION

Transformation of APIs from their original form into co-crystals or salts has gained a lot of interest in the recent years. Cocrystals can be defined as *homogeneous solid phases containing two or more neutral compounds in a crystal lattice with defined stoichiometry, which are solids in their pure form in ambient conditions*.[1] A pharmaceutical cocrystal is a *multi-component crystalline material in which the active pharmaceutical ingredient is in a stoichiometric ratio with a second compound that is generally a solid*.[2] It is expected to exhibit modified physical and chemical properties than the pure compounds, which enables us to improve the physico-chemical properties of the drug without reducing its therapeutic efficiency. It can help in creating an attractive route for drug development.[3] Besides, co-crystals/salts of a drug are known to be more stable and less prone to phase transformations. Pharmaceutical cocrystals can exhibit distinctively different molecular arrangements and solid-state thermodynamics, which can lead to significant changes in physicochemical and pharmacokinetic properties. While molecular cocrystals offer formation of only a single combination with one conformer, ionic cocrystals (salts) of an API can be formed using counter ions, coformers and a combination of both (Figure 2.1). Hence, salts/ionic cocrystals are more versatile in the sense that a vast library can be created to prepare as much number of compounds as desired.[2] (A conformer is a molecule selected from the list of benign chemicals for human consumption, approved by the FDA (Generally Regarded As Safe, GRAS)).

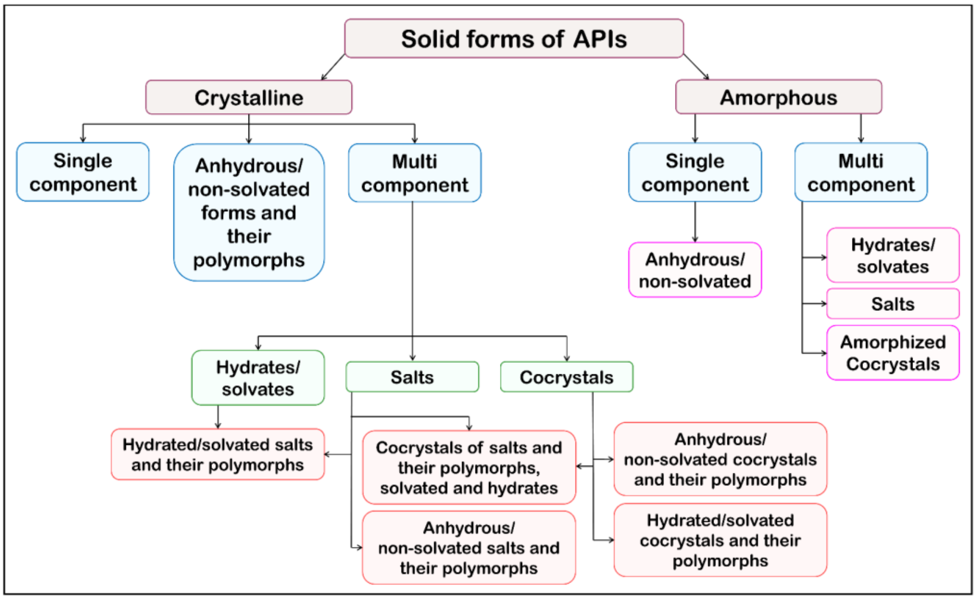

Figure 2.1 Various solid forms of APIs that can be created to fine tune the drug properties[4]

The supramolecular interactions in crystalline solids can profoundly impact the properties of drugs, viz. solubility, dissolution rate, bioavailability, melting point, stability and compressibility and hence, crystal engineering can be explored for modifying the properties of drugs.[5] An approach based on crystal engineering or supramolecular synthons is the most commonly employed method in the design of such systems (Figure 2.2). This approach focusses on implementing the frequently occurring motifs from the literature and synthesizing pre-designed networks of molecules which might be applicable to the API of interest.[6] This method is complemented by the work of Etter[7] who the proposed rules for graph set representation of hydrogen bonds in organic compounds, which were based upon their predictability/stability. An alternative approach was reported by Fàbiàn[8] based on quantitative structure activity relationship (QSAR), wherein molecular descriptors were calculated for each set of reliable cocrystals (extracted from Cambridge Structural Database). This study led to identification of molecular properties that influence formation of cocrystals and could provide constructive guidelines for their rational design. In a unique paper, Pidcock and coworkers have discussed at length how rational designing of cocrystals has been carried out in the past using crystal engineering approach and can be useful for devising knowledge-based approaches in the future.[9]

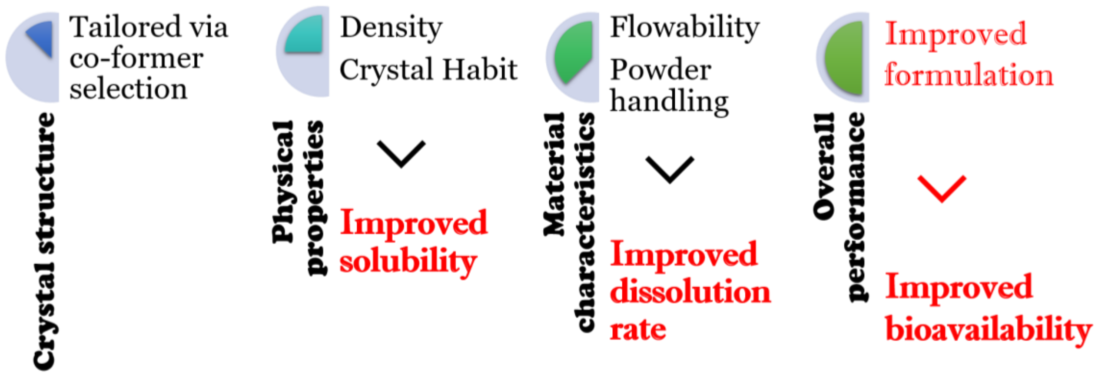

Figure 2.2 An illustration highlighting the role of improved processing attributes in salt/cocrystal preparation leading to improved therapeutic effects in drugs

Over 80% of the drugs are sold in the form of tablets and about 40% of the marketed drugs are reported to have less than optimal solubility. Surprisingly, about 80% of the drugs in R&D pipeline are likely to fail because of solubility issues.[10] It is believed that the dissolution behavior of any drug results from a complex interplay of the interactions between – (1) molecules inside a crystal, (2) the solvent and solute molecules at the crystal faces, and (3) molecules of the dissolved crystals and their solvation shell in solution.[11] This means that modifications in the intermolecular interactions in a crystal structure and enhancing the solute-solvent interactions may have a constructive effect on the solubility.[11] This is why cocrystals are believed to have better solubilities than the parent compounds. Because of their crystalline nature, cocrystals are more stable to humidity, drug processing and tableting, and hence, less likely to undergo phase transformations. They can be considered as supramolecular prodrugs that are capable of achieving high solubilities *in vivo*. There have been various reports where salts and cocrystals have significantly improved the aqueous solubility[12–14], intrinsic dissolution[15], stability[16], and mechanical properties[17] of the drug molecules. As per the regulatory classification proposed by the FDA, different polymorphic forms of a drug are considered the same API, whereas different salt forms of the same active moiety are considered different APIs.[4]

Numerous drugs have been studied and modified using the principles of supramolecular syntheses. As an example, well-known and widely prescribed drugs have been refined by employing crystallographic principles like gabapentin[18], pyrimethanamine[19], triamterene[20], lornoxicam[21,22], tadalafil[23], to name a few. Ciprofloxacin (Figure 2.3(a)), a second-generation fluoroquinolone broad-spectrum antibiotic, is prescribed for the treatment of several types of bacterial infections. However, it suffers from demerits like poor solubility and bioavailability. Mandal and coworkers reported a hippurate salt of ciprofloxacin, which possessed superior intrinsic dissolution rate and a better stability than the parent API.[24] In another study, meloxicam (Figure 2.3(b)), a nonsteroidal anti-inflammatory drug, which shows low solubility in acidic aqueous media and a slow onset of action in biological systems, was manipulated using a similar approach. A more soluble variant of meloxicam is desirable since it can have faster onset of action and hence can be used for treating mild-to-medium level pain. In this study, meloxicam was treated with various carboxylic acids and their salts so obtained were found to be having better dissolution and enhanced oral absorption than that of pure meloxicam.[25]

Interestingly, the idea of creating cocrystals is not just limited to molecules that carry desired functional groups such as –COOH, $–NH_2$, $–CONH_2$, –OH, –X, etc., (which can promote H-bonding) in order to fine-tune the drug properties. Propyphenazone (Figure 2.3(c)), a well-known antipyretic and analgesic drug, does not contain any H-bonding donor groups in its structure. It contains only one H-bonding acceptor atom, that too is sterically hindered because of the presence of neighboring iso-propyl group. Aitipamula and coworkers synthesized cocrystals of propyphenazone with various compounds bearing carboxylic acid and phenolic backbones, with comparable stability and in some cases, higher solubility.[6]

In another classic study, apixaban (Figure 2.3(d)), which is a highly potent and selective drug for inhibition of blood coagulation and suffers from poor water solubility and low oral bioavailability, was modified. A cocrystal of apixaban with oxalic acid was obtained, and it was found to have *c.a.* 2 times higher solubility and improved bioavailability.[26] In a study reported by Tjandrawinata and coworkers, the tabletability of a well-known antipyretic drug, paracetamol (Figure 2.3(e)) was modified by creating a conformer with 5-nitroisopthalic acid, which exhibited a similar dissolution profile as paracetamol with decent stability.[27]

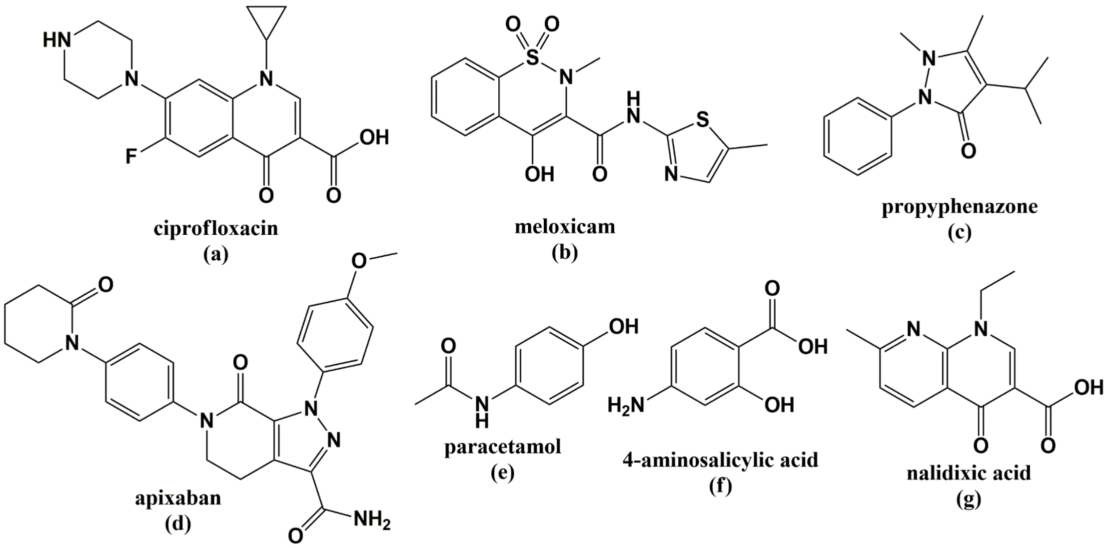

Figure 2.3 Some drug molecules modified using the salt/cocrystal approach

One of the most impressive and sought-after applications of pharmaceutical cocrystals is the synthesis of multidrug cocrystals. They contain multiple APIs combined in a single dose for effective treatment of complex disorders like HIV/AIDS, cancer, diabetes, etc.[28] These can be in the form of salts, complexes or cocrystals. Multidrug cocrystals are defined as *dissociable solid crystalline supramolecular complexes comprising two or more therapeutically effective components in a stoichiometric ratio within the same crystal lattice*, *wherein the components may predominantly interact via* *non-ionic interactions and rarely through hybrid interactions (a combination of ionic and nonionic interactions involving partial proton transfer and hydrogen bonding) with or without the presence of solvate molecules*.[29,30] They offer various merits, like enhanced solubility and dissolution rate of at least one of the components[31], improved bioavailability[32], increased stability of unstable APIs by virtue of intermolecular interactions[33,34], added mechanical strength, to name a few. Since the approach is still in its infant stages, the prediction and screening of multidrug formulations mostly follows knowledge-based approach, which considers H-bond formation ability, pK_a differences, supramolecular synthon approach, etc. In case of acid-base moieties, ΔpK_a is one of the most crucial tools employed; it is believed that a difference between pK_a values of acid and base (ΔpK_a) > 3 leads to the formation of salts, while ΔpK_a < 3 generally results in formation of cocrystals.

2.2 MEMANTINE AND ITS COMPOUNDS

Based on an extensive literature search, we discovered a promising candidate, memantine (*3,5-dimethyl-1-aminoadamantane*), because of its pharmaceutical activity and unique structural features. Despite being a well-known drug for treatment of dementia, memantine (MEM) does not have sufficient literature on its solid-state properties. It is commercially available and administered in the form of memantine hydrochloride (MEM.HCl).

Memantine hydrochloride is an NMDA (N-methyl-D-aspartate) receptor antagonist, and a clinically useful drug for the treatment of various neurological disorders, like the Alzheimer's disease. It is approved by the US Food and Drug Administration (US-FDA) for use in moderate-to-severe Alzeimer's disease.[35] Memantine (MEM) has a great therapeutic utility, as it is also utilized in the treatment of other forms of dementia, like the Parkinson's and Huntington's diseases. It happens to be a promising candidate for other diseases associated with NMDAR (N-methyl-D-aspartate receptor) activation in the central nervous system, namely, glaucoma, multiple sclerosis, epilepsy, and neuropathic pain.[36,37] The formulations of memantine hydrochloride are available for daily administration in the form of tablets (immediate release), oral solution and a once-daily extended-release capsules. However, the advantage of memantine therapy is somewhat jeopardized by the requirement of taking the medication on a daily basis, as oral administration of the drug for patients suffering from various types of dementia is generally a difficult task, with high chances of drug failure due to noncompliance with the scheduled self-medication.[38] Therefore, suitable modification of the drug is necessary to maintain its therapeutic concentration in the body. Additionally, hydrochloride salts come with their own set of disadvantages, like unacceptably high acidity in formulations, risk of corrosion of manufacturing plant and equipment, less than optimal solubility inside the body due to the salting out, poor stability (if the drug is hygroscopic), etc. And rightly so, parameters like corrosion, taste, wettability and flowability are important in drug formulation and scalability. Interestingly, MEM.HCl is also hygroscopic in nature if kept for a longer period of time, as established by crystal structure prediction and study on the solvent accessible volume in the crystal lattice. The crystal structure of memantine hydrochloride contains solvent-accessible voids ranging from 3-14% of the unit-cell volume.[39,40]

Considering above facts, we employed memantine for design and synthesis of new organic salts of memantine, which could have improved solubility and bioavailability, based on the presumption that the presence of charged moieties can substantially enhance ionic and electrostatic interactions in aqueous medium. To the best of our knowledge, only one example of memantine salt is reported in literature.[38] Mishra and coworkers reported a pamoic acid salt of memantine and optimized it to maximize the loading efficiency and to make it suitable for long acting injection. In the present work, we have synthesized a combinatorial library of memantine containing salts with various mono-, di- and tri-carboxylic acids with aliphatic and aromatic backbones (Scheme 2.2). The series of salts synthesized were explored for their propensity to form various supramolecular synthons, as primary ammonium monocarboxylate (PAM) is known to form 1-D (one dimensional) columnar hydrogen bonded networks (Scheme 2.1(a)).[41] PAM can be easily extended to 2-D (two-dimensions) by the presence of an additional carboxylic acid functionality (Scheme 2.1(b)). Interestingly, dicarboxylate primary ammonium (PAD) salts are also reported to form 2-D networks[42] (Scheme 2.1(c)). We were curious to see the effect of methyl functionalities and the bulky adamantane group of memantine on the resulting PAM and PAD hydrogen bonded assemblies, as adamantane based compounds are not only attractive for their pharmaceutical applications[43], but also for exploring weak non-covalent interactions in the crystal structures.[44–48]

In the present work, efforts were also directed to quantify various supramolecular synthons observed in the crystal structures using graph set analysis.[7] Graph sets were framed by M. C. Etter to define the morphology of H-bonded motifs. For the motifs generated from intermolecular H-bonds, the designators are **C** (chain), **R** (ring), **D** (dimer or other finite set) and **S** (intramolecular hydrogen bond). The number of ***d***onor and ***a***cceptor atoms involved in each motif are assigned as subscripts and superscripts, respectively, and the size (degree/number of atoms in repeat unit) of the motif is indicated in parentheses, forming a graph set of the general form - $\boldsymbol{R_d^a(degree\ of\ motif)}$ (Scheme 2.1).

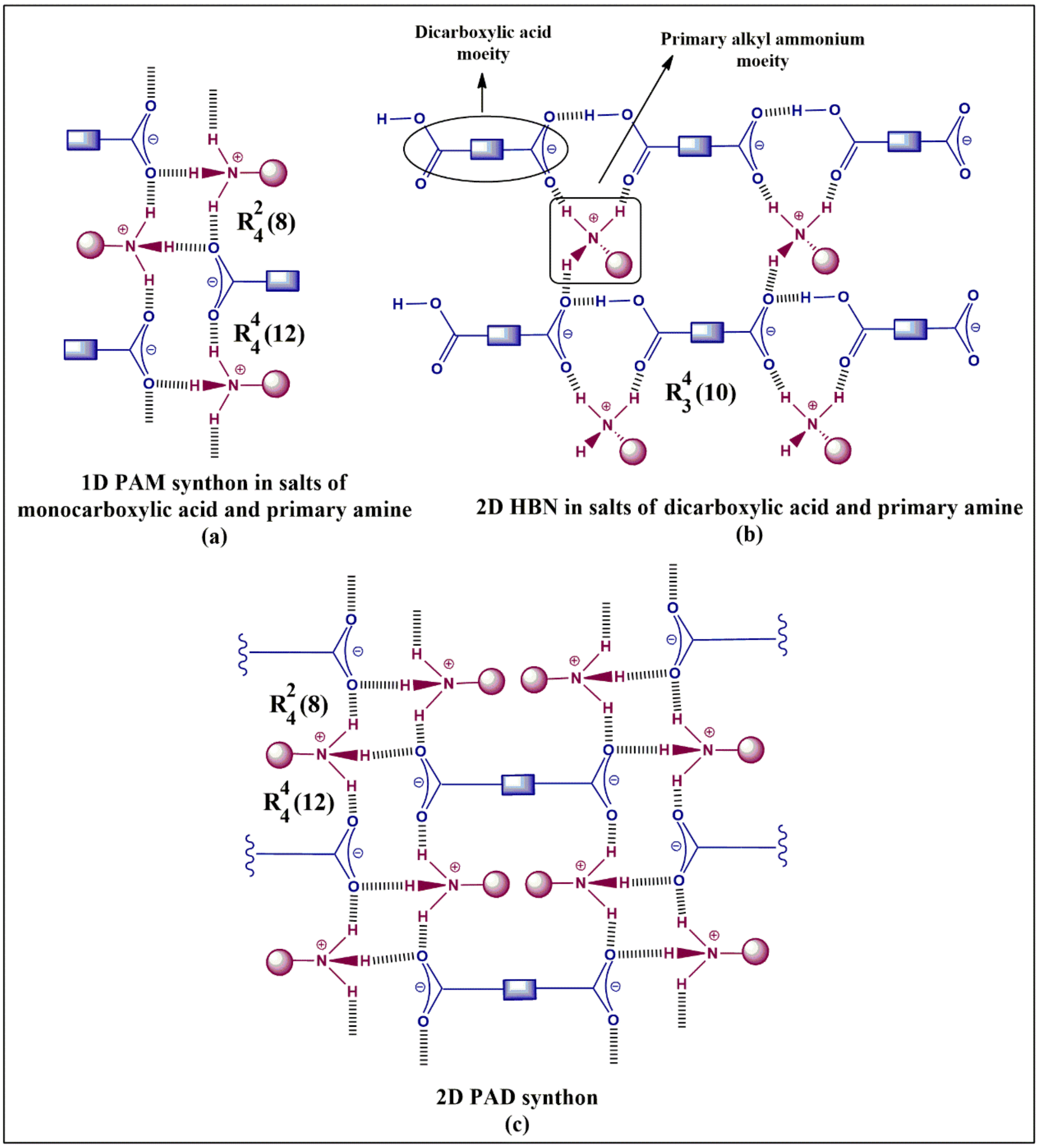

Scheme 2.1 Probable supramolecular synthons in (a) salts of monocarboxylic acid and primary amine (b) mono carboxylate -dicarboxylic acid salt with primary amine (c) di-carboxylate salts with primary amine

All the newly synthesized salts were subjected to Hirshfeld analyses to understand the contribution of various non-covalent interactions towards overall stability and packing in the crystalline state.

Single crystal structure is known to directly impact the solubility of a given molecule in solution. In order to be bioavailable, drug molecules require a certain solubility in the body. It is estimated that 40% of existing drug products and up to 90% of new chemical entities have limited aqueous solubility[28] and hence cannot be delivered to the body using conventional techniques. Cocrystal/salt formation with suitable compounds offer the potential of improved solubility *via* modification of underlying crystal structure, thus potentially rendering the drug bioavailable. This inspired us to perform a comparative study of weak non-covalent interactions present in the parent compound MEM.HCl[39] and newly synthesized salts of memantine in order to obtain better understanding of the trends obtained from the dissolution studies of the newly synthesized MEM salts.

2.3 EXPERIMENTAL PROCEDURES

2.3.1 Synthesis

Free MEM was isolated from MEM.HCl by dissolving 1 g of salt in 25 mL water. Then, a solution of 2 g sodium hydroxide dissolved in 15 mL water was added to it with continuous stirring. Free memantine separated out on the surface of the solvent in the form of yellow oil after an hour. It was extracted using dichloromethane (DCM) and dried over anhydrous sodium sulphate. The solution was then distilled in a rotary evaporator to remove the DCM and free memantine was obtained in the form of oil. All the salts were obtained by refluxing the free memantine and acid in equimolar ratios ((1:1) and (2:1) for dicarboxylic acids) in methanol for 1 hour. The solid salts obtained were kept for recrystallization in pure solvents (methanol, ethanol, and acetonitrile) as well as solvents mixtures (at room temperature (25-30°C) or slightly lower temperatures (15-20°C)). Crystals suitable for single crystal X-ray studies were obtained by slow evaporation of solvents.

For dicarboxylic acids (**A-F**), the salts were synthesized in the ratios of (1:1) and (2:1), however, only for oxalic acid, we could isolate both mono- and di-carboxylate salts (**1A** and **1(2)A**). For all the other dicarboxylic acids, we could obtain only one of the mono-or di-carboxylate salts. Also, in some cases, the same salt in both (1:1) and (1:2) solutions was obtained (Table 2.1). We believe that the salt which is thermodynamically most stable (of all possible structures[49]) is formed and falls out of the system as a solid. In nutshell, it is extremely difficult to gain control over the resulting stoichiometry of the salts.

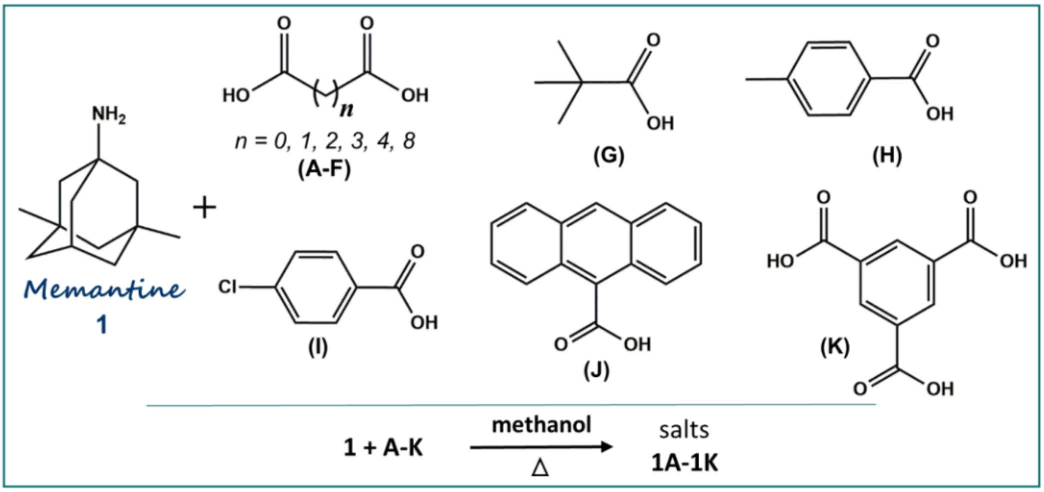

Scheme 2.2 List of memantine salts (1A-1K) synthesized

2.3.2 Materials and Methods

All the chemicals were obtained from Sigma Aldrich and TCI and the solvents were obtained from SD Fine Chemicals, India and were used without any further purification. Memantine hydrochloride was obtained from TCI India.

Table 2.1 Stoichiometric ratios of the salts formed, and solvents employed for crystallization

Salt	Reactants Ratio	Solvents
1A	1 + A (1:1)	MeOH + ACN
1(2)A	1 + A (2:1)	MeOH + H_2O
1(2)B	1 + B (2:1)	EtOH
1C	1 + C (1:1)	MeOH
1D	1 + D (1:1)	EtOH + MeOH
1(2)E	1 + E (2:1)	EtOH + ACN
1F	1 + F (1:1)	MeOH
1G	1 + G	MeOH
1H	1 + H	MeOH + ACN
1I	1 + I	EtOH
1J	1 + J	MeOH
1K	1 + K (1:1)	MeOH + H_2O

2.3.2.1 NMR studies

NMR data was recorded on BRUKER AVANCE, 400 MHz spectrometer in DMSO-d6 with TMS as internal standard. The ^{1}H NMR spectra of all compounds can be found in Supplementary Data* at the end of the chapter.

2.3.2.2 FT-IR studies

FT-IR studies were performed on Bruker Alpha FT-IR spectrometer. The solid sample was ground together with anhydrous KBr using mortar pestle and the pellet so formed was subjected to FT-IR analysis. The FT-IR spectra of all compounds can be found in Supplementary Data* at the end of the chapter.

2.3.2.3 Single crystal X-ray diffraction

Single crystal diffraction data for all compounds was collected on an Xcalibur, EOS, Gemini diffractometer with graphite monochromatic Mo Kα radiation (0.71073 Å). All structures were solved and refined using the Olex2[50] software and ShelXL[51] refinement package. Graphics were generated using MERCURY (version 4.3.1). All structures were solved by direct methods and refined in a regular pattern. In all the cases, non-hydrogen atoms were treated anisotropically. Whenever possible, the hydrogen atoms were refined by locating on a difference Fourier map. In other cases, hydrogen atoms were geometrically fixed. The ORTEP images of all salts are combined in Figure S2.1*.

2.3.2.4 Hirshfeld surface analysis

The 3D Hirshfeld surfaces[52–54] and two-dimensional Hirshfeld fingerprint plots of all the salts were obtained using Crystal Explorer 3.1.[55] software. Intermolecular interaction energies of the salts were also measured for CE-HF model with HF/3-21G basis sets. The 3D Hirshfeld surfaces of all salts are combined in Figure S2.2*.

2.3.2.5 Dissolution studies of memantine salts

The solubility studies of all the salts were performed gravimetrically and compared with that of MEM.HCl. A known amount of salt was dissolved in 5 mL of distilled water and the solution stirred (550–600 RPM) at RT (~ 25-27°C) for 48 h. The solution was then filtered with a pre-weighed filter paper. The weight of undissolved salt subtracted from the total amount taken gave the amount of dissolved salt in the solution, which was further confirmed by evaporation of water from the solution obtained and weighing the amount of salt left behind.

2.3.2.6 Powder X-ray diffraction (PXRD)

PXRD studies of salts **1(2)E** and **1G** were carried out using a Bruker D2 Phaser X-ray diffractometer equipped with a Cu Kα radiation (λ = 1.54056 Å) source. For these studies, crystalline fresh samples of the salts were scanned for 'before dissolution' (B.D.) studies and approximately 20 mg of the same salts were dissolved completely in distilled water and the solutions filtered, and these solutions were kept at a temperature of 35°C- 40°C for 4-5 days. These solutions had their water dried up which eventually yielded the salts samples, which were scanned for 'after dissolution' (A.D.) studies.

2.3.2.7 DSC studies

DSC studies were performed for before and after dissolution samples of salts **1(2)E** and **1G** on a METTLER DSC 3 instrument with Ceramic FRS5+ sensor in alumina crucibles. Approximately 2 mg of samples were scanned under N_2 atmosphere on a temperature range of 25°C-250°C with a scan rate of 10°C/min. Plots of sample temperature vs. Heat flow (mW) were prepared.

2.3.3 Analytical Data

The monocarboxylate salts of dibasic acids (**1A, 1C, 1D** and **1F**) contain one deprotonated carboxylate ion and one free carboxylic acid group. They show strong IR bands for carboxylate ion around 1650-1550 cm^{-1} and 1280-1400 cm^{-1}, which attribute to asymmetric and symmetric vibrations of carbonyl respectively; a band around 1760-1690 cm^{-1} was observed which confirm the carbonyl of free carboxylic acid group. A broad trough around 2800-3400 cm^{-1} was also observed, a characteristic of O-H stretching of free carboxylic acid group. The IR bands representing free –COOH group were found to be absent in salts **1(2)A**, **1(2)B** and **1(2)E**, which are dicarboxylate salts of dibasic acids and the spectrum only showed characteristic carboxylate bands. Salts **1G**, **1H**, **1I** and **1J** are formed with monobasic acids and have their -COOH group deprotonated, as shown by their carboxylate bands around 1650-1550 cm^{-1} and 1280-1400 cm^{-1}. Salt **1K** is a monocarboxylate salt of trimesic acid and thus displayed bands corresponding to both, carboxylate ion and free carboxylic acid groups.

^{1}H-NMR analysis of salts (**1A-1K**) confirmed the formation of mono-carboxylate as well as di-carboxylate salts of memantine.

Compound 1A. M.P.= 205°C, ^{1}H NMR (400 MHz, DMSO-d6, TMS) = δ (ppm) 5.2 (6H, NH),δ 2.134 (*s*, 1H, CH), δ 1.576 (*s*, 2H, CH_2), δ 1.418-1.329 (*q*, 4H, 2(CH_2)), δ 1.276 (*s*, 4H, 2(CH_2)), δ 1.154-1.052 (*q*, 2H, CH_2), δ 0.835 (*s*, 6H, 2(CH_3)).

FT-IR, cm^{-1} (KBr) – 3471, 3408, 3257, 3003, 2921, 2643, 1773, 1719, 1632, 1404, 1360, 1325, 852, 781, 719, 577.

Compound 1(2)A. M.P.= 239°C, ^{1}H NMR (400 MHz, DMSO-d6, TMS) = δ (ppm) 4.2 (NH), δ 2.094 (*s*, 1H, CH), δ 1.476 (*s*, 2H, CH_2), δ 1.318-1.232 (*m*, 8H, 4(CH_2)), δ 1.128-1.036 (*q*, 2H, CH_2), δ 0.822 (*s*, 6H, 2(CH_3)).

FT-IR, cm^{-1} (KBr) – 3367, 2908, 2698, 2645, 2225, 1638, 1600, 1529, 1361, 1345, 1294, 1193, 766, 685, 580, 479.

Compound 1(2)B. M.P.= 184°C, ^{1}H NMR (400 MHz, DMSO-d6, TMS) = δ (ppm) 4.396 (6H, NH), δ 2.090 (*s*, 1H, CH), δ 1.454 (*s*, 2H, CH_2), δ 1.302-1.214 (*m*, 8H, 4(CH_2)), δ 1.122-1.030 (*q*, 2H, CH_2), δ 0.818 (*s*, 6H, 2(CH_3)).

FT-IR, cm^{-1} (KBr) – 3454, 2947, 2631, 2211, 1702, 1645, 1578, 1453, 1415, 1363, 1241, 1119, 1044, 1027, 952, 937, 803, 697, 647, 550, 480.

Compound 1C. M.P.= 137°C, ^{1}H NMR (400 MHz, DMSO-d6, TMS) = δ (ppm) 2.223 (*s*, 2H, CH_2), δ 2.088 (*s*, 1H, CH), δ 1.462 (*s*, 2H, CH_2), δ 1.305-1.221 (*m*, 10H, 5(CH_2)), δ 1.119-1.025 (*q*, 2H, CH_2), δ 0.813 (*s*, 6H, 2(CH_3)).

FT-IR, cm^{-1} (KBr) – 3428, 2911, 2862, 2639, 2168, 1630, 1561, 1514, 1474, 1386, 1281, 1173, 1061, 1027, 812, 655, 544.

Compound 1D. M.P.= 176°C, ^{1}H NMR (400 MHz, DMSO-d6, TMS) = δ (ppm) 2.181-2.146 (*m*, 4H, 2(CH_2)), δ 2.114 (*s*, 1H, CH), δ 1.701-1.630 (*m*, 2H, CH_2), δ 1.529 (*s*, 2H, CH_2), δ 1.373-1.230 (*m*, 8H, 4(CH_2)), δ 1.143-1.043 (*q*, 2H, CH_2), δ 0.829 (*s*, 6H, 2(CH_3)).

FT-IR, cm^{-1} (KBr) – 3448, 2916, 2849, 2697, 2597, 2527, 2079, 1729, 1687, 1535, 1447, 1397, 1227. 1152, 886, 789, 662.

Compound 1(2)E. M.P.= 160°C, ^{1}H NMR (400 MHz, DMSO-d6, TMS) = δ (ppm) 2.098-2.050 (*m*, 4H, 2(CH_2)), δ 1.476-1.442 (*m*, 4H, 2(CH_2)), δ 1.411 (*s*, 2H, CH_2), δ 1.254-1.168 (*m*, 8H, 4(CH_2)), δ 1.094-1.007 (*q*, 2H, CH_2), δ 0.799 (*s*, 6H, 2(CH_3)).

FT-IR, cm^{-1} (KBr) – 3429, 2945, 2902, 2199, 1633, 1580, 1529, 1452, 1399, 1135, 919, 795, 629.

Compound 1F. M.P.= 98°C, ^{1}H NMR (400 MHz, DMSO-d6, TMS) = δ (ppm) 2.142-2.106 (*m*, 4H, 2(CH_2)), δ 2.067 (*s*, 1H, CH), δ 1.487-1.452 (*m*, 4H, 2(CH_2)), δ 1.425 (*s*, 2H, CH_2), δ 1.266 (*m*, 12H, 4+2(CH_2)), δ 1.079-1.049 (*q*, 2H, CH_2), δ 0.808 (*s*, 6H, 2(CH_3)).

FT-IR, cm^{-1} (KBr) – 3156, 2935, 2626, 2563, 2103, 1977, 1694, 1635, 1556, 1457, 1389, 1272, 1233, 1113, 904, 878, 767, 685.

Compound 1G. M.P.= 159°C, ^{1}H NMR (400 MHz, DMSO-d6, TMS) = δ (ppm) 2.071 (*s*, 1H, CH), δ 1.446 (*s*, 2H, CH_2), δ 1.288-1.199 (*m*, 8H, 4(CH_2)), δ 1.068 (*s*, 11H, CH_2+3(CH_3)), δ 0.803 (*s*, 6H, 2(CH_3)).

FT-IR, cm^{-1} (KBr) – 3416, 2950, 2908, 2174, 1642, 1574, 1480, 1455, 1401, 1358, 1220, 1059, 1028, 964, 879, 793, 591.

Compound 1H. M.P.= 150°C, ^{1}H NMR (400 MHz, DMSO-d6, TMS) = δ (ppm) 7.766-7.747 (*d*, 2H, 2(CH)), δ 7.133-7.114 (*d*, 2H, 2(CH)), δ 2.306 (*s*, 3H, CH_3), δ 2.113 (*s*, 1H, CH), δ 1.600 (*s*, 2H, CH_2), δ 1.441-1.347 (*q*, 4H, 2(CH_2)), δ 1.264 (*s*, 4H, 2(CH_2)), δ 1.136-1.040 (*q*, 2H, CH_2), δ 0.820 (*s*, 6H, 2(CH_3)).

FT-IR, cm^{-1} (KBr) – 3413, 2944, 2171, 1930, 1630, 1548, 1454, 1376, 1172, 1018, 842, 773, 695, 609, 548, 478.

Compound 1I. M.P.= 142°C, ^{1}H NMR (400 MHz, DMSO-d6, TMS) = δ (ppm) 7.891-7.869 (*d*, 4H, 4(CH)), δ 7.442-7.421 (*d*, 4H, 4(CH)), δ 2.076 (*s*, 1H, CH), δ 1.639 (*s*, 2H, CH_2), δ 1.477-1.384 (*q*, 4H, 2(CH_2)), δ 1.277 (*s*, 4H, 2(CH_2)), δ 1.156-1.052 (*q*, 2H, CH_2), δ 0.831 (*s*, 6H, 2(CH_3)).

FT-IR, cm^{-1} (KBr) – 3450, 2945, 2155, 1930, 1680, 1590, 1553, 1424, 1375, 1164, 1088, 1014, 934, 834, 685, 548.

Compound 1J. M.P.= 194°C, ^{1}H NMR (400 MHz, DMSO-d6, TMS) = δ (ppm) 8.335 (*s*, 1H, CH), δ 8.149-8.128 (*d*, 2H, 2(CH)), δ 8.002-7.999 (*d*, 2H, 2(CH)), δ 7.456-7.379 (*m*, 4H, 4(CH)), δ 2.061 (*s*, 1H, CH), δ 1.525 (*s*, 2H, CH_2), δ 1.341-1.159 (*q*, 8H, 4(CH_2)), δ 1.082-1.051 (*d*, 1H, CH_2), δ 0.938-0.907 (*d*, 1H, CH_2), δ 0.754 (*s*, 6H, 2(CH_3)).

FT-IR, cm^{-1} (KBr) – 3452, 3032, 2892, 2623, 1786, 1680, 1554, 1485, 1448, 1344, 1292, 1255, 916, 891, 724, 639.

Compound 1K. M.P.= 196°C, ^{1}H NMR (400 MHz, DMSO-d6, TMS) = δ (ppm) 8.572 (*s*, 3H, 3(CH)), δ 2.143 (*s*, 1H, CH), δ 1.656 (*s*, 2H, CH_2), δ 1.497-1.403 (*q*, 4H, 2(CH_2)), δ 1.283 (*s*, 4H, 2(CH_2)), δ 1.155-1.059 (*q*, 2H, CH_2), δ 0.834 (*s*, 6H, 2(CH_3)).

FT-IR, cm^{-1} (KBr) – 3389, 3121, 2904, 1948, 1690, 1613, 1556, 1321, 1257, 1181, 1057, 1020, 899, 752, 676, 606, 519.

2.4 SALT FORMATION – EXPERIMENTAL AND STRUCTURAL CONCEPTS

A simple mixing of amine with mono- and di-carboxylic acids in methanolic solutions resulted in the formation of salts, depending upon the pK_a difference of amine and various mono-/di-carboxylic acids (Table 2.2). 12 binary salt complexes were synthesized by reacting acid and amine in 1:1 and 1: 2 molar ratios. The salt formation was confirmed by FT-IR, ^{1}H NMR and single crystal X-ray studies.

pK_a for memantine= 10.7

Table 2.2 pK_a values for various acids used in the study

Salts/Acids	pK_a1*	pK_a2*	ΔpK_a
1A/oxalic acid (1:1)	1.23	4.19	9.47
1(2)A/oxalic acid (2:1)	1.23	4.19	9.47, 6.51
1(2)B/malonic acid (2:1)	2.85	5.69	7.85, 5.01
1C/succinic acid (1:1)	4.16	5.28	6.54, 5.42
1D/glutaric acid (1:1)	4.31	5.35	6.31
1(2)E/adipic acid (2:1)	4.43	5.44	6.27, 5.26
1F/sebacic acid (1:1)	4.72	5.45	5.98
1G/pivalic acid	5.03	-	5.67
1H/4-methylbenzoic acid	4.37	-	6.33
1I/4-chlorobenzoic acid	3.98	-	6.72
1J/9-anthracenecarboxylic acid	3.68	-	7.02
1K/trimesic acid (1:1)	3.12	3.89, 4.70	7.58

(Source for pK_a values- https://pubchem.ncbi.nlm.nih.gov/)

2.4.1 Single crystal X-ray diffraction studies

Single crystal X-ray studies of salts **1A-1K** were carried out to get an insight about the packing modes and supramolecular synthons present in these salts. The crystallographic parameters and H-bond parameters are listed in Tables S2.1* and S2.2*.

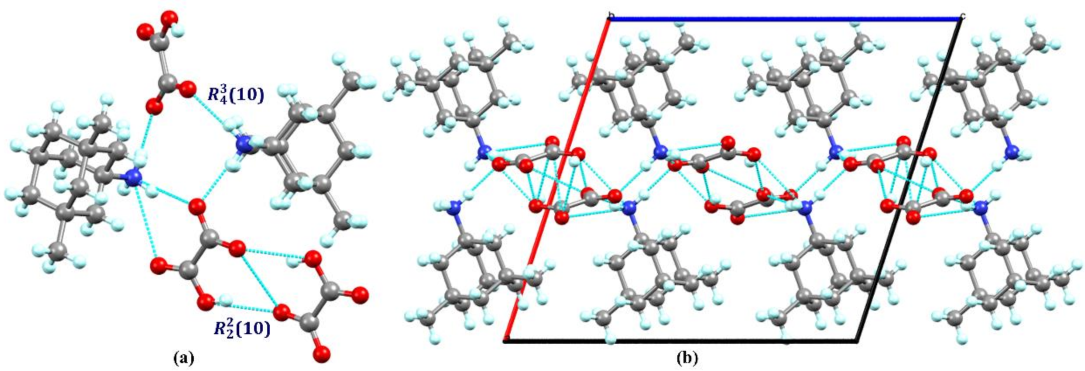

Figure 2.4 (a) the primary hydrogen bonded network of salt 1A, (b) overall assembly as viewed from *b* axis.

Salt 1A ***[3,5-dimethyladamantan-1-aminium hydrogenoxalate)]*** Crystals suitable for single crystal X-ray study of **1A** were obtained from methanol and acetonitrile mixture (1:1). **1A** crystallizes out in monoclinic, *P2₁/c* space group and the asymmetric unit contains one molecule each of oxalic acid and memantine. A persistent cyclic dimeric COOH…COOH acid interaction (O-H...O bond length= 2.777 Å and bond angle= 143.84°) along with cyclic hetero supramolecular synthon between ammonium ion and carboxylate moiety, with graph set $R_4^3(10)$ is found in the crystal structure. The packing of **1A** extends in 3D *via* multiple weak non-covalent interactions such as C-H…O, N-H...C, N-H...O, and van der Waals. (Figure 2.4)

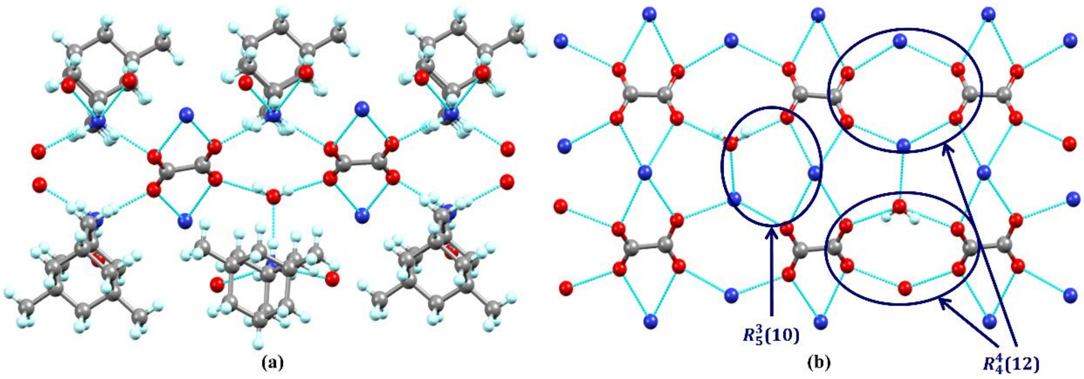

Figure 2.5 (a) dicarboxylate oxalic acid salt of memantine, (b) 2D network formed by N-H...O and O-H...O interactions as viewed from *b* axis (memantine moiety is not shown for clarity of the picture).

Salt 1(2)A ***[di(3,5-dimethyladamantan-1-aminium) oxalate]*** Crystals of dicarboxylate salt of MEM with oxalic acid (**1(2)A**) were obtained from methanol and water mixture (1:1). The structure crystallizes in triclinic *P-1* space group and the asymmetric unit of **1(2)A** contains three molecules of oxalate, six molecules of memantine, and two molecules of water (no suitable higher symmetry crystal system could be obtained). A zig-zag two-dimensional hydrogen bonded network is created with oxalate ion, memantine ammonium ion and water molecules. Overall, the hydrogen bonded network of **1(2)A** contains some well-known supramolecular synthons represented by $R_4^2(8), R_4^4(12)$ graph set representations, along with the unique hydrogen bonded patterns with graph sets $R_5^3(10)$ and $R_2^2(7)$ (Figure 2.5). The structure further extends in three dimensions through multiple van der Waals interactions.

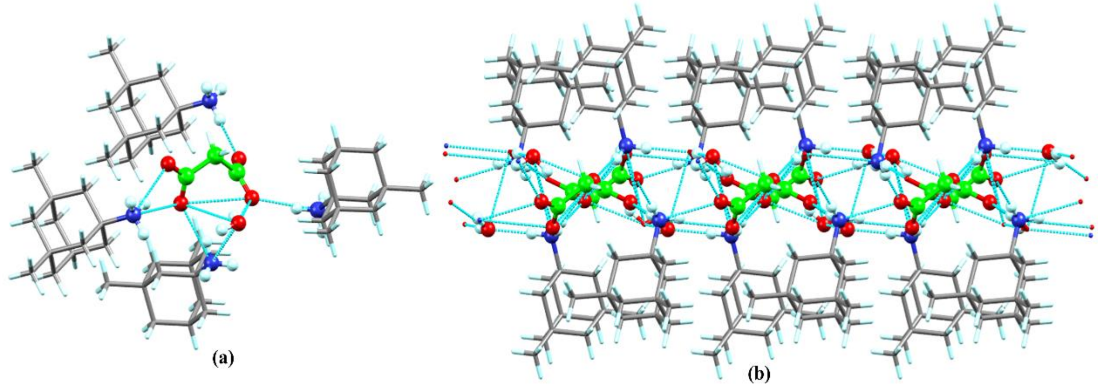

Figure 2.6 (a) primary H-bonding unit of Salt 1(2)B, (b) network of various non-covalent interactions found in Salt 1(2)B, as viewed from *c* axis (carbons of malonate ion are represented in bright green)

Salt 1(2)B ***[di(3,5-dimethyladamantan-1-aminium) malonate]*** Diffraction quality crystals of MEM and dimalonate salt were obtained from ethanol and water mixture (1:1). Salt **1(2)B** crystallizes out in monoclinic, *P2₁/c* space group, consisting of two molecules of MEM, one molecule of malonate ion, and two molecules of water in the asymmetric unit. A unique supramolecular synthon pattern with graph set representation $R_4^4(10)$ is observed involving two malonate ions and one MEM ion (Figure 2.6). However, frequently observed 1D PAM synthon ($R_4^2(8)$, (Scheme 2.1)) is also found in the crystal structure of **1(2)B**. 1D network of **1(2)B** extends in 2D through C-H…O and van der Waals interactions.

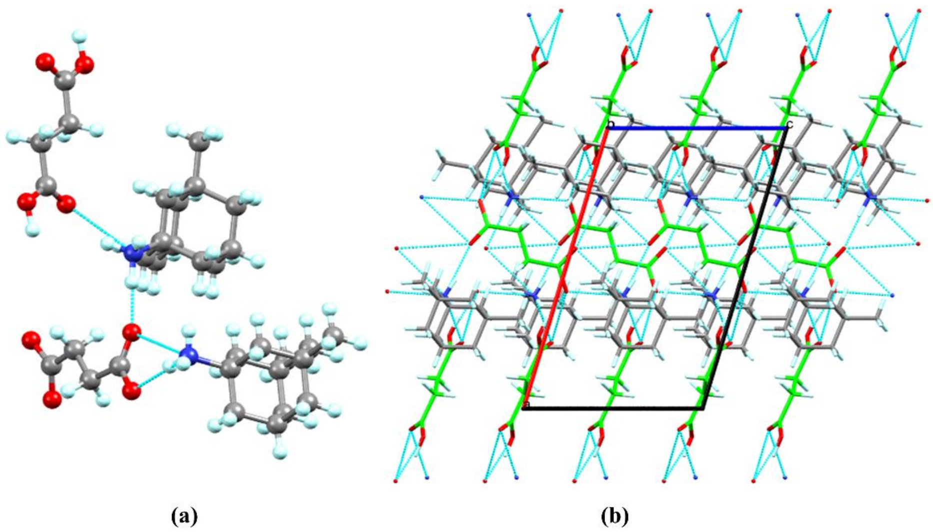

Figure 2.7 (a) bonding in salt 1C, (b) dense supramolecular assembly of the salt as viewed from *b* axis (carbons of succinic acid and succinate moiety are shown in bright green, for clarity of image)

Salt 1C ***[bis(3,5-dimethyladamantan-1-aminium) succinate-succinic acid]*** A good crystal of salt **1C** was obtained from methanolic solution by slow evaporation method at room temperature. **1C** crystallizes out in monoclinic, *P2₁/c* space group and its asymmetric unit contains two molecules each of MEM cations and succinic acid. The crystal structure is quite a unique one, as one of the succinic acid molecules forms a dicarboxylate and one of them remains as dicarboxylic acid only. This type of structure has rarely been reported in the literature. We find a $R_4^4(12)$ type of synthon, frequently occurring (Scheme 2.1) in dicarboxylate salts with primary ammonium cations (PAD). The structure also possesses carboxylate-carboxylic acid interactions which extend in three dimensions (Figure 2.7).

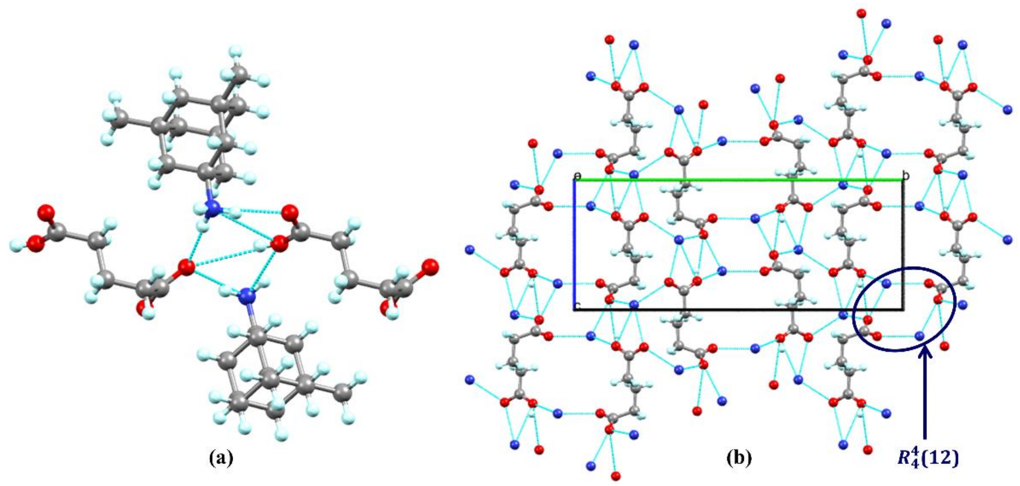

Figure 2.8 (a) asymmetric unit of 1D as viewed from *b* axis, (b) network of intermolecular H-bonds as viewed from *a* axis (memantine moiety is not shown for clarity of image)

Salt 1D ***[3,5-dimethyladamantan-1-aminium) hydrogenglutarate]*** The crystals of monocarboxylate salt of glutaric acid with memantine were obtained from methanol and ethanol mixture (2:1). The salt **1D** crystallizes in monoclinic crystal system, with centrosymmetric *P2₁/c* space group. Primarily, the eight membered ($R_4^4(12)$) supramolecular synthon was observed in the crystal structure (Figure 2.8). The average N-H...O bond length in the synthon is around 2.8 Å. Other than participation in forming supramolecular synthons, the carboxylate moiety of the acid is also making hydrogen bond with the neighboring ammonium ion forming hydrogen bonded network with graph set representation $R_2^2(6)$. Overall, the assembly was found to be 2D due to the presence of multiple weak non-bonded interactions such as C-H…O, N-H…C and van der Waals forces.

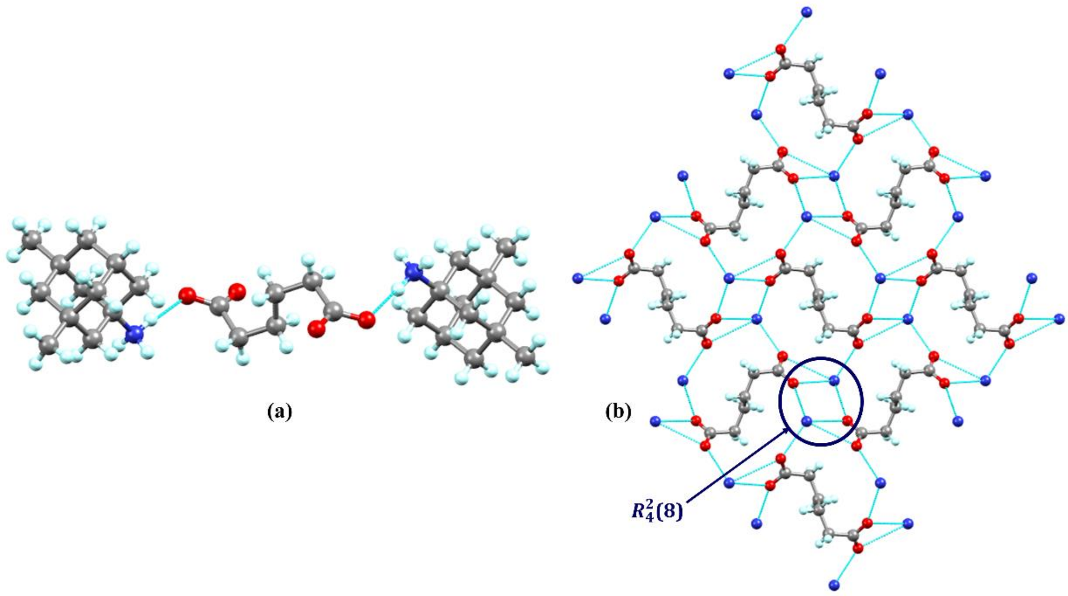

Figure 2.9 (a) Salt 1(2)E, (b) extended assembly of salt as viewed from *c* axis (memantine moiety is not shown for clarity of image)

Salt 1(2)E ***[di(3,5-dimethyladamantan-1-aminium) adipate]*** Memantine reacted with adipic acid forming a dicarboxylate salt and a suitable crystal of **1(2)E** was obtained from ethanol and acetonitrile (2:1) mixture. Single crystal structure of **1(2)E** belongs to chiral $P2_1$ space group of monoclinic crystal system with two molecules of MEM and one molecule of adipate dicarboxylate ion in the asymmetric unit. The frequently occurring PAD supramolecular synthon, $R_4^2(8)$ is also observed in the structure (the average N-H....O bond length of 1.9Å and average bond angle of 163^o) (Figure 2.9). **1(2)E** displays multiple weak C-H…O interactions forming a 2D network, which extends in 3D through multiple van der Waals interactions.

Salt 1F ***[3,5-dimethyladamantan-1-aminium sebacitate]*** Good diffraction quality crystals of sebacic acid monocarboxylate salt with memantine were obtained from methanolic solution. The crystal structure belongs to monoclinic, $P2_1$ space group with one molecule each of sebacic acid monocarboxylate and MEM ion in the asymmetric unit. The structure contains a unique supramolecular synthon with graph set $R_5^5(14)$ (Figure 2.10). The crystal structure of **1F** contains multiple C-H…O interactions leading to a 3D supramolecular network.

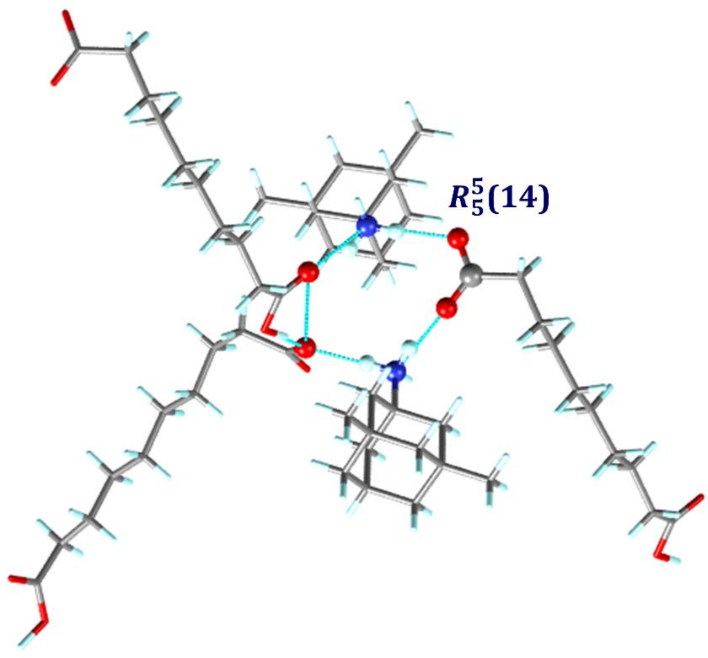

Figure 2.10 Hetero-synthon in 1F

Salt 1G ***[3,5-dimethyladamantan-1-aminium pivalate]*** Pivalic acid forms (1:1) salt with memantine, and a suitable crystal of **1G** was obtained from methanolic solution by slow evaporation method at room temperature (25°C). The salt **1G** crystallizes in *I2/a* space group of monoclinic system with two molecules each of MEM and pivalate ion in the asymmetric unit. The hydrogen bonded network of **1G** is a zero-dimensional (0D) unit with four molecules each of acid and base participating in the hydrogen bonded cluster (Figure 2.11).

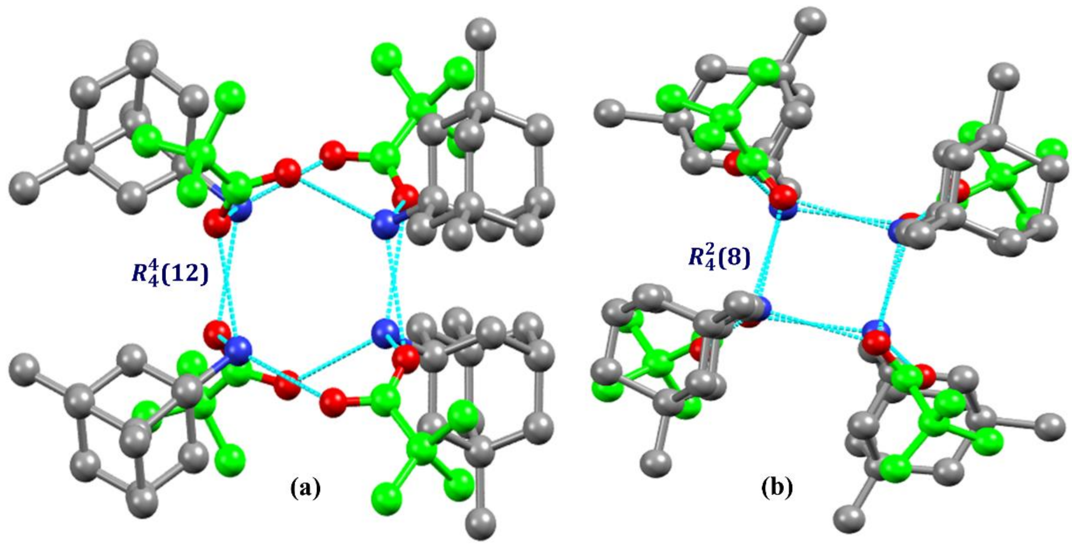

Figure 2.11 (a) 0D cluster patterns of 1G as viewed from *a* axis, (b) 3D 4-membered patterns as viewed from *b* axis (hydrogens are hidden for the clarity of image, pivalic acid moiety is shown in neon green color to distinguish it from the MEM moiety)

Even though, the structure contains the commonly occurring PAM supramolecular synthons $R_4^4(12)$ and $R_4^2(8)$, the hydrogen bonded network is a 0D instead of 1D (Scheme 2.1 (a)).

The supramolecular isomerism of this hydrogen bonded network may be attributed to the presence of bulky *tert*-butyl functional group of pivalic acid in the structure. Interestingly, the hydrogen bonded cluster of **1G** also contains a well-defined void of about 4.2 Å.

Salt 1H ***[3,5-dimethyladamantan-1-aminium 4-methylbenzoate]*** The salt of 4-methylbenzoic acid with memantine was obtained by reacting acid and amine in 1:1 molar ratio, and diffraction quality crystals of **1H** were obtained from methanol and acetonitrile (1:1) mixture.

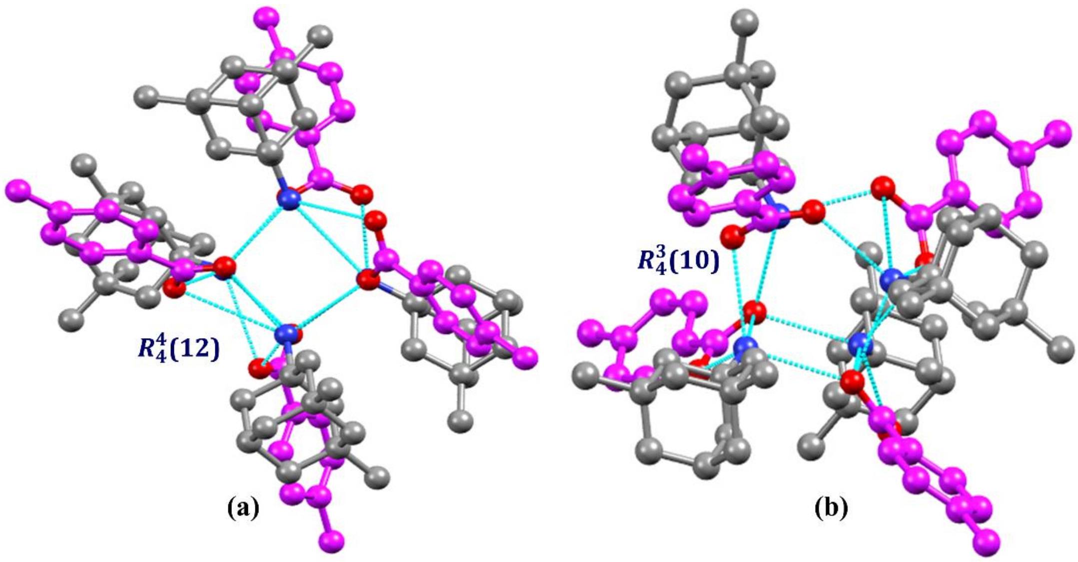

Figure 2.12 (a), (b) 0D synthon pattern of 1H (acid moiety is shown in purple for clarity of picture)

Salt **1H** crystallizes in a centrosymmetric, *P-1* space group of triclinic crystal system, and the asymmetric unit contains four molecules each of MEM and 4-methyl benzoate, forming a closed hydrogen bonded cluster (0D network) comprising of $R_4^3(10)$ and $R_4^4(12)$ type supramolecular synthons (Figure 2.12). Unlike the 0D network of **1G**, the structure of **1H** extends in 3D space through multiple van der Waals interactions among the hydrogen bonded clusters.

Salt 1I ***[3,5-dimethyladamantan-1-aminium) 4-chlorobenzoate]*** Crystals of **1I** were obtained from ethanolic solution by slow evaporation method. **1I** crystallizes in monoclinic, $P2_1/c$ space group and the asymmetric unit contains one molecule each of MEM and 4-chlorobenzoate anion. The crystal structure of **1I** displays the PAM supramolecular synthon (Figure 2.13) forming a 1D network (Scheme 2.1) as expected for primary ammonium salts. No other weak non-covalent interactions were observed in the structure.

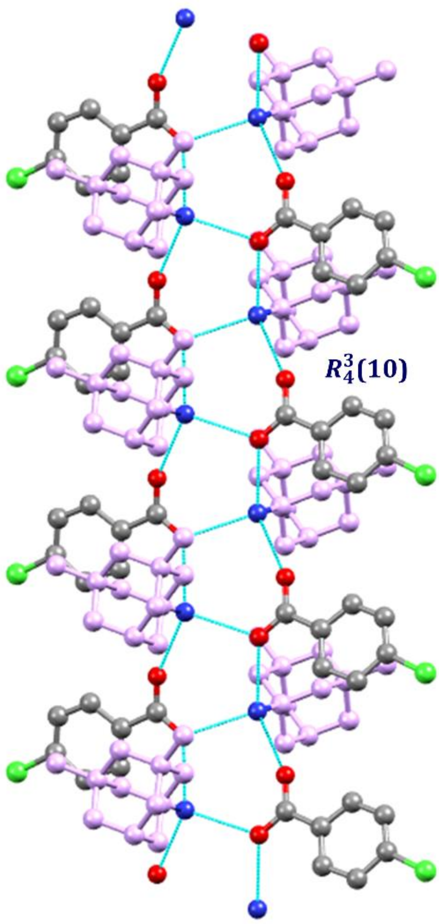

Figure 2.13 Arrangement pattern in 1I as viewed from *c* axis (memantine moiety is shown in very light color for clarity of image)

Salt 1J ***[3,5-dimethyladamantan-1-aminium 9-anthracenecarboxylate]*** (1:1) equimolar salt of MEM and 9-anthracenecarboxylic acid was synthesized and crystallized from methanolic solution. **1J** crystallizes out in centrosymmetric, *P-1* space group of triclinic crystal system and the asymmetric unit contains two molecules each of acid and amine.

The supramolecular assembly of **1J** extends in 1D as a result of the alternating arrangement of synthons ($R_4^2(8)$ and $R_4^4(12)$) (Figure 2.14), as expected for PAM salts (Scheme 2.1). Along with robust charge assisted hydrogen bonds ($^{+}$N-H…$^{-}$O), multiple weak non-covalent interactions were also observed in the crystal structure, viz. C-H…π and van der Waals interactions.

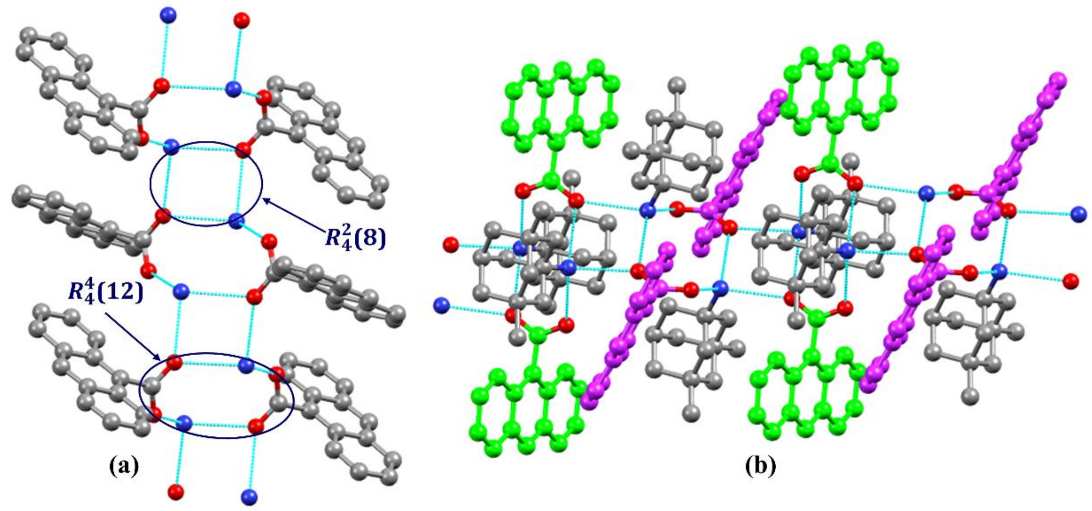

Figure 2.14 (a) synthon pattern of 1J as viewed from *b* axis, (b) the overall extended assembly showing anthracene rings arranged at an angle of ~34^o (hydrogens are hidden for the clarity of picture, anthracene rings are multi-colored for showing their cross-orientation)

Salt 1K ***[3,5-dimethyladamantan-1-aminium dihydrogentrimesate]*** Reaction of MEM with trimesic acid resulted into salt with only one proton transfer from acid to amine, i.e. (1:1) molar salt. A crystal suitable for single crystal X-ray study was obtained from methanol and water mixture. The asymmetric unit of **1K** (monoclinic, $P2_1/n$) contains a pair of acid and base along with solvent molecules of crystallization (water and methanol).

The supramolecular synthons observed in PAM couldn't be identified in the structure mainly due to the presence of solvent molecules capable of forming interfering hydrogen bonds with the parent compounds. Interestingly, π…π stacking between the benzene rings is observed (distance between benzene ring=3.3Å) in the structure (Figure 2.15).

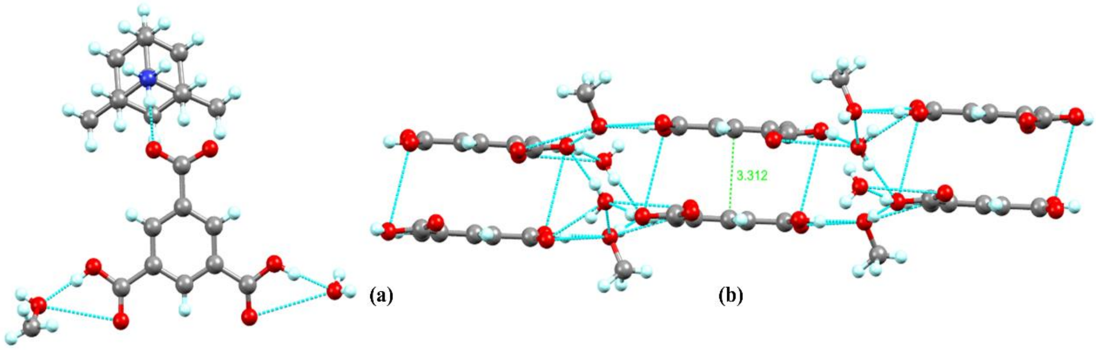

Figure 2.15 (a)monocarboxylatetrimesic acid salt 1K; (b) stacking in benzene rings of the acid in 1K (memantine moiety is not shown for clarity of image)

From the X-ray studies, we now observe that the 1D PAM synthon (as shown in Scheme 2.1), which occurs in salts **1(2)A**, **1D**, **1G**, **1H** and **1J** is a robust supramolecular arrangement and is likely is to occur in organic salt linkages. Also, we find a couple of unique synthon patterns in the crystal structures, which were expected as a result of the intervention caused by the bulky adamantane moiety and the methyl groups. Some salts exhibit unique patterns such as, $R_5^3(10)$ and $R_2^2(7)$ by Salt **1(2)A**; $R_4^4(10)$ by Salt **1(2)B** and $R_5^5(14)$ by **1F**. A hetero synthon belonging to $R_4^3(10)$ graph set was found in Salts **1A**, **1H** and **1I**. Notably, the salts with smaller dibasic acids have more deviation in their supramolecular assembly pattern than the monobasic acids, which mostly comprise of the 1D PAM synthon as shown in Scheme 2.1. This also implies that the smaller dibasic acid moieties are more competent to form unique H-bonded patterns and hence, unique supramolecular assemblies.

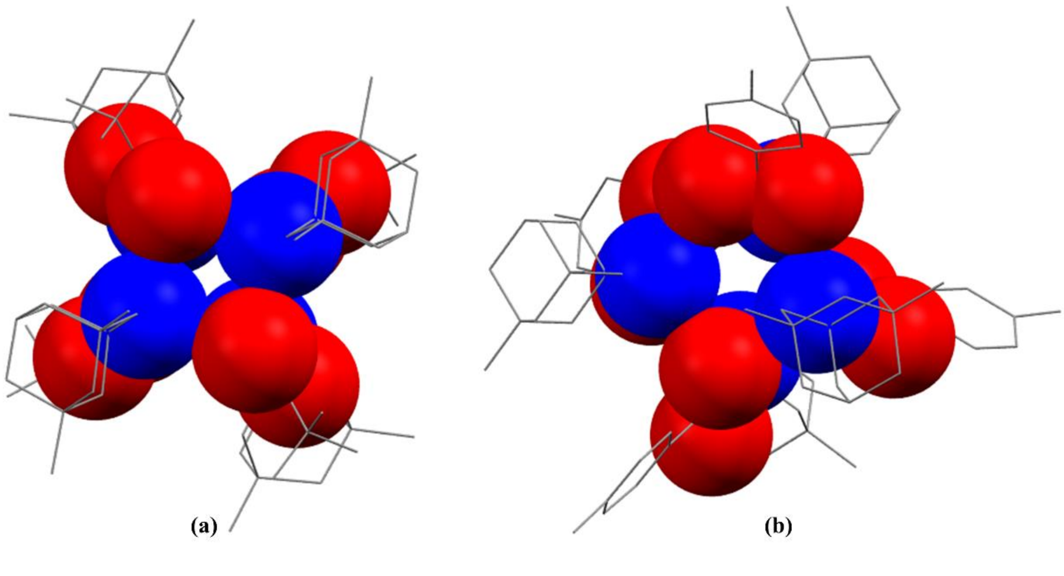

Figure 2.16 Hydrogen bonded cluster network in salts (a) 1G (as viewed from *b* axis) and (b) 1H (for clarity, contacts atoms are shown in space fill model and hydrogens are not shown)

Comparing the single crystal structures with that of MEM.HCl, we found that it displayed a columnar structure having water molecules sitting at the center of a void where the overall 3-D structure is governed by strong N-H…Cl interactions. When the N-H…Cl interaction is replaced by charged N-H…O interactions, similar hydrogen bonded networks were observed as in the case of salts **1G** and **1H**, where the conventional PAM supramolecular synthons have converged into a unique molecular cluster with well-defined voids (Figure 2.16).

2.4.2 Hirshfeld analyses

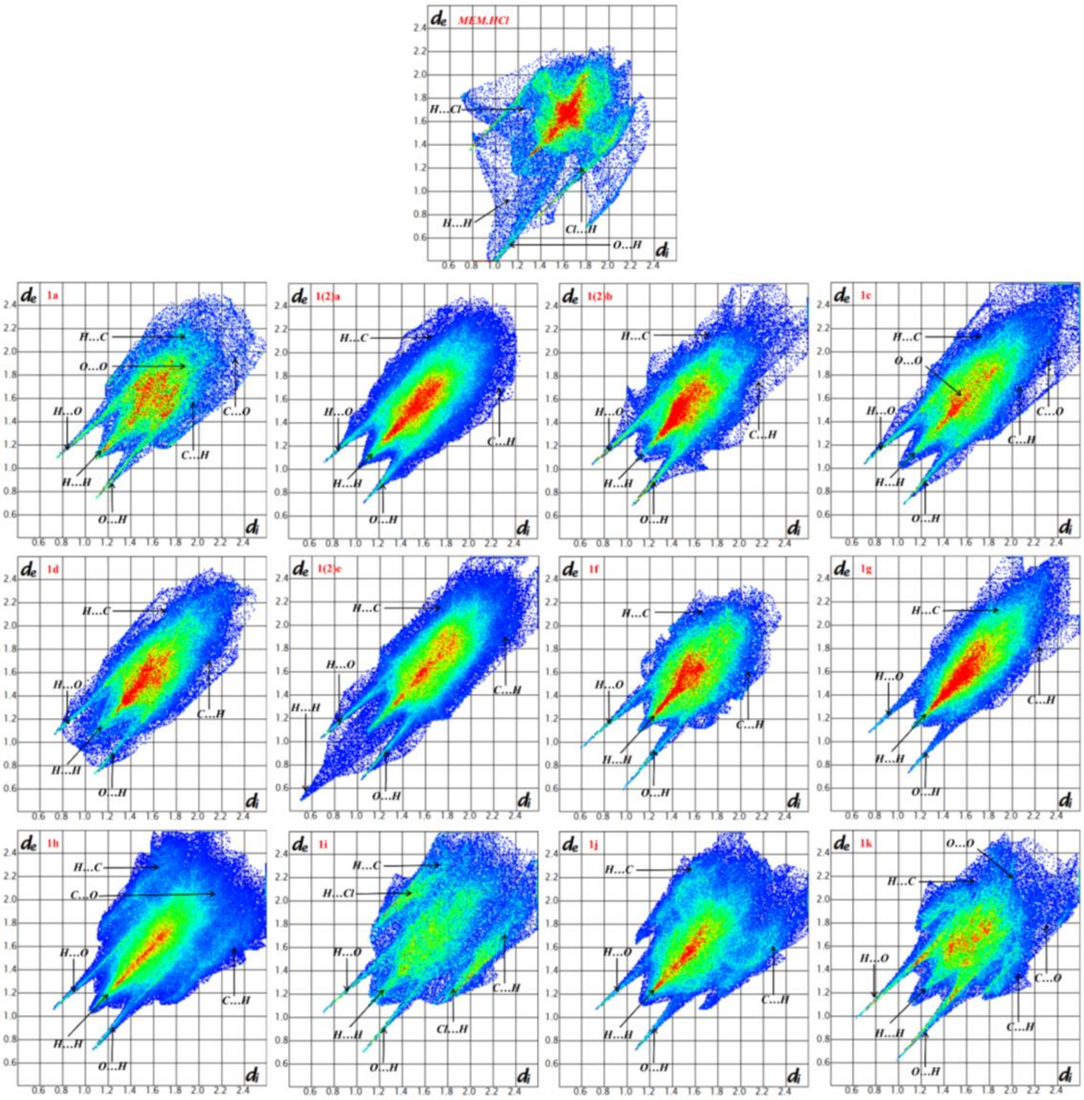

Figure 2.17 Two-Dimensional Hirshfeld fingerprint plots of structures of MEM.HCl and MEM salts (1A-1K). The color in the sequence white-blue-green-red is a summary of the frequencies of each combination of distances d_e and d_i across the Hirshfeld surfaces of a molecule (in increasing order), where d_i is internal distance and d_e external distance from the Hirshfeld surface to the nearest molecule

The 3D Hirshfeld surfaces and 2D fingerprint plots are unique for any crystal structure as well as polymorphs and serve as powerful tools for gaining insight into a crystal structure by giving a quantitative summarization of the nature and type of intermolecular contacts experienced by the molecules in the crystal. In this study, we performed the Hirshfeld studies on the 12 salts as well as on the standard memantine hydrochloride structure to investigate the influence of different acids with varied backbones on overall packing in the crystal. Hirshfeld surfaces provide a three-dimensional picture of close contacts in a crystal, and these contacts can be summarized in a fingerprint plot (Figure 2.17). The contribution of non-covalent interactions in overall packing of the crystals is represented by Figure 2.18. The structure of MEM.HCl shows H…Cl, H…H and O…H interactions, however no O…Cl and C…Cl contacts were found.

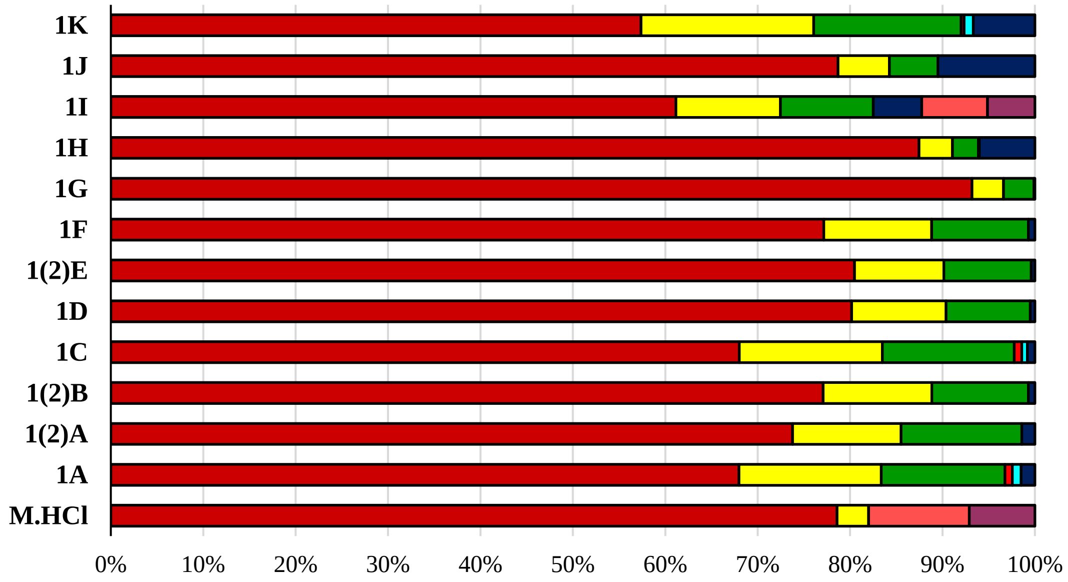

	M.H Cl	1A	1(2)A	1(2)B	1C	1D	1(2)E	1F	1G	1H	1I	1J	1K
H-H	78.6	77.7	72.9	76.7	67.2	80	80	76.7	93.2	84.4	58.4	72	52.5
O-H	3.4	17.6	11.6	11.7	15.3	10.2	9.6	11.6	3.4	3.5	10.8	5.1	17.1
H-O	0	15.3	12.9	10.4	14.1	9.1	9.4	10.4	3.3	2.7	9.6	4.8	14.6
O-O	0	0.9	0	0	0.8	0	0	0	0	0	0	0	0.3
C-O	0	1.1	0	0	0.6	0	0	0	0	0.1	0	0	0.9
C-H	0	1.7	1.4	0.7	0.8	0.5	0.4	0.7	0.1	5.8	5	9.6	6.1
Cl-H	10.9	0	0	0	0	0	0	0	0	0	6.8	0	0
H-Cl	7.1	0	0	0	0	0	0	0	0	0	4.9	0	0

Figure 2.18 Distribution of contacts on the Hirshfeld surfaces sorted according to the types of contacting atoms in MEM.HCl.2H_2O and synthesized MEM salts (1A-1K) (represented in graphical and tabular form)

In **1A**, the N-H…O bonding interactions appear as two sharp spikes, as shown in the figure, having 16.7% of the total interaction contributions, second highest after the H-H interactions which appear in the lower middle region of the graph going till the top, having 61.7% of the total contributions. The sharp features to the lower left of the plot are characteristic of the carboxylic-carboxylic dimer. We also observe a small contribution of O…O (0.9%) and C…O (12%) interactions.

The 2D fingerprint plot of **1C** was similar to **1A**. In **1(2)A, 1(2)B** and **1(2)E**, no significant O…O and C…O interactions were found. However, the crystal structures **1(2)A, 1(2)B, 1(2)E** and **1F** displayed various non-covalent interactions such as H…H, N-H…O, C…H etc. **1G** mostly comprises of the H…H interactions, having 93% contribution, and N-H…O interactions making 3.4% contribution with 0.1% of the C...H interactions. Interactions in **1H** are comparable with those of **1G**. **1H** also follows a similar pattern, except for the fact that it has considerably good amount of C…H interactions (7.2%) and 0.1% C…O interactions in its structure. **1K** follows similar trend, in nearly the same amounts. **1I** contains a halogen atom and thus, other than the usual H…H, O…H, C…H interactions, it also has a good contribution of non-covalent Cl…H (6.8%) and C…Cl (0.5%) interactions. Interestingly, MEM.HCl also has 10.9% Cl…H interactions in its structure, which is comparable with Cl…H interactions of **1I** (6.8%).

Overall, all the fingerprint plots of **1A-1K** displayed significant contribution of van der Waals interactions comparable with those found in MEM.HCl. However, there is a significant increase in the amount of other non-covalent interactions such as O…H, O…O, C…O, C…H which were present in all the crystal structures.

2.4.2.1 Hirshfeld energies

Intermolecular interaction energies of all salts were measured for CE-HF model with HF/3-21G basis set to evaluate the contribution of stabilizing and destabilizing interactions in the crystal structures. We would like to point out that these energy values can be slightly misleading while exploring interactions in charged species, as understandably, salts are expected show higher % electrostatic contributions as compared with % dispersion contribution. (Table 2.3)

Salt	Solubility (mg/mL)	E_ele kJ/mol	E_pol kJ/mol	E_rep kJ/mol	E_dis kJ/mol	E_tot kJ/mol	% Electrostatic contribution	% Dispersion contribution
1A	25.03	-30.4	-3.4	113.9	-17.4	43.5	66.01563	33.98438
1(2)A	12.97	-35	-0.7	100.1	-10.8	35.3	76.77419	23.22581
1(2)B	20.23	-36.1	-5.7	131.3	-18.5	49.3	69.32007	30.67993
1C	19.97	-46.3	-1.5	135.3	-15.2	47.9	75.87302	24.12698
1D	46.1	-43.2	-3.6	134.6	-16.3	48.1	74.16799	25.83201
1(2)E	59.93	-55.5	-7.4	145.8	-14.2	44.1	81.58236	18.41764
1F	5.4	-39.4	-1.1	136.4	-13.5	57.6	75.0	25.0
1G	40.83	-56.5	-5.4	163	-14	58.4	81.55468	18.44532
1H	10.17	-71.9	-9.4	185.6	-12.3	59.9	86.85897	13.14103
1I	7.47	-3.1	-0.5	11.9	-26.2	-17.5	12.08054	87.91946
1J	0.806	-36.7	-25.6	135	-29	29.3	68.23658	31.76342
1K	1.737	-21.9	-6.6	76.7	-11.6	25.2	71.07232	28.92768

Table 2.3 Intermolecular interaction energy values for salts 1A-1K and %electrostatic and %dispersion contribution to the total stabilization

Where $\boldsymbol{E_{tot} = k_{ele}E_{ele} + k_{pol}E_{pol} + k_{dis}E_{dis} + k_{rep}E_{rep}}$

$k_{ele} = 1.019$, $k_{pol} = 0.651$, $k_{dis} = 0.901$, $k_{rep} = 0.811$ for **HF/3-21G model**

E_{ele} = classical electrostatic energy of interaction between monomer charge distributions,

E_{pol} = polarization energy, E_{dis} = dispersion energy and E_{rep} = exchange–repulsion energy

Electrostatic contribution to the total stabilization of a particular molecular pair

$= [(E_{ele} + E_{pol}) / (E_{ele} + E_{pol} + E_{disp})] \times 100\%$.

Dispersion contribution to the total stabilization of a particular molecular pair

$= [(E_{disp}) / (E_{ele} + E_{pol} + E_{disp})] \times 100\%$.

2.4.3 Dissolution studies

Equilibrium concentration (thermodynamic solubility) and maximum concentration (kinetic solubility) are critical in predicting and optimizing performance of a drug.[56–59] Thus, to analyze the efficiency of a drug, it is important to determine its solubility. In this work, the dissolution studies were performed to obtain an idea about the change in physical properties (solubility) of the salts by changing the types of acids used based on their aromatic/aliphatic backbone, length of carbon chain, introducing bulky groups, etc. The solubility studies were carried out in 3 sets (to ensure accuracy of results) and an average value of solubility (mg/mL) was plotted along with the standard deviation for each salt (Figure 2.19).

The solubilities of MEM.HCl and the newly synthesized salts of memantine clearly show a dependency of solubility on the aliphatic chain length as well as the number of memantine molecules involved in the salt formation. In salts **1(2)A** and **1(2)B**, where ratio of memantine to acid is (2:1) as well as in **1C,** the solubility is lower than that of MEM.HCl. Contrary to our expectations that an increase in chain length of acid moiety should decrease the solubility of salt, **1D** and **1(2)E** showed higher solubilities in water despite an increase in carbon chain length of the carboxylic acids involved in salt formation. However, salt **1F** showed the lowest solubility in the aliphatic carboxylic acid based salts, which is quite intuitive. This also suggests that a delicate balance between the hydrophobic and hydrophilic part of carboxylic acid is a prerequisite for controlling the solubility. Pivalic acid based salt, even though contains a bulky trimethyl functionality, displays excellent solubility in water. The strong dependence of solubility of MEM salts on number of carbon atoms in aliphatic chain of carboxylic acid, is quite evident from the experimentally measured solubility values.

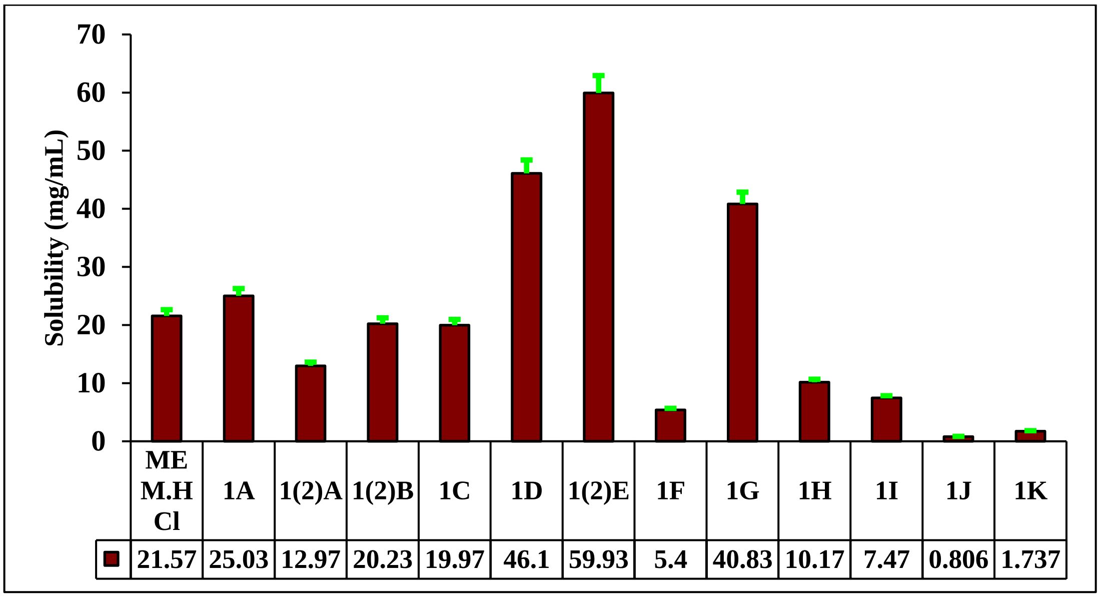

Figure 2.19 Bar graph representing average solubility (in mg/mL) with standard deviation of MEM.HCl and MEM salts in water

To further quantify the role of hydrophobicity of carboxylic acids on solubility of MEM salts in water, a plot of hydrophobicity index of the aliphatic carboxylic acids (**1A-1G**) vs. solubility values (irrespective of the salt being a mono- or di-carboxylate) was prepared (Figure 2.20); where hydrophobicity of an acid was calculated by the following formula-

$$Hydrophobicity = \frac{total\ number\ of\ carbon\ atoms}{number\ of\ -COOH\ groups\ present}$$

The plot displays a gradual increase in solubility with increase in hydrophobicity index with a peak value for salt **1(2)E** and then suddenly decreases the solubility with further increase in hydrophobicity index in salt **1F**. Interestingly, salts **1F** and **1G**, with comparable hydrophobicity indices, display significantly different solubility values, which may be attributed to the presence of bulky group i.e. *tert*-butyl group in **1G** and a long aliphatic chain in **1F**.

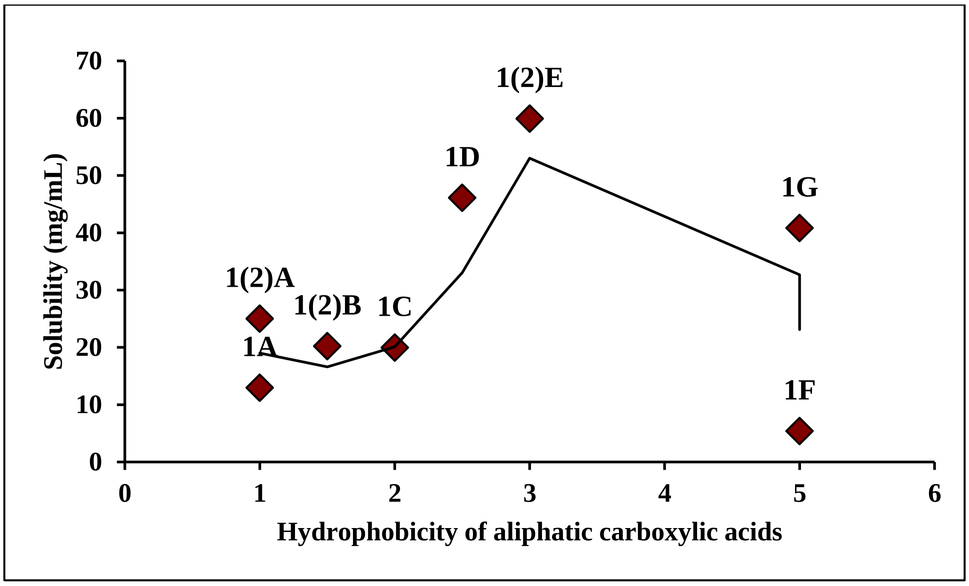

Figure 2.20 Hydrophobicity of aliphatic carboxylic acids vs. solubility

Moreover, the salts of aromatic carboxylic acids were found to be poorly soluble in water and showed strong dependency on number of aromatic rings in the structure and number of carboxylic acid groups attached to the aromatic ring (**1K**). We are now able to show a whole range of solubility of memantine salts in water with a possibility to tune the solubility by suitable choice of carboxylic acids.

While an increase in solubility of a drug is generally more desirable, it comes with its set of disadvantages too, for example, increase in solubility of a drug may lead to higher toxicity and unwanted rapid release of the drug, causing discomfort to the system.

Understandably, due to these difficulties many of the high dosage tablets of various drugs come in CR (controlled release) variants.

Two salts (**1C** and **1(2)E**) out of 12 salts may be considered as promising candidates for developing memantine based formulation as the acids used in these salts belong to GRAS (Generally recognized as safe) class of FDA (Food and Drug Administration) approved compounds.

2.4.4 PXRD studies

To ascertain whether there is a change in the morphology of the salt samples after dissolution, representative DSC and Powder XRD studies were performed on two salts, **1(2)E** and **1G**. These salts were chosen on account of their impressive solubilities in water. Also, the crystal structure of salt **1G** shows an exceptional 3D cluster which might be responsible for its high solubility, and it was essential to validate that the salt does not lose its supramolecular arrangement after dissolution.

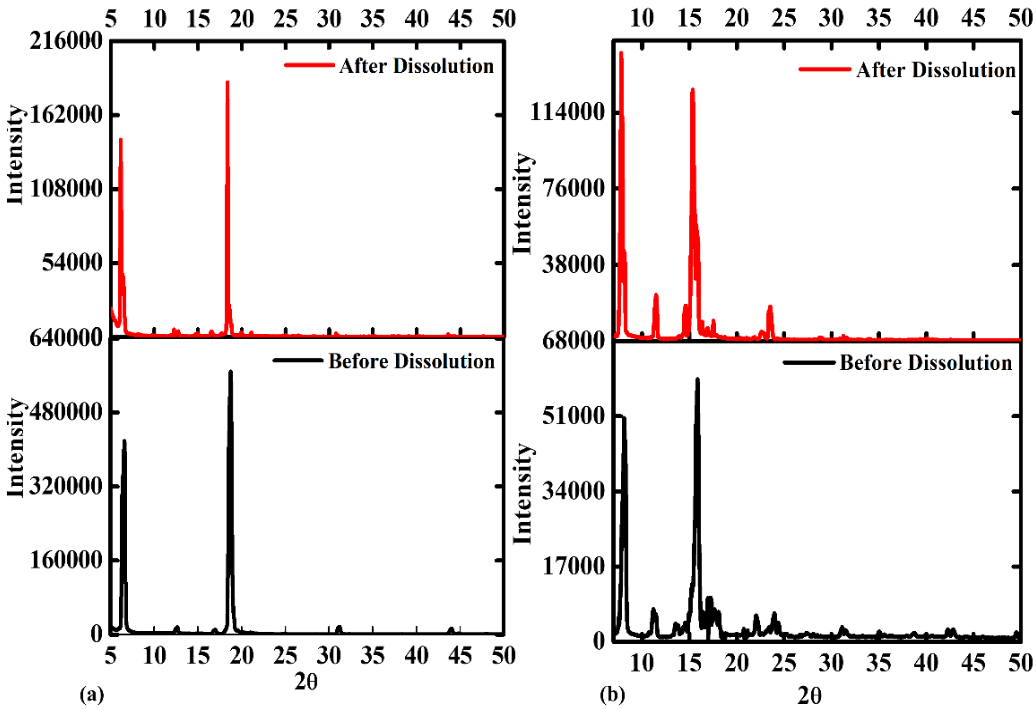

Figure 2.21 Powder XRD patterns of salts (a) 1(2)E and (b) 1G before (B.D.) and after dissolution (A.D.)

We found that powder XRD spectra of both the salts, before and after dissolution to be overlapping with each other (Figure 2.21), which verified that the overall packing did not change after dissolution of the salts.

2.4.5 DSC studies

The DSC studies also confirmed that that the morphology of the salts remained similar before and after dissolution (Figure 2.22). Plots of sample temperature vs. Heat flow (mW) were prepared as shown.

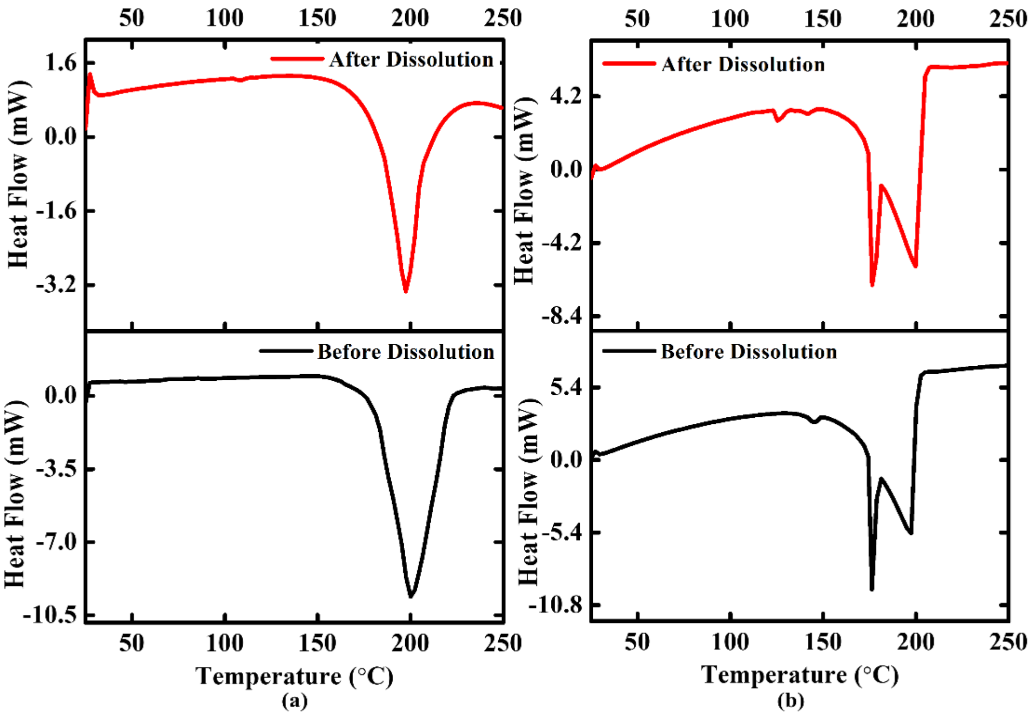

Figure 2.22 DSC patterns of salts (a) 1(2)E and (b) 1G before (B.D.) and after dissolution (A.D.)

Albeit the fact a change in polymorph can change the solubility and the dissolution rate and it is always exciting to establish structure-property relationship in a drug (or drug-like molecule), our quest for finding polymorphs for this set of compounds could not be fulfilled, and we can say that this set of compounds may be more or less, monomorphic in nature. As is known, once an organic molecule is close packed within a crystal, there is a significant barrier to rearrangement.

Also, all the molecular transitions follow first order kinetics, where the phase change requires change in nucleation and growth mechanism, not just a change from one crystal symmetry to another. The simplest way this could have been achieved was by either desolvating the crystal structure or by allowing the nucleation to occur at a higher temperature, both of which could result in a higher symmetric, high-energy form, stabilized kinetically. The former method didn't work out quite well, as shown in the DSC and PXRD studies, the latter one, too, yielded similar results as we happened to obtain the same crystal symmetries when we carried out the crystallization at higher (and even lower) temperatures. Statistically, the CSD (Cambridge Structural Database) reports that there are only 5% of the molecules having polymorphic crystal structures[60] and this study highlights the importance of growing diffraction quality single crystals rather than the occurrence of polymorphism.

Also, the very process of crystallization is highly complex and specific to every molecule, making it even more complicated to go looking for different crystal symmetries for a set of bulky compounds like this!

2.5 CONCLUSIONS

In this work, a series of 12 salts of memantine were designed and synthesized using combinatorial library approach. A variety of acids (aliphatic and aromatic) were utilized to critically examine the nature and diversity of various supramolecular synthons observed in their crystal structures. It was found that most of the structures displayed supramolecular synthons with graph set representation $R_4^2(8)$ and $R_4^4(12)$ which are very common in PAM and PAD salts. Also, the dissolution behavior of PAD salts in this series showed a gradual increase in solubility with increase in carbon chain length up to 6 carbons (**1(2)A** to **1(2)E**), and the PAM salt **1F** with longer aliphatic carbon chain length demonstrated very less solubility in water suggesting the dependence of solubility on carbon chain length of the carboxylate ion.

The unique supramolecular assembly shown by compounds **1G** and **1H**, has well-defined voids very similar to the parent compound MEM.HCl.H_2O, which is suggestive of the fact that steric hindrance (such as presence of *tert*-butyl group in pivalic acid salt **1G** and a benzene ring in **1H**) may force a commonly occurring PAM or PAD hydrogen bonded network to converge to a different, more confined supramolecular synthon. Interestingly, salt **1G** displayed better a solubility behavior as compared to MEM.HCl suggesting that the zero-dimensional (0D) molecular cluster with well-defined void may be the driving force for better solubility. Also, the lower solubility of **1H** despite having well-defined void in the crystal structure may be attributed to the presence of aromatic ring in the carboxylate ion, as all the aromatic ring containing salts have necessarily shown poor solubility in water.

Moreover, a comparison of Hirshfeld studies with respect to MEM.HCl salt revealed the presence of multiple weak interactions in all the newly synthesized MEM salts. However, the amount of H…H interactions was more or less similar except for two salts (**1(2)E** and **1G**), where the value drastically increases. These salts also showed decent solubility behavior and a strong dependence on van der Waals interactions as their C-H…H-C contribution is found to be highest in the Hirshfeld studies.

As far as drug performance is concerned, it is believed that an increase in solubility of the drug can be beneficial for its fast release action. However, a decrease in solubility of a drug is also crucial for its controlled release variants, which could be more beneficial to patients suffering from various forms of dementia. During the course of this study, we expected that the organic acid salts of memantine will be more useful for the latter purpose on account of their lower solubility, but it turns out that the hydrochloride salt can also be replaced by some organic salt with almost comparable solubility values and we can consider this study as a promising one for development of memantine formulations in future, as similar principles are involved in the task of comprehensive co-crystal screening as those in pure compounds.

REFERENCES

1. Aakeröy, C. B. & Salmon, D. J. Building co-crystals with molecular sense and supramolecular sensibility. *CrystEngComm* **7**, 439–448 (2005).
2. Shan, N., Perry, M. L., Weyna, D. R. & Zaworotko, M. J. Impact of pharmaceutical cocrystals : the effects on drug pharmacokinetics. *Expert Opin. Drug Metab. Toxicol.* **10**, 1255–1271 (2014).
3. Gopi, S. P., Banik, M. & Desiraju, G. R. New Cocrystals of Hydrochlorothiazide: Optimizing Solubility and Membrane Diffusivity. *Cryst. Growth Des.* **17**, 308–316 (2017).
4. Aitipamula, S., Banerjee, R., Bansal, A. K., Biradha, K., Cheney, M. L., Choudhury, A. R., Desiraju, G. R., Dikundwar, A. G., Dubey, R., Duggirala, N., Ghogale, P. P., Ghosh, S., Goswami, P. K., Goud, N. R., Jetti, R. R. K. R., Karpinski, P., Kaushik, P., Kumar, D., Kumar, V., *et al.* Polymorphs, salts, and cocrystals: What's in a name? *Cryst. Growth Des.* **12**, 2147–2152 (2012).
5. Blagden, N., de Matas, M., Gavan, P. T. & York, P. Crystal engineering of active pharmaceutical ingredients to improve solubility and dissolution rates. *Adv. Drug Deliv. Rev.* **59**, 617–630 (2007).
6. Mapp, L. K., Coles, S. J. & Aitipamula, S. Design of Cocrystals for Molecules with Limited Hydrogen Bonding Functionalities: Propyphenazone as a Model System. *Cryst. Growth Des.* **17**, 163–174 (2017).
7. Etter, M. C. Encoding and Decoding Hydrogen-Bond Patterns of Organic Compounds. *Acc. Chem. Res.* **23**, 120–126 (1990).
8. Fábián, L. Cambridge structural database analysis of molecular complementarity in cocrystals. *Cryst. Growth Des.* **9**, 1436–1443 (2009).
9. Wood, P. A., Feeder, N., Furlow, M., Galek, P. T. A., Groom, C. R. & Pidcock, E. Knowledge-based approaches to co-crystal design. *CrystEngComm* **16**, 5839–5848 (2014).
10. Babu, N. J. & Nangia, A. Solubility Advantage of Amorphous Drugs and Pharmaceutical Cocrystals. *Cryst. Growth Des.* **11**, 2662–2679 (2011).
11. Tumanov, N. A., Myz, S. A., Shakhtshneider, T. P. & Boldyreva, E. V. Are meloxicam dimers really the structure-forming units in the ' meloxicam – carboxylic acid ' co-crystals family? Relation between crystal structures and dissolution behaviour. *CrystEngComm* **14**, 305–313 (2012).
12. Tao, Q., Chen, J. M., Ma, L. & Lu, T. B. Phenazopyridine cocrystal and salts that exhibit enhanced solubility and stability. *Cryst. Growth Des.* **12**, 3144–3152 (2012).
13. Childs, S. L., Chyall, L. J., Dunlap, J. T., Smolenskaya, V. N., Stahly, B. C., Stahly, G. P., Kent, A. V & Lafayette, W. Crystal Engineering Approach To Forming Cocrystals of Amine Hydrochlorides with Organic Acids. Molecular Complexes of Fluoxetine Hydrochloride with Benzoic, Succinic, and Fumaric Acids. *J. Am. Chem. Soc.* **126**, 13335–13342 (2004).
14. Smith, A. J., Kavuru, P., Wojtas, L., Zaworotko, M. J. & Shytle, R. D. Cocrystals of quercetin with improved solubility and oral bioavailability. *Mol. Pharm.* **8**,

1867–1876 (2011).
15. Cherukuvada, S., Babu, N. J. & Nangia, A. Nitrofurantoin–p-Aminobenzoic Acid Cocrystal: Hydration Stability and Dissolution Rate Studies. *J. Pharm. Sci.* **100**, 3233–3244 (2011).
16. Trask, A. V. & Jones, W. Crystal engineering of organic cocrystals by the solid-state grinding approach. *Top. Curr. Chem.* 254, 41–70 (2005).
17. Karki, S., Friščić, T., Fabián, L., Laity, P. R., Day, G. M. & Jones, W. Improving mechanical properties of crystalline solids by cocrystal formation: new compressible forms of paracetamol. *Adv. Mater.* **21**, 3905–3909 (2009).
18. Reddy, L. S., Bethune, S. J., Kampf, J. W. & Rodríguez-Hornedo, N. Cocrystals and salts of gabapentin: pH dependent cocrystal stability and solubility. *Cryst. Growth Des.* **9**, 378–385 (2009).
19. Faroque, M. U. & Noureen, S. Electrostatic properties of the pyrimethamine – 2 , 4-dihydroxybenzoic acid cocrystal in methanol studied using transferred electron-density parameters. *Acta Crystallogr. C Struct. Chem.* **C78**, 100–107 (2018).
20. Rehman, A., Delori, A., Hughes, D. S., Jones, W. & Mate-, C. Structural studies of crystalline forms of triamterene with carboxylic acid, GRAS and API molecules. *IUCrJ* **5**, 309–324 (2018).
21. Nijhawan, M., Santhosh, A., Babu, P. R. S. & Subrahmanyam, C. V. S. Solid state manipulation of lornoxicam for cocrystals – physicochemical characterization. *Drug Dev. Ind. Pharm.* **40**, 1163–1172 (2013).
22. Suresh, K. & Nangia, A. Lornoxicam Salts: Crystal Structures, Conformations, and Solubility. *Cryst. Growth Des.* **14**, 2945–2953 (2014).
23. Weyna, D. R., Cheney, M. L., Shan, N., Hanna, M., Wojtas, L. & Zaworotko, M. J. Crystal engineering of multiple-component organic solids : Pharmaceutical cocrystals of tadalafil with persistent hydrogen bonding motifs. *CrystEngComm* **14**, 2377–2380 (2012).
24. Chadha, R., Singh, P., Khullar, S. & Mandal, S. K. Ciprofloxacin Hippurate Salt: Crystallization Tactics, Structural Aspects, and Biopharmaceutical Performance. *Cryst. Growth Des.* **16**, 4960–4967 (2016).
25. Weyna, D. R., Cheney, M. L., Shan, N., Hanna, M., Zaworotko, M. J., Sava, V., Song, S. & Sanchez-ramos, J. R. Improving Solubility and Pharmacokinetics of Meloxicam via Multiple-Component Crystal Formation. *Mol. Pharm.* **9**, 2094–2102 (2012).
26. Chen, Y., Li, L., Yao, J., Chen, J. & Lu, T. Improving the Solubility and Bioavailability of Apixaban via Apixaban − Oxalic Acid Cocrystal. *Cryst. Growth Des.* **16**, 2923–2930 (2016).
27. Hiendrawan, S., Veriansyah, B., Widjojokusumo, E., Soewandhi, S. N., Wikarsa, S. & Tjandrawinata, R. R. Physicochemical and mechanical properties of paracetamol cocrystal with 5-nitroisophthalic acid. *Int. J. Pharm.* **497**, 106–113 (2015).
28. Karimi-Jafari, M., Padrela, L., Walker, G. M. & Croker, D. M. Creating cocrystals: A review of pharmaceutical cocrystal preparation routes and applications. *Cryst. Growth Des.* **18**, 6370–6387 (2018).

29. Thipparaboina, R., Kumar, D., Chavan, R. B. & Shastri, N. R. Multidrug co-crystals: Towards the development of effective therapeutic hybrids. *Drug Discov. Today* **21**, 481–490 (2016).
30. Kaur, R., Cavanagh, K. L., Rodríguez-Hornedo, N. & Matzger, A. J. Multidrug cocrystal of anticonvulsants: Influence of strong intermolecular interactions on physiochemical properties. *Cryst. Growth Des.* **17**, 5012–5016 (2017).
31. Aitipamula, S., Chow, P. S. & Tan, R. B. H. Trimorphs of a pharmaceutical cocrystal involving two active pharmaceutical ingredients: Potential relevance to combination drugs. *CrystEngComm* **11**, 1823–1827 (2009).
32. Cheney, M. L., Weyna, D. R., Shan, N., Hanna, M., Wojtas, L. & Zaworotko, M. J. Coformer Selection in Pharmaceutical Cocrystal Development: a Case Study of a Meloxicam Aspirin Cocrystal That Exhibits Enhanced Solubility and Pharmacokinetics. *J. Pharm. Sci.* **100**, 2172–2181 (2011).
33. Chadha, R., Saini, A., Arora, P., Jain, D. S., Dasgupta, A. & Guru Row, T. N. Multicomponent solids of lamotrigine with some selected coformers and their characterization by thermoanalytical, spectroscopic and X-ray diffraction methods. *CrystEngComm* **13**, 6271–6284 (2011).
34. Luszczki, J. J., Czuczwar, M., Kis, J., Krysa, J., Pasztelan, I., Swiader, M. & Czuczwar, S. J. Interactions of lamotrigine with topiramate and first-generation antiepileptic drugs in the maximal electroshock test in mice: An isobolographic analysis. *Epilepsia* **44**, 1003–1013 (2003).
35. Johnson, J. W. & Kotermanski, S. E. Mechanism of action of memantine. *Curr. Opin. Pharmacol.* **6**, 61–67 (2006).
36. Rammes, G., Danysz, W. & Parsons, C. G. Pharmacodynamics of Memantine : An Update. *Curr. Neuropharmacol.* **6**, 55–78 (2008).
37. Witt, A., Macdonald, N. & Kirkpatrick, P. Memantine hydrochloride. *Nat. Rev. Drug Discov.* **3**, 109–110 (2004).
38. Mittapelly, N., Rachumallu, R., Pandey, G., Sharma, S. & Arya, A. Investigation of salt formation between memantine and pamoic acid: Its exploitation in nanocrystalline form as long acting injection. *Eur. J. Pharm. Biopharm.* **101**, 62–71 (2016).
39. Lou, W. J., Hu, X. R. & Gu, J. M. Memantinium chloride 0.1-hydrate. *Acta Crystallogr. Sect. E Struct. Reports Online* **E65**, 2191 (2009).
40. Mohamed, S., Karothu, D. P. & Naumov, P. Using crystal structure prediction to rationalize the hydration propensities of substituted adamantane hydrochloride salts. *Acta Crystallogr. Sect. B Struct. Sci. Cryst. Eng. Mater.* **B72**, 551–561 (2016).
41. Ballabh, A., Adalder, T. K. & Dastidar, P. Structures and gelation properties of a series of salts derived from an alicyclic dicarboxylic acid and n-alkyl primary amines. *Cryst. Growth Des.* **8**, 4144–4149 (2008).
42. Das, U. K. & Dastidar, P. Extending primary ammonium dicarboxylate (PAD) to diprimary ammonium dicarboxylate (DPAD) synthon and its implication in supramolecular gelation. *Cryst. Growth Des.* **13**, 4559–4570 (2013).
43. Buschmann, H. H., Tesson, N., Farran, J. & RAFECAS, L. Patent EP2257517 A1

- Salts of memantine and cox-inhibitors and their crystal form in the treatment of pain. at (2010).

44. Lemmerer, A., Bernstein, J. & Spackman, M. A. Supramolecular polymorphism of the 1:1 molecular salt (adamantane-1-carboxylate-3,5,7-tricarboxylic acid)·(hexamethylenetetraminium). A ‘failed’ crystal engineering attempt. *Chem. Commun.* **48**, 1883–1885 (2012).
45. Lemmerer, A. Steric effects in hydrogen bonded columns of salts of benzoic acid and 1-adamantanecarboxylic acid with the cyclic amines $C_nH_{2n+1}NH_2$, n = 5, 6, 7, 8 and 12. *CrystEngComm* **13**, 2849–2862 (2011).
46. Kawahata, M., Matsuura, M., Tominaga, M., Katagiri, K. & Yamaguchi, K. Hydrogen-bonded structures from adamantane-based catechols. *J. Mol. Struct.* **1164**, 116–122 (2018).
47. Tominaga, M., Masu, H. & Azumaya, I. Hydrogen-Bonding Networks of Adamantane-Based Bisphenol Molecules : Toward the Preparation of Molecular Crystals with Channels. *Cryst. Growth Des.* **11**, 542–546 (2011).
48. Manjare, Y. & Pedireddi, V. R. Co-Crystals of 1,3-Adamantanedicarboxylic Acid with N-Oxide and Aza Compounds. *Cryst. Growth Des.* **11**, 5079–5086 (2011).
49. Price, S. L. Predicting crystal structures of organic compounds. *Chem. Soc. Rev.* **43**, 2098–2111 (2014).
50. Dolomanov, O. V., Bourhis, L. J., Gildea, R. J., Howard, J. A. K. & Puschmann, H. OLEX2: A complete structure solution, refinement and analysis program. *J. Appl. Crystallogr.* **42**, 339–341 (2009).
51. Sheldrick, G. M. A short history of SHELX. *Acta Crystallogr. Sect. A Found. Crystallogr.* **64**, 112–122 (2008).
52. Spackman, M. A. & Mckinnon, J. J. Fingerprinting intermolecular interactions in molecular crystals. *CrystEngComm* **4**, 378–392 (2002).
53. Spackman, M. A. & Byrom, P. G. A novel definition of a molecule in a crystal. *Chem. Phys. Lett.* **267**, 215–220 (1997).
54. McKinnon, J. J., Mitchell, A. S. & Spackman, M. A. Hirshfeld surfaces: A new tool for visualising and exploring molecular crystals. *Chem. Eur. J.* **4**, 2136–2141 (1998).
55. Spackman, M. A. & Jayatilaka, D. Hirshfeld surface analysis. *CrystEngComm* **11**, 19–32 (2009).
56. Luo, Y. & Sun, B. Pharmaceutical Co-Crystals of Pyrazinecarboxamide (PZA) with Various Carboxylic Acids: Crystallography, Hirshfeld Surfaces, and Dissolution Study. *Cryst. Growth Des.* **13**, 2098–2106 (2013).
57. Aitipamula, S., Chow, P. S. & Tan, R. B. H. Crystal engineering of tegafur cocrystals: Structural analysis and physicochemical properties. *Cryst. Growth Des.* **14**, 6557–6569 (2014).
58. Langer, R. Drug delivery and targeting. *Nature* vol. **392**, 5–10 (1998).
59. Andre, V., Duarte, M. T., Braga, D. & Grepioni, F. Polymorphic Ammonium Salts of the Antibiotic 4-Aminosalicylic Acid. *Cryst. Growth Des.* **12**, 3082–3090 (2012).
60. Allen, F. H. & Taylor, R. Research applications of the Cambridge Structural Database (CSD). *Chem. Soc. Rev.* **33**, 463–475 (2004).

*SUPPLEMENTARY DATA

Crystallographic Data for salts 1A-1K.

Table S2.1 Crystallographic Data and Structure refinement parameters for 1A-1K.

	1A	1(2)A	1(2)B	1C
Empirical Formula	$C_{14}H_{23}NO_4$	$C_{78}H_{136}N_6O_{14}$	$C_{27}H_{50}N_2O_6$	$C_{32}H_{54}N_2O_8$
Formula weight	269.33	1381.92	498.69	594.77
Temperature/K	293	293	293	293
Crystal system	monoclinic	triclinic	monoclinic	monoclinic
Space group	$P2_1/c$	*P-1*	$P2_1/c$	$P2_1/c$
a/Å	14.653(3)	13.8479(8)	7.9175(3)	14.1625(19)
b/Å	6.8183(10)	15.3401(10)	29.0478(16)	30.102(4)
c/Å	15.269(4)	18.6581(9)	12.2374(7)	8.3719(11)
α/°	90	101.607(5)	90	90
β/°	107.97(3)	91.279(4)	94.084(4)	106.161(14)
γ/°	90	93.140(5)	90	90
Volume/Å^3	1451.1(6)	3874.4(4)	2807.3(2)	3428.1(8)
Z	4	2	4	4
ρ_{calc}g/cm^3	1.233	1.185	1.180	1.152
μ/mm^{-1}	0.090	0.080	0.082	0.082
F(000)	584.0	1516.0	1096.0	1296.0
Crystal size/mm^3	0.12 × 0.06 × 0.04	0.05 × 0.05 × 0.01	0.06 × 0.03 × 0.02	0.05 × 0.03 × 0.02
2Θ range for data collection/°	6.602 to 52.73	6.292 to 52.74	6.104 to 52.74	5.79 to 52.744
Index ranges	$-17 \le h \le 18, -8 \le k \le 7, -19 \le l \le 15$	$-17 \le h \le 17, -16 \le k \le 19, -22 \le l \le 23$	$-9 \le h \le 9, -36 \le k \le 36, -15 \le l \le 15$	$-17 \le h \le 17, -37 \le k \le 37, -10 \le l \le 10$
Reflections collected	5993	35739	29248	35898
Independent reflections	2954 [R_{int} = 0.0269, R_{sigma} = 0.0437]	15798 [R_{int} = 0.0585, R_{sigma} = 0.0847]	5712 [R_{int} = 0.0405, R_{sigma} = 0.0296]	6971 [R_{int} = 0.1732, R_{sigma} = 0.1338]
Data/restraints/parameters	2954/0/176	15798/0/907	5712/0/328	6971/0/411
Goodness-of-fit on F^2	1.021	1.105	1.049	0.950
Final R indexes [I>=2σ (I)]	R_1 = 0.0448, wR_2 = 0.1024	R_1 = 0.0804, wR_2 = 0.2062	R1 = 0.0618, wR2 = 0.1304	R_1 = 0.0885, wR_2 = 0.1979
Final R indexes [all data]	R_1 = 0.0742, wR_2 = 0.1167	R_1 = 0.1366, wR_2 = 0.2432	R1 = 0.0835, wR2 = 0.1429	R_1 = 0.2231, wR_2 = 0.2811
Largest diff. peak/hole / e Å^{-3}	0.18/-0.15	0.29/-0.28	0.29/-0.24	0.30/-0.23
CCDC No.	1569275	1837210	1866047	1858608

	1D	1(2)E	1F	1G
Empirical Formula	$C_{29}H_{51}N_2O_4$	$C_{30}H_{52}N_2O_4$	$C_{22}H_{39}NO_4$	$C_{34}H_{62}N_2O_4$
Formula weight	491.71	504.73	381.54	562.85
Temperature/K	293	293	293	298
Crystal system	monoclinic	monoclinic	monoclinic	monoclinic
Space group	$P2_1/c$	$P2_1/c$	$P2_1$	$I2/a$
a/Å	15.292(3)	8.9613(10)	12.5085(16)	23.7014(18)
b/Å	21.781(9)	11.9787(12)	7.5502(8)	13.3523(7)
c/Å	8.908(2)	29.373(3)	13.4237(18)	23.010(2)
α/°	90	90	90	90
β/°	104.829(19)	98.395(11)	117.649(17)	94.789(8)
γ/°	90	90	90	90
Volume/Å^3	2868.0(14)	3119.3(6)	1123.0(3)	7256.4(9)
Z	4	4	2	8
ρ_{calc}g/cm^3	1.139	1.075	1.128	1.030
μ/mm^{-1}	0.075	0.070	0.076	0.066
F(000)	1084.0	1112.0	420.0	2496.0
Crystal size/mm^3	0.05 × 0.03 × 0.01	0.12 × 0.05 × 0.03	0.94 × 0.217 × 0.164	0.04 × 0.04 × 0.03
2Θ range for data collection/°	6.552 to 49.42	6.044 to 52.742	6.392 to 52.744	6.824 to 52.74
Index ranges	$-17 \le h \le 16$, $-20 \le k \le 14$, $-8 \le l \le 10$	$-11 \le h \le 11$, $-14 \le k \le 14$, $-36 \le l \le 36$	$-15 \le h \le 15$, $-9 \le k \le 9$, $-16 \le l \le 16$	$-29 \le h \le 26$, $-10 \le k \le 16$, $-15 \le l \le 28$
Reflections collected	5699	30375	11717	12360
Independent reflections	3424 [R_{int} = 0.0579, R_{sigma} = 0.0618]	6105 [R_{int} = 0.1231, R_{sigma} = 0.0931]	4525 [R_{int} = 0.0380, R_{sigma} = 0.0638]	7128 [R_{int} = 0.0379, R_{sigma} = 0.0677]
Data/restraints/parameters	3424/0/326	6105/0/331	4525/1/251	7128/0/373
Goodness-of-fit on F^2	1.146	0.989	0.897	1.008
Final R indexes [I>=2σ (I)]	R_1 = 0.1024, wR_2 = 0.2855	R_1 = 0.0945, wR_2 = 0.2256	R_1 = 0.0494, wR_2 = 0.0984	R_1 = 0.1053, wR_2 = 0.2658
Final R indexes [all data]	R_1 = 0.1291, wR_2 = 0.3113	R_1 = 0.1937, wR_2 = 0.2894	R_1 = 0.0834, wR_2 = 0.1078	R_1 = 0.2255, wR_2 = 0.3624
Largest diff. peak/hole / e Å^{-3}	0.46/-0.31	0.31/-0.23	0.16/-0.16	0.40/-0.20
CCDC No.	1561184	1858609	1560003	1876954

	1H	1I	1J	1K
Empirical Formula	$C_{80}H_{115}N_4O_8$	$C_{19}H_{26}ClNO_2$	$C_{54}H_{62}N_2O_4$	$C_{22}H_{33}NO_8$
Formula weight	1261.76	335.86	803.05	439.49
Temperature/K	293	293	293	293
Crystal system	triclinic	monoclinic	triclinic	monoclinic
Space group	*P-1*	$P2_1/c$	*P-1*	$P2_1/n$
a/Å	15.5569(11)	14.3827(19)	10.8809(7)	12.6174(7)
b/Å	15.8750(15)	6.6848(6)	15.1512(10)	11.9470(7)
c/Å	16.9242(10)	20.716(2)	15.1598(11)	15.0863(8)
α/°	92.407(6)	90	64.825(7)	90
β/°	97.341(5)	107.498(13)	83.155(6)	92.038(5)
γ/°	113.927(8)	90	79.424(6)	90
Volume/Å^3	3768.8(5)	1899.6(4)	2221.0(3)	2272.7(2)
Z	2	4	2	4
ρ_{calc}g/cm^3	1.112	1.174	1.201	1.284
μ/mm^{-1}	0.071	0.210	0.075	0.097
F(000)	1376.0	720.0	864.0	944.0
Crystal size/mm^3	0.07 × 0.04 × 0.02	0.04 × 0.03 × 0.02	0.06 × 0.03 × 0.02	0.07 × 0.04 × 0.02
2Θ range for data collection/°	5.928 to 54.204	6.434 to 52.744	6.624 to 52.744	6.39 to 52.74
Index ranges	$-19 \le h \le 19$, $-20 \le k \le 20$, $-21 \le l \le 21$	$-16 \le h \le 17$, $-8 \le k \le 8$, $-24 \le l \le 25$	$-13 \le h \le 9$, $-18 \le k \le 18$, $-18 \le l \le 18$	$-14 \le h \le 15$, $-7 \le k \le 14$, $-16 \le l \le 18$
Reflections collected	79451	9391	16967	8890
Independent reflections	16547 [R_{int} = 0.2362, R_{sigma} = 0.2466]	3872 [R_{int} = 0.0563, R_{sigma} = 0.0768]	9028 [R_{int} = 0.0344, R_{sigma} = 0.0769]	4630 [R_{int} = 0.0212, R_{sigma} = 0.0363]
Data/restraints/parameters	16547/0/849	3872/0/211	9028/0/547	4630/0/304
Goodness-of-fit on F^2	0.934	0.997	0.995	1.043
Final R indexes [I>=2σ (I)]	R_1 = 0.0977, wR_2 = 0.2044	R_1 = 0.0943, wR_2 = 0.2861	R_1 = 0.0551, wR_2 = 0.1092	R_1 = 0.0732, wR_2 = 0.2185
Final R indexes [all data]	R_1 = 0.3289, wR_2 = 0.3160	R_1 = 0.1684, wR_2 = 0.3581	R_1 = 0.1099, wR_2 = 0.1352	R_1 = 0.1010, wR_2 = 0.2440
Largest diff. peak/hole / e Å^{-3}	0.72/-0.23	0.64/-0.53	0.16/-0.18	1.60/-0.41
CCDC No.	1876955	1837561	1561187	1561186

H-bonds for salts 1A-1K

Table S2.2 Hydrogen bond parameters for salts 1A-1K

D	H	A	d(D-H) /Å	d(H-A) /Å	d(D-A)/Å	D-H-A /°	Symmetry operation for A
Salt 1A							
O3	H3	O2	0.82	2.16	2.6410(16)	117.3	+X, +Y, +Z
O3	H3	O2	0.82	2.07	2.7774(17)	143.8	1-X, 2-Y, 1-Z
N1	H1A	O1	0.89	1.96	2.8394(17)	172.0	1-X, -1/2+Y, 1/2-Z
N1	H1B	O2	0.89	2.02	2.8942(17)	169.1	+X, -1+Y, +Z
N1	H1C	O1	0.89	1.98	2.8442(17)	163.4	+X, +Y, +Z
Salt 1(2)A							
N5	H5A	O13	0.89	1.88	2.770(3)	176.0	+X, +Y, +Z
N5	H5B	O9	0.89	1.95	2.801(3)	160.6	+X, +Y, +Z
N5	H5C	O10	0.89	1.88	2.750(3)	164.4	1-X, 1-Y, 1-Z
N1	H1A	O1	0.89	2.16	2.900(3)	140.5	+X, +Y, +Z
N1	H1A	O4	0.89	2.16	2.923(3)	143.5	+X, +Y, +Z
N1	H1B	O1	0.89	2.01	2.885(3)	168.1	1-X, -Y, -Z
N1	H1C	O8	0.89	1.96	2.839(3)	168.3	1-X, 1-Y, -Z
N4	H4A	O2	0.89	1.95	2.820(3)	164.5	+X, 1+Y, +Z
N4	H4B	O14	0.89	1.92	2.805(3)	174.8	+X, +Y, +Z
N4	H4C	O7	0.89	1.92	2.786(3)	164.3	+X, +Y, +Z
N2	H2A	O8	0.89	2.21	2.976(3)	143.5	+X, +Y, +Z
N2	H2A	O5	0.89	2.16	2.916(3)	141.8	+X, +Y, +Z
N2	H2B	O5	0.89	2.00	2.880(3)	172.0	1-X, 1-Y, -Z
N2	H2C	O4	0.89	1.97	2.843(3)	165.8	1-X, 1-Y, -Z
N6	H6A	O2	0.89	1.94	2.794(3)	161.5	1-X, 1-Y, 1-Z
N6	H6B	O3	0.89	2.21	2.817(3)	125.2	1-X, 1-Y, 1-Z
N6	H6C	O10	0.89	2.32	2.879(3)	121.1	+X, +Y, +Z
N6	H6C	O11	0.89	2.00	2.858(3)	161.9	+X, +Y, +Z
N3	H3A	O6	0.89	1.96	2.784(3)	153.5	1+X, +Y, +Z
N3	H3B	O9	0.89	2.09	2.905(3)	151.5	1+X, +Y, +Z
N3	H3B	O12	0.89	2.22	2.892(3)	131.8	1+X, +Y, +Z
N3	H3C	O7	0.89	2.12	2.801(3)	132.3	1+X, +Y, +Z
C21	H21B	O2	0.97	2.63	3.536(3)	156.4	1-X, -Y, -Z
C25	H25A	O4	0.97	2.63	3.350(3)	131.0	+X, +Y, +Z
C47	H47A	O9	0.97	2.65	3.384(3)	132.6	+X, +Y, +Z
C47	H47B	O6	0.97	2.64	3.500(3)	148.3	+X, +Y, +Z
C11	H11A	O9	0.97	2.58	3.315(3)	132.6	1+X, +Y, +Z
C55	H55A	O11	0.97	2.63	3.475(3)	145.8	1-X, 2-Y, 1-Z
C68	H68B	O11	0.97	2.55	3.300(3)	133.9	+X, +Y, +Z
C37	H37A	O8	0.97	2.54	3.284(3)	133.9	+X, +Y, +Z
C37	H37B	O4	0.97	2.64	3.380(3)	133.9	1-X, 1-Y, -Z
Salt 1(2)B							
N2	H2A	O1	0.89	1.94	2.779(2)	157.0	+X, +Y, +Z
N2	H2B	O4	0.89	1.99	2.869(2)	168.1	-X, 1-Y, 1-Z
N2	H2C	O5	0.89	1.91	2.801(2)	174.1	+X, +Y, +Z
N1	H1A	O3	0.89	1.87	2.754(2)	173.2	+X, +Y, +Z
N1	H1B	O2	0.89	1.91	2.796(2)	176.4	-X, 1-Y, 2-Z
N1	H1C	O2	0.89	2.01	2.854(2)	158.3	-1+X, +Y, +Z
Salt 1C							
O5	H5A	O3	0.98(7)	1.58(7)	2.522(4)	162(6)	+X, 1/2-Y, 1/2+Z

O7	H7	O1	0.99(8)	1.55(8)	2.515(4)	165(7)	-1+X, +Y, +Z
N2	H2A	O6	0.93(4)	1.99(4)	2.867(5)	157(3)	+X, +Y, +Z
N2	H2B	O2	1.00(4)	1.75(4)	2.753(4)	176(3)	+X, +Y, +Z
N2	H2C	O3	0.84(4)	1.96(4)	2.792(5)	170(4)	+X, +Y, 1+Z
C14	H14B	O6	0.97	2.59	3.350(5)	135.0	+X, +Y, +Z
N1	H1A	O8	0.84(4)	2.10(4)	2.898(5)	157(4)	1+X, 1/2-Y, 1/2+Z
N1	H1B	O4	0.88(4)	1.92(4)	2.787(4)	170(4)	+X, +Y, 1+Z
N1	H1C	O1	1.01(4)	1.77(4)	2.751(5)	165(4)	+X, +Y, +Z
N1	H1C	O2	1.01(4)	2.44(4)	3.206(5)	133(3)	+X, +Y, +Z
C6	H6A	O8	0.97	2.49	3.267(6)	136.6	1+X, 1/2-Y, 1/2+Z
Salt 1D							
N1	H1A	O1	0.89	1.87	2.743(5)	164.7	+X, +Y, +Z
N1	H1B	O2	0.89	1.93	2.813(7)	174.3	1-X, 1-Y, 1-Z
N1	H1C	O3	0.89	2.01	2.810(6)	149.6	+X, +Y, 1+Z
N2	H2C	O4	0.89	1.94	2.819(6)	171.2	+X, +Y, +Z
N2	H2D	O1	0.89	1.95	2.842(6)	175.1	+X, 1/2-Y, -1/2+Z
N2	H2E	O4	0.89	2.06	2.937(5)	169.7	+X, 1/2-Y ,1/2+Z
N2	H2E	O3	0.89	2.39	3.047(6)	130.3	+X, 1/2-Y, 1/2+Z
C2	H2A	O1	0.97	2.57	3.498(9)	159.4	1-X, 1-Y, 1-Z
O3	H3A	N2	0.74(16)	2.47(17)	3.047(6)	136(16)	+X, 1/2-Y, -1/2+Z
Salt 1(2)E							
N2	H2A	O1	0.89	1.85	2.731(4)	170.0	+X, +Y, +Z
N2	H2B	O2	0.89	1.88	2.754(4)	167.2	1-X, 1/2+Y, 3/2-Z
N2	H2C	O3	0.89	2.58	3.341(4)	143.7	2-X, 2+Y, 3/2-Z
N2	H2C	O4	0.89	1.92	2.773(4)	161.0	2-X, 1/2+Y, 3/2-Z
N1	H1A	O1	0.89	2.51	3.261(4)	142.7	1-X, -1/2+Y, 3/2-Z
N1	H1A	O2	0.89	1.99	2.843(4)	160.9	1-X, -1/2+Y, 3/2-Z
N1	H1B	O4	0.89	1.88	2.740(4)	162.2	2-X, -1/2+Y, 3/2-Z
N1	H1C	O3	0.89	1.83	2.706(4)	169.5	+X, +Y, +Z
C24	H24B	O1	0.97	2.60	3.435(5)	144.4	1-X, -1/2+Y, 3/2-Z
C6	H6A	O3	0.97	2.57	3.429(5)	147.2	2-X, 1/2+Y, 3/2-Z
Salt 1F							
N1	H1A	O2	0.89	1.90	2.773(3)	168.3	1-X, -1/2+Y, 1-Z
N1	H1B	O1	0.89	1.89	2.776(3)	173.4	+X, +Y, +Z
N1	H1C	O4	0.89	2.07	2.833(4)	143.3	-1+X, -1+Y, +Z
O3	H3	O1	1.13(6)	1.41(6)	2.532(3)	171(5)	2-X, 3/2+Y, 1-Z
Salt 1G							
N1	H1A	O4	0.89	2.02	2.895(5)	168.2	1/2-X, +Y, -Z
N1	H1B	O4	0.89	1.94	2.805(4)	163.5	+X, +Y, +Z
N1	H1C	O1	0.89	1.81	2.686(6)	169.6	+X, +Y, +Z
N2	H2C	O2	0.89	1.94	2.815(6)	165.8	1/2-X, +Y, -Z
N2	H2D	O2	0.89	1.98	2.844(6)	164.6	+X, +Y, +Z
N2	H2E	O3	0.89	1.79	2.677(6)	170.5	+X, +Y, +Z
Salt 1H							
N2	H2A	O8	0.82	1.92	2.736(6)	177.0	+X, +Y, +Z
N1	H1A	O6	0.89	1.98	2.846(5)	165.1	+X, +Y, +Z
N1	H1A	O5	0.89	2.56	3.191(5)	128.7	+X, +Y, +Z
N1	H1B	O2	0.89	1.90	2.787(5)	177.3	+X, +Y, +Z
N1	H1C	O3	0.89	1.88	2.757(6)	167.5	+X, +Y, +Z
N4	H4A	O5	0.89	1.85	2.734(5)	172.3	+X, +Y, +Z
N4	H4B	O4	0.89	1.88	2.748(5)	163.2	+X, +Y, +Z
N4	H4C	O7	0.89	1.90	2.782(5)	170.2	+X, +Y, +Z
N3	H3A	O6	0.89	2.01	2.895(5)	171.4	+X, +Y, +Z

N3	H3B	O7	0.89	1.95	2.834(6)	170.3	+X, +Y, +Z
N3	H3C	O1	0.89	1.79	2.674(5)	171.6	+X, +Y, +Z
N2	H2B	O2	0.71(3)	2.16(4)	2.849(7)	164(4)	+X, +Y, +Z
Salt 1I							
N1	H1A	O2	0.89	1.96	2.845(4)	172.6	+X, 3/2-Y, -1/2+Z
N1	H1B	O1	0.89	1.87	2.755(4)	172.0	+X, 5/2-Y, -1/2+Z
N1	H1C	O2	0.89	1.86	2.747(4)	174.4	-X, 2-Y, 1-Z
Salt 1J							
N1	H1A	O3	0.89	1.95	2.810(2)	161.8	+X, +Y, +Z
N1	H1B	O2	0.89	1.91	2.774(2)	164.6	+X, +Y, +Z
N1	H1C	O4	0.89	1.98	2.848(2)	165.9	-X, 1-Y, 2-Z
N2	H2C	O1	0.89	1.88	2.7652(18)	170.4	+X, +Y, +Z
N2	H2D	O2	0.89	1.96	2.816(2)	161.2	1-X, 1-Y, 2-Z
N2	H2E	O4	0.89	1.92	2.8019(19)	168.8	1+X, +Y, +Z
Salt 1K							
O7	H7	O8	0.82	1.75	2.571(3)	174.5	+X, +Y, +Z
N1	H1A	O3	0.89	2.06	2.927(3)	165.1	+X, +Y, +Z
N1	H1B	O8	0.89	2.60	3.241(3)	129.9	-1/2+X, -1/2-Y, 1/2+Z
N1	H1B	O1	0.89	2.22	2.951(3)	139.8	+X, +Y, +Z
N1	H1C	O5	0.89	1.87	2.759(3)	175.7	+X,-1+Y,+Z
C9	H9B	O2	0.97	2.55	3.438(4)	151.7	1/2-X, -1/2+Y, 1/2-Z
O8	H8	O4	0.82	1.78	2.599(3)	177.0	1/2+X, 1/2-Y,-1/2+Z
O2	H2	O1	0.85(5)	1.78(5)	2.622(3)	171(5)	+X, +Y, +Z

ORTEP images

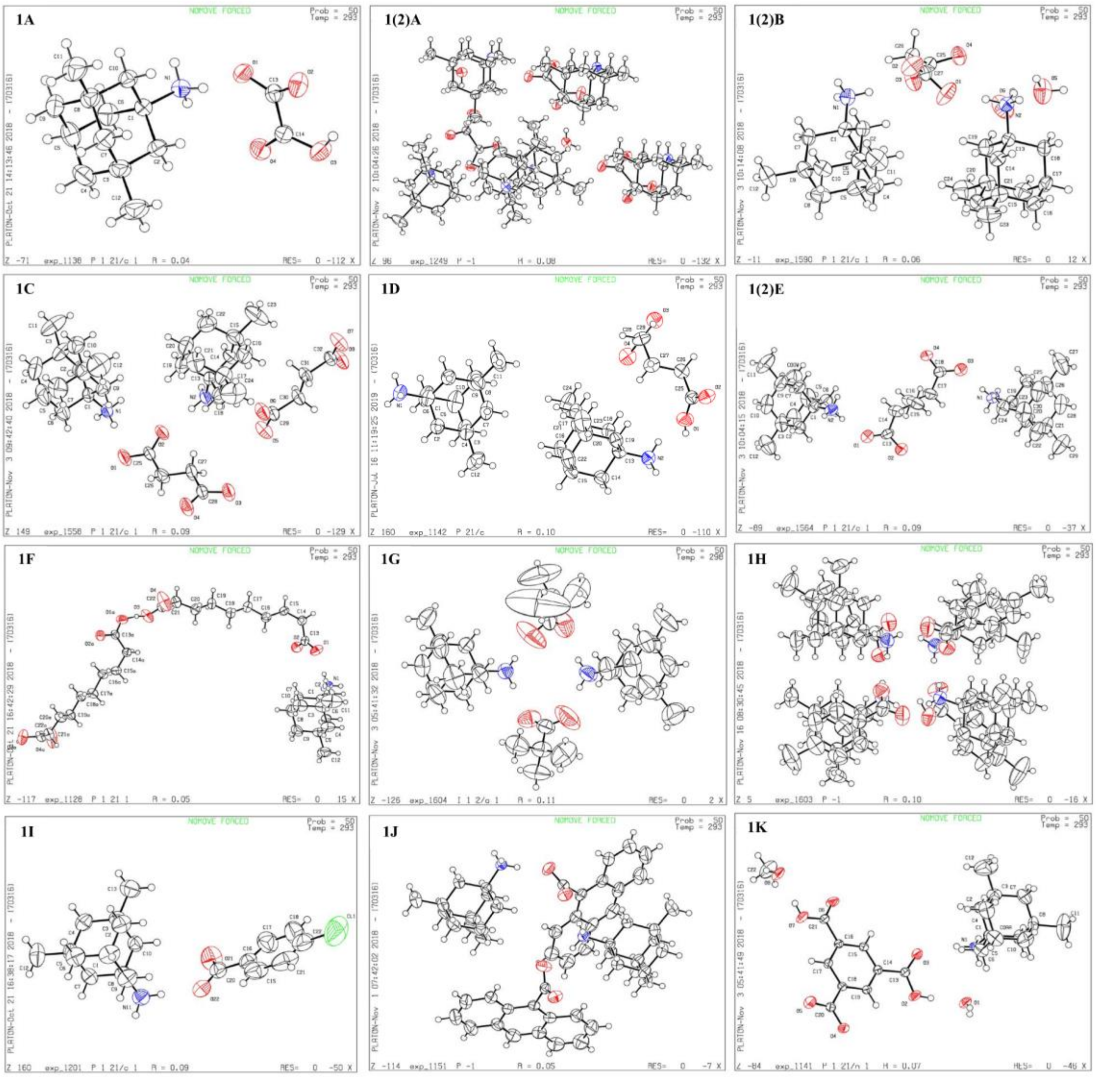

Figure S2.1 ORTEP images of all salts

3D Hirshfeld surfaces

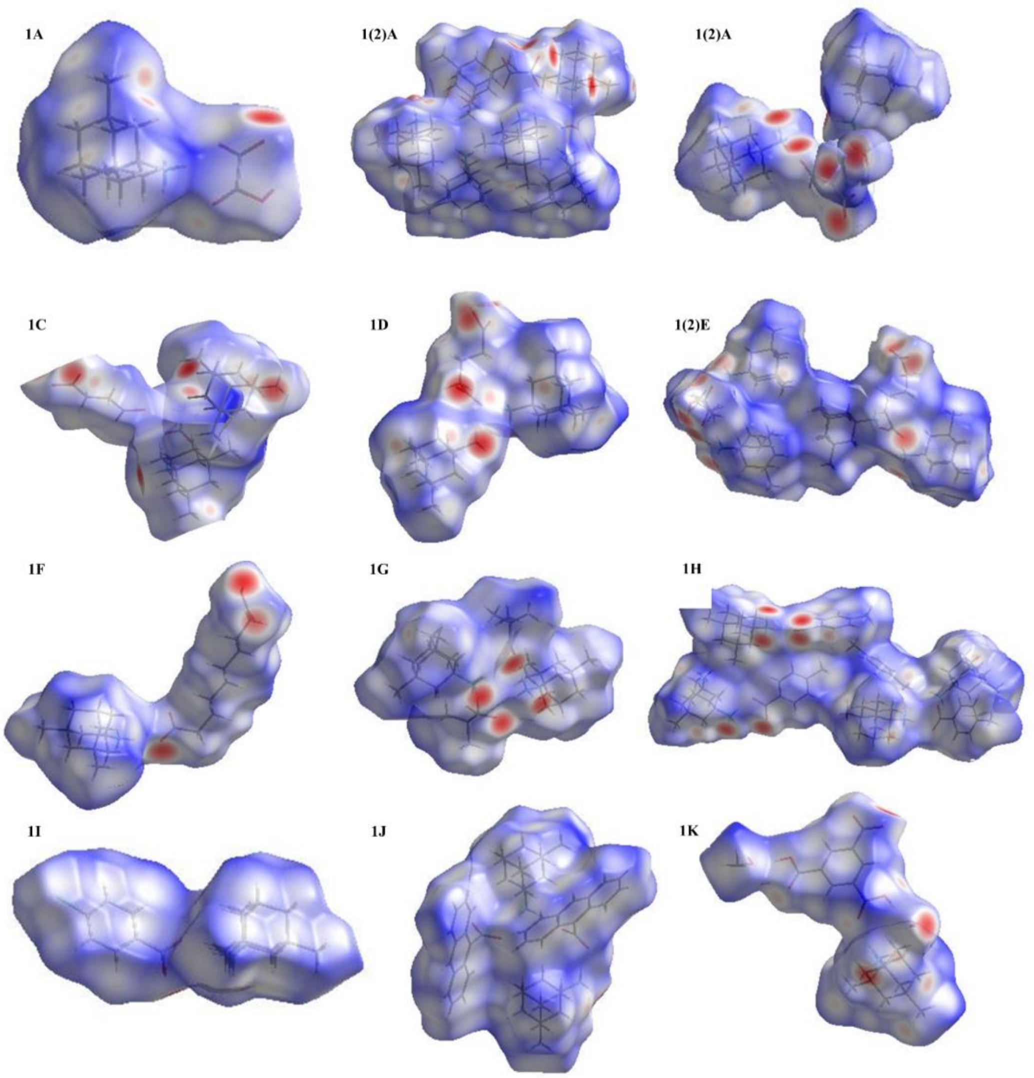

Figure S2.2 3D Hirshfeld surfaces of all salts

Spectral Data

^{1}H and FT-IR

Salt 1A

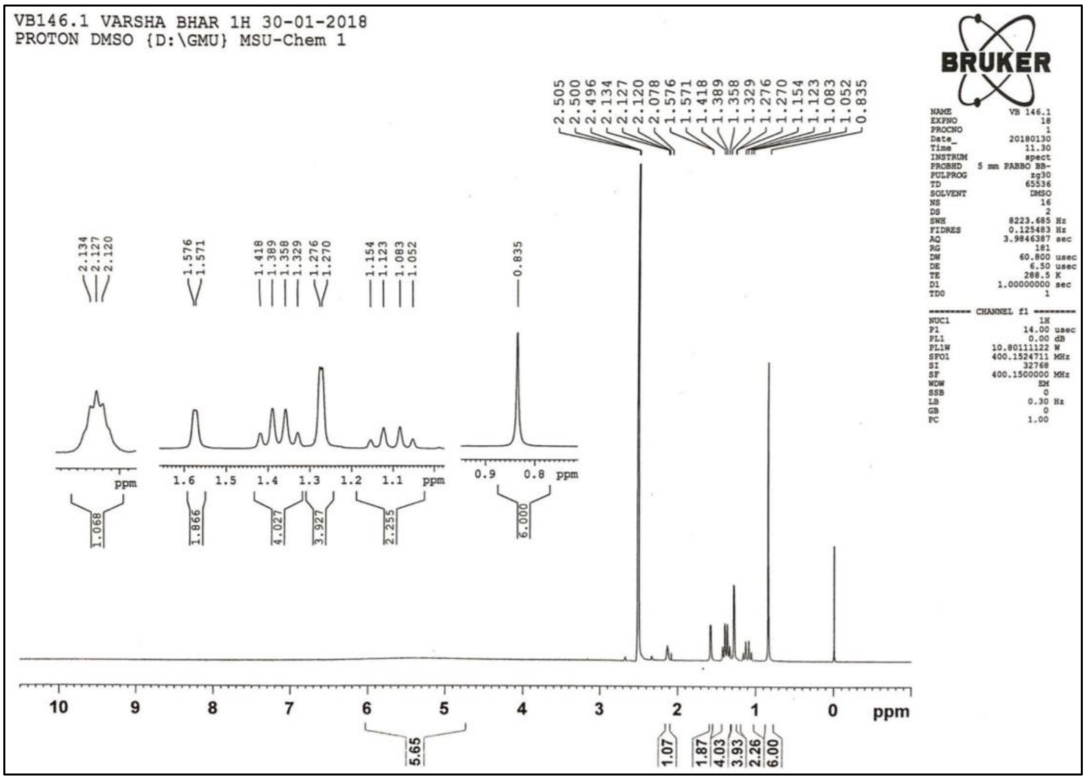

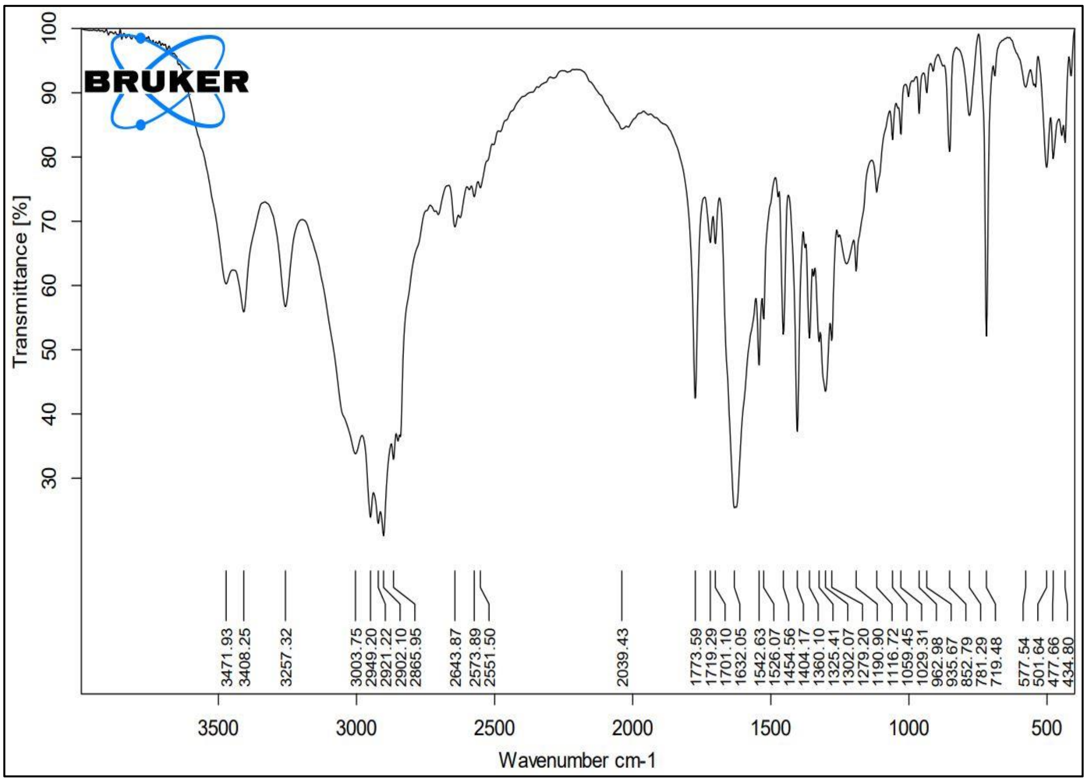

Salt 1(2)A

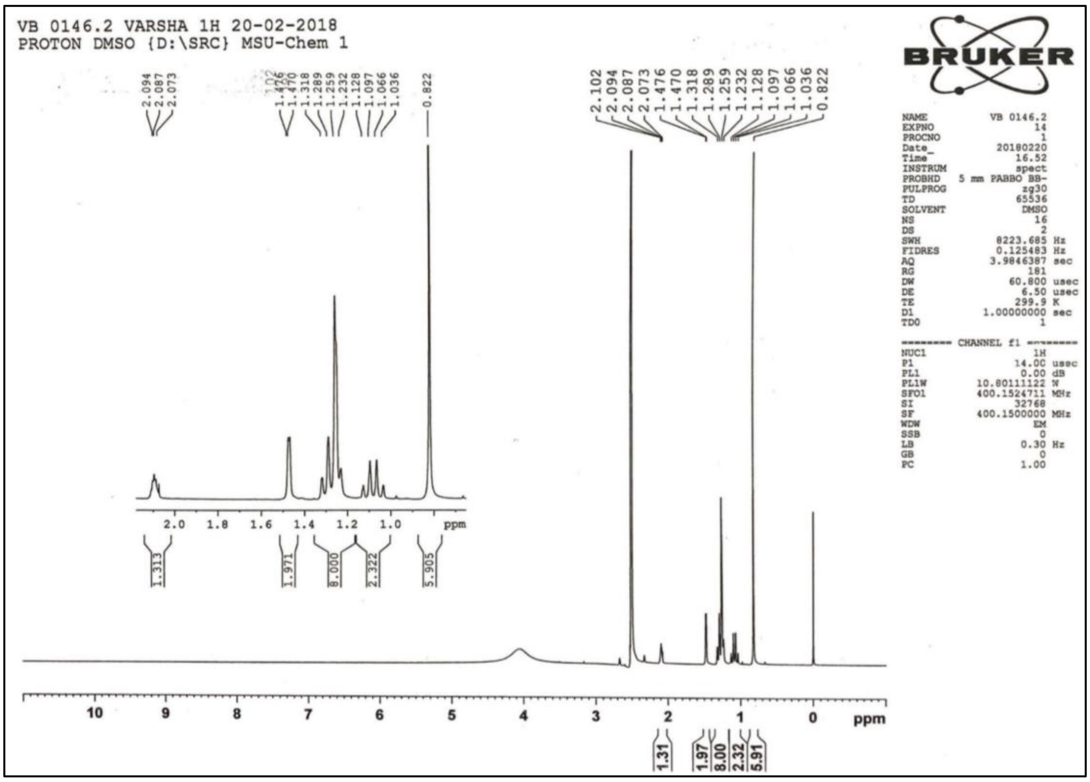
VB 0146.2 VARSHA 1H 20-02-2018
PROTON DMSO {D:\SRC} MSU-Chem 1
BRUKER
NAME VB 0146.2
EXPNO 14
PROCNO 1
Date_ 20180220
Time 16.52
INSTRUM spect
PROBHD 5 mm PABBO BB-
PULPROG zg30
TD 65536
SOLVENT DMSO
NS 16
DS 2
SWH 8223.685 Hz
FIDRES 0.125483 Hz
AQ 3.9846387 sec
RG 181
DW 60.800 usec
DE 6.50 usec
TE 299.9 K
D1 1.00000000 sec
TD0 1
======== CHANNEL f1 ========
NUC1 1H
P1 14.00 usec
PL1 0.00 dB
PL1W 10.80111122 W
SFO1 400.1524711 MHz
SI 32768
SF 400.1500000 MHz
WDW EM
SSB 0
LB 0.30 Hz
GB 0
PC 1.00
ppm

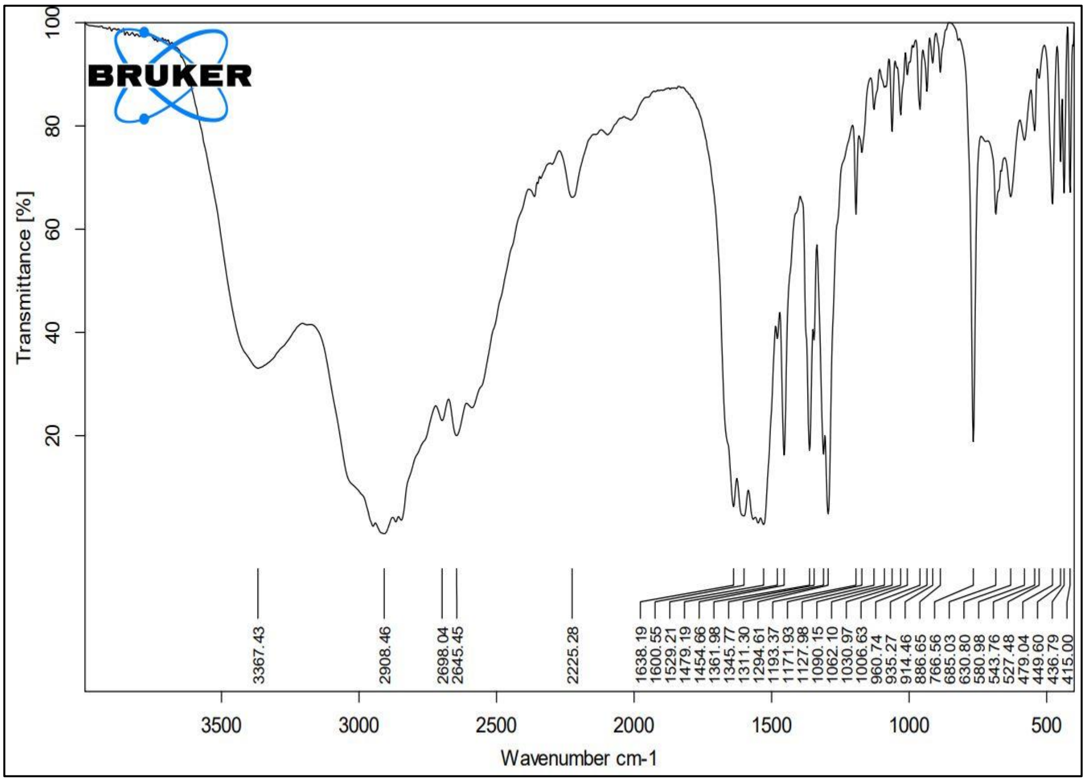
BRUKER
Transmittance [%]
Wavenumber cm-1
3367.43
2908.46
2698.04
2645.45
2225.28
1638.19
1600.55
1529.21
1479.19
1454.66
1361.98
1345.77
1311.30
1294.61
1193.37
1171.93
1127.98
1090.15
1062.10
1030.97
1006.63
960.74
935.27
914.46
886.65
766.56
685.03
630.80
580.98
543.76
527.48
479.04
449.60
436.79
415.00

Salt 1(2)B

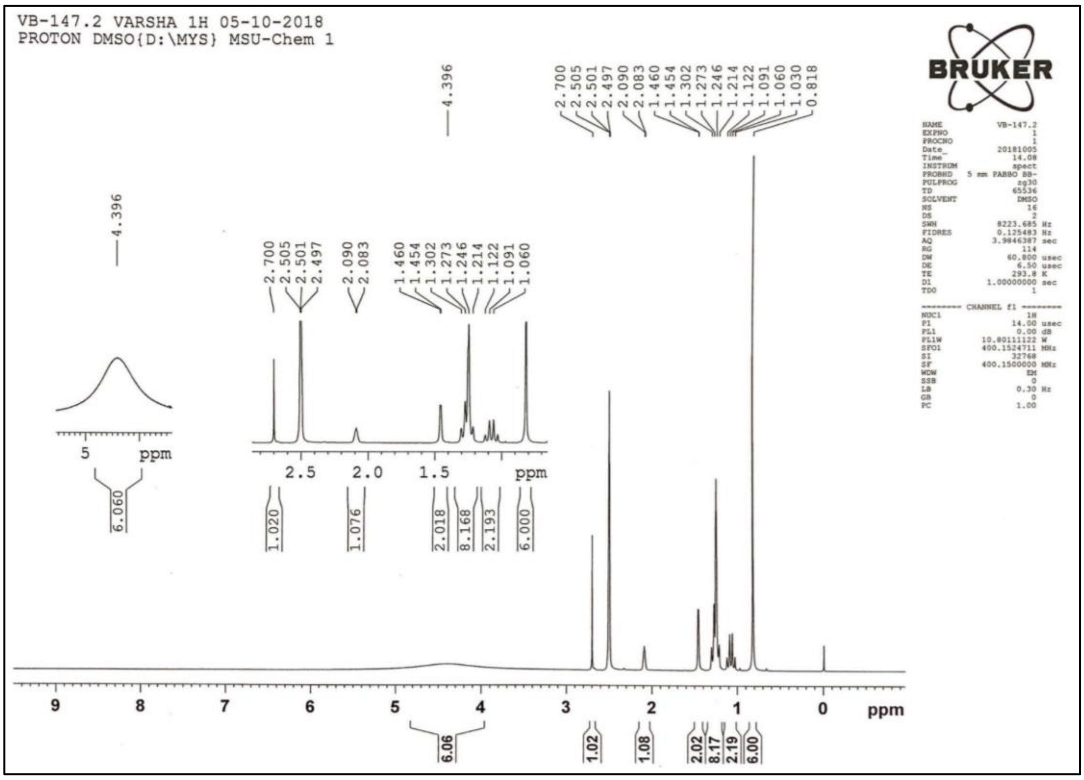
VB-147.2 VARSHA 1H 05-10-2018
PROTON DMSO{D:\MYS} MSU-Chem 1
BRUKER
4.396
2.700
2.505
2.501
2.497
2.090
2.083
1.460
1.454
1.302
1.273
1.246
1.214
1.122
1.091
1.060
1.030
0.818
6.060
1.020
1.076
2.018
8.168
2.193
6.000
6.06
1.02
1.08
2.02
8.17
2.19
6.00
ppm

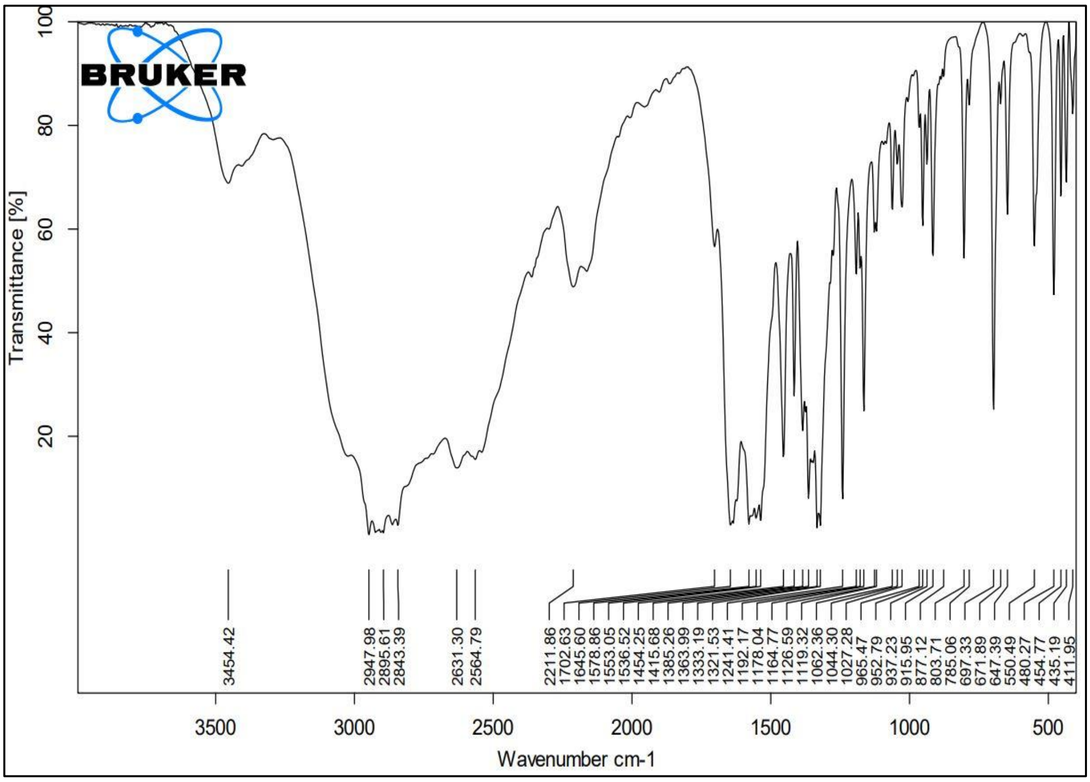
BRUKER
Transmittance [%]
Wavenumber cm-1
3454.42
2947.98
2895.61
2843.39
2631.30
2564.79
2211.86
1702.63
1645.60
1578.86
1553.05
1536.52
1454.25
1415.68
1385.26
1363.99
1333.19
1321.53
1241.41
1192.17
1178.04
1164.77
1126.59
1119.32
1062.36
1044.30
1027.28
965.47
952.79
937.23
915.95
877.12
803.71
785.06
697.33
671.89
647.39
550.49
480.27
454.77
435.19
411.95

Salt 1C

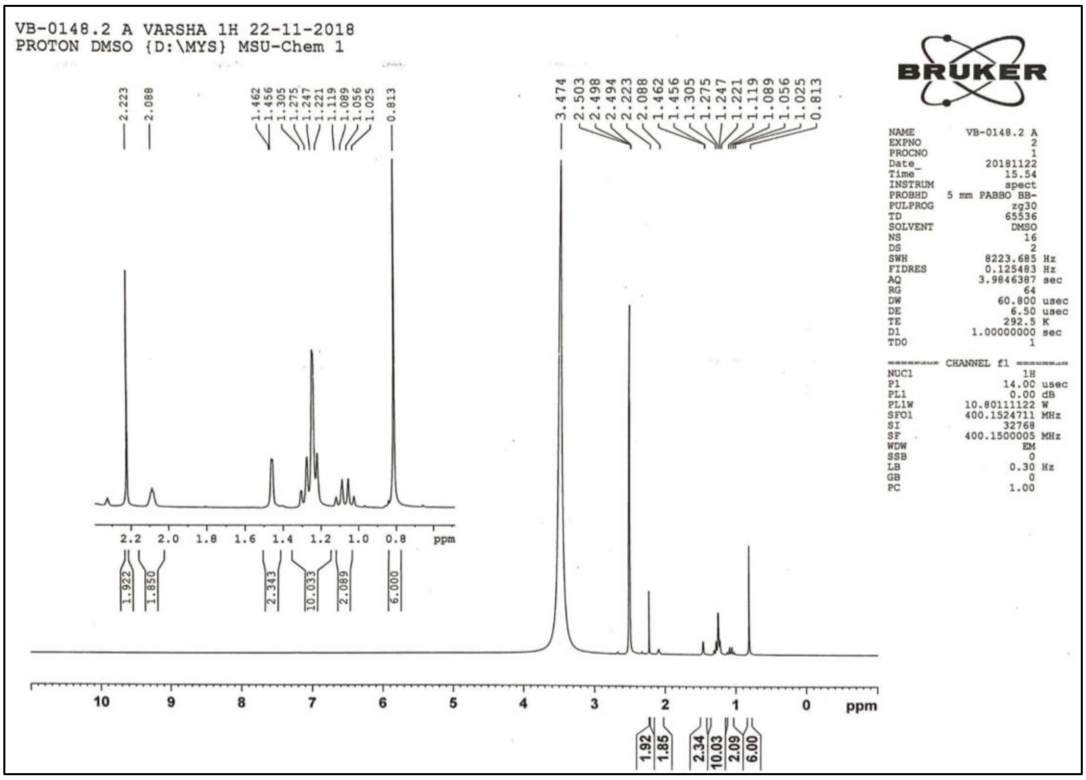
VB-0148.2 A VARSHA 1H 22-11-2018
PROTON DMSO {D:\MYS} MSU-Chem 1
BRUKER
NAME VB-0148.2 A
EXPNO 2
PROCNO 1
Date_ 20181122
Time 15.54
INSTRUM spect
PROBHD 5 mm PABBO BB-
PULPROG zg30
TD 65536
SOLVENT DMSO
NS 16
DS 2
SWH 8223.685 Hz
FIDRES 0.125483 Hz
AQ 3.9846387 sec
RG 64
DW 60.800 usec
DE 6.50 usec
TE 292.5 K
D1 1.00000000 sec
TD0 1
CHANNEL f1
NUC1 1H
P1 14.00 usec
PL1 0.00 dB
PL1W 10.80111122 W
SFO1 400.1524711 MHz
SI 32768
SF 400.1500005 MHz
WDW EM
SSB 0
LB 0.30 Hz
GB 0
PC 1.00
ppm

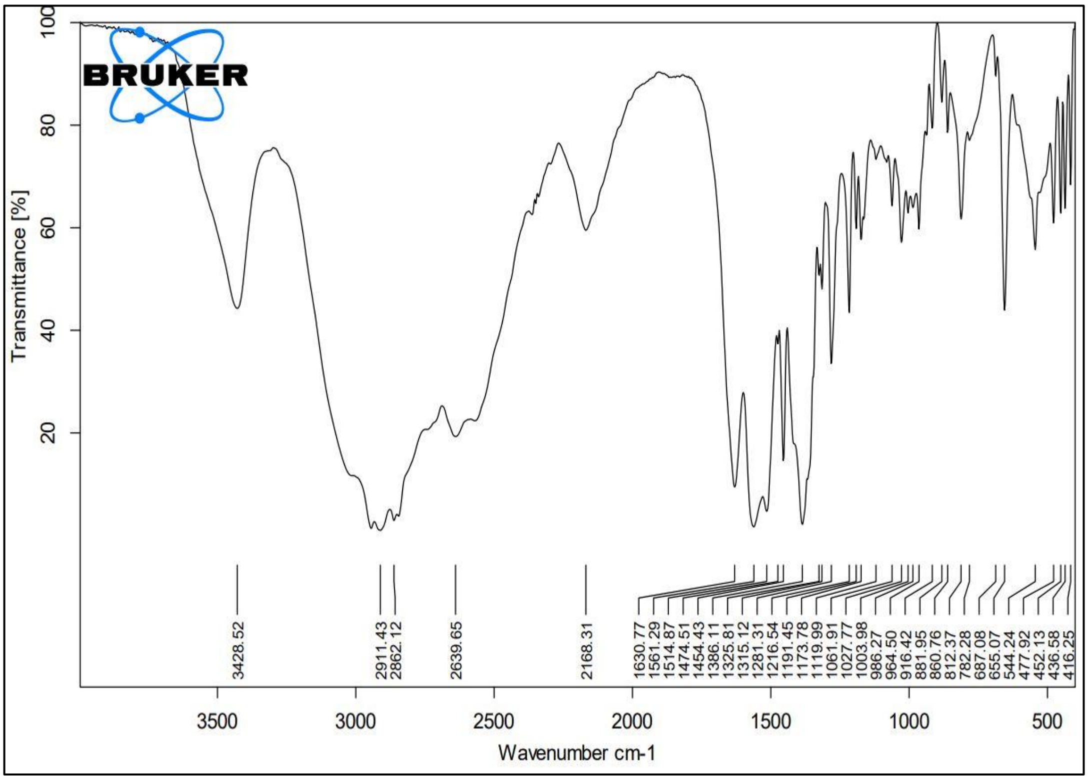
BRUKER
Transmittance [%]
Wavenumber cm-1
3428.52
2911.43
2862.12
2639.65
2168.31
1630.77
1561.29
1514.87
1474.51
1454.43
1386.11
1325.81
1315.12
1281.31
1216.54
1191.45
1173.78
1119.99
1061.91
1027.77
1003.98
986.27
964.50
916.42
881.95
860.76
812.37
782.28
687.08
655.07
544.24
477.92
452.13
436.58
416.25

Salt 1D

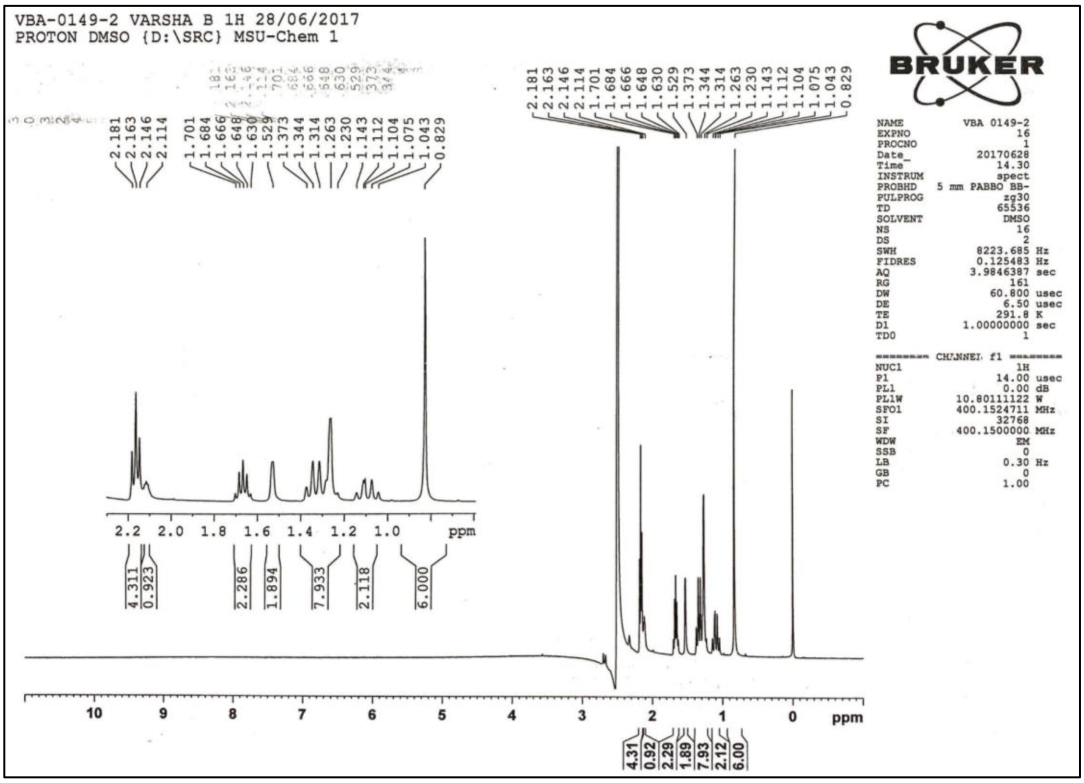
VBA-0149-2 VARSHA B 1H 28/06/2017
PROTON DMSO {D:\SRC} MSU-Chem 1
BRUKER
NAME VBA 0149-2
EXPNO 16
PROCNO 1
Date_ 20170628
Time 14.30
INSTRUM spect
PROBHD 5 mm PABBO BB-
PULPROG zg30
TD 65536
SOLVENT DMSO
NS 16
DS 2
SWH 8223.685 Hz
FIDRES 0.125483 Hz
AQ 3.9846387 sec
RG 161
DW 60.800 usec
DE 6.50 usec
TE 291.8 K
D1 1.00000000 sec
TD0 1
CHANNEL f1
NUC1 1H
P1 14.00 usec
PL1 0.00 dB
PL1W 10.80111122 W
SFO1 400.1524711 MHz
SI 32768
SF 400.1500000 MHz
WDW EM
SSB 0
LB 0.30 Hz
GB 0
PC 1.00
2.181 2.163 2.146 2.114 1.701 1.684 1.666 1.648 1.630 1.529 1.373 1.344 1.314 1.263 1.230 1.143 1.112 1.104 1.075 1.043 0.829
4.311 0.923 2.286 1.894 7.933 2.118 6.000
4.31 0.92 2.29 1.89 7.93 2.12 6.00
ppm

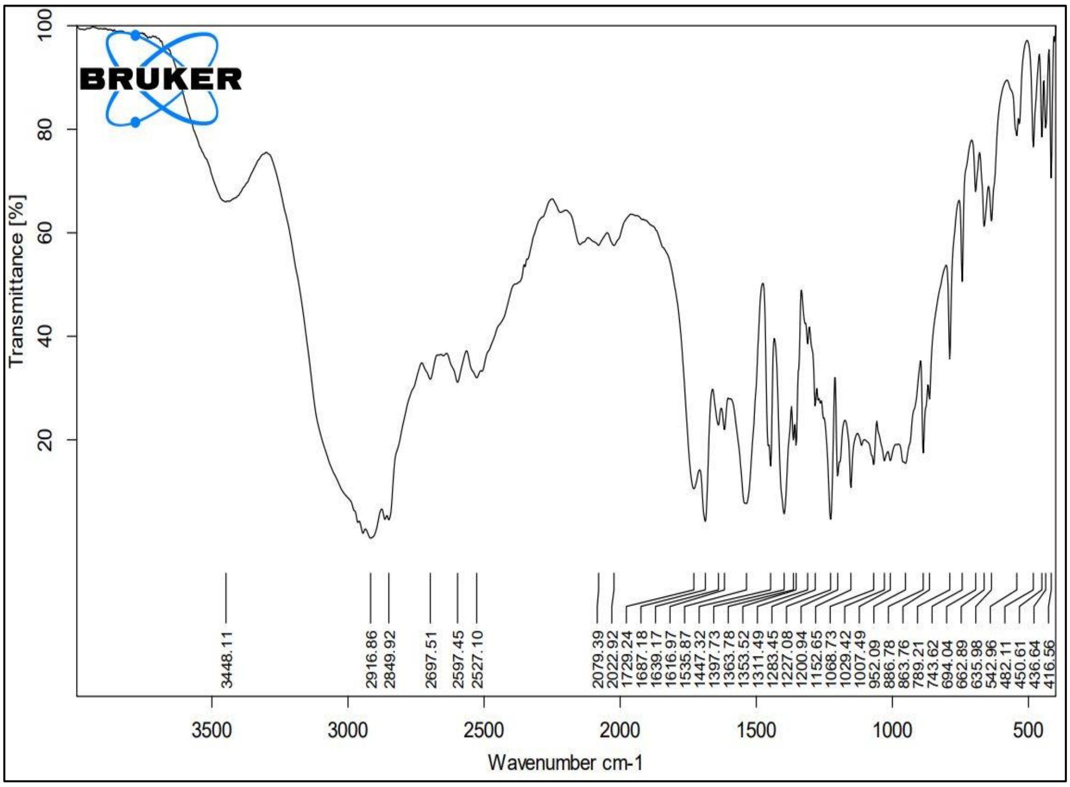
BRUKER
Transmittance [%]
Wavenumber cm-1
3448.11
2916.86
2849.92
2697.51
2597.45
2527.10
2079.39
2022.92
1729.24
1687.18
1639.17
1616.97
1535.87
1447.32
1397.73
1363.78
1353.52
1311.49
1283.45
1227.08
1200.94
1152.65
1068.73
1029.42
1007.49
952.09
886.78
863.76
789.21
743.62
694.04
662.89
635.98
542.96
482.11
450.61
436.64
416.56

Salt 1(2)E

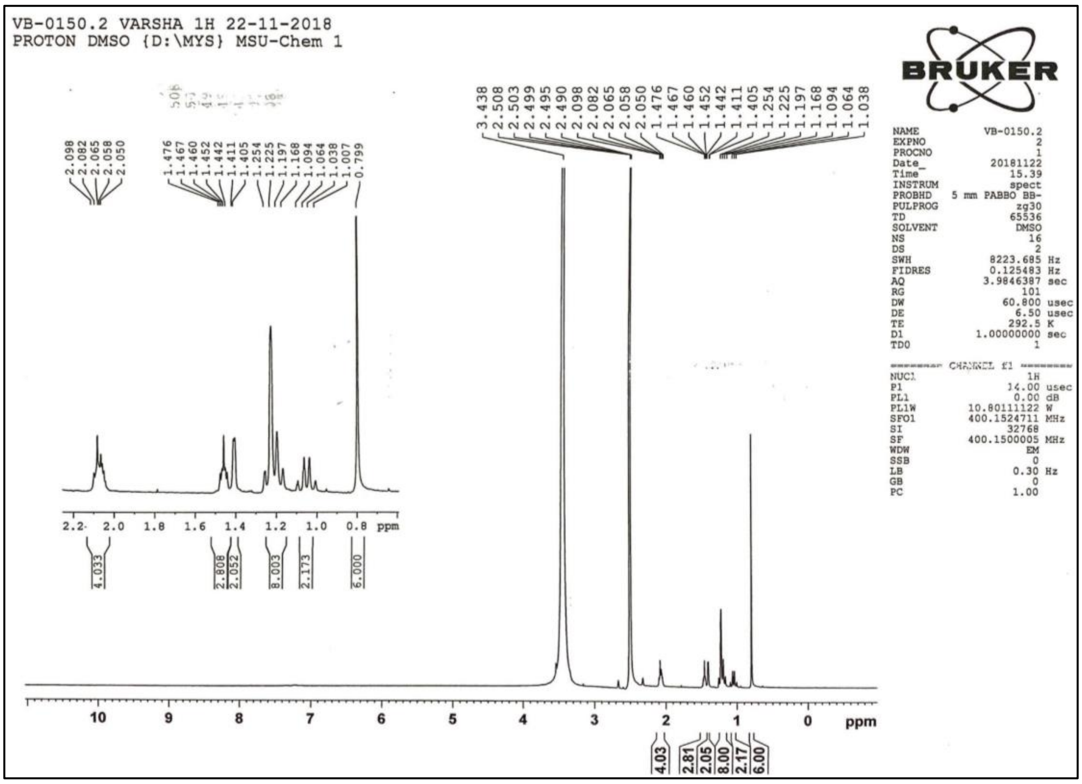
VB-0150.2 VARSHA 1H 22-11-2018
PROTON DMSO {D:\MYS} MSU-Chem 1
BRUKER
NAME VB-0150.2
EXPNO 2
PROCNO 1
Date_ 20181122
Time 15.39
INSTRUM spect
PROBHD 5 mm PABBO BB-
PULPROG zg30
TD 65536
SOLVENT DMSO
NS 16
DS 2
SWH 8223.685 Hz
FIDRES 0.125483 Hz
AQ 3.9846387 sec
RG 101
DW 60.800 usec
DE 6.50 usec
TE 292.5 K
D1 1.00000000 sec
TD0 1
NUC1 1H
P1 14.00 usec
PL1 0.00 dB
PL1W 10.80111122 W
SFO1 400.1524711 MHz
SI 32768
SF 400.1500005 MHz
WDW EM
SSB 0
LB 0.30 Hz
GB 0
PC 1.00
ppm

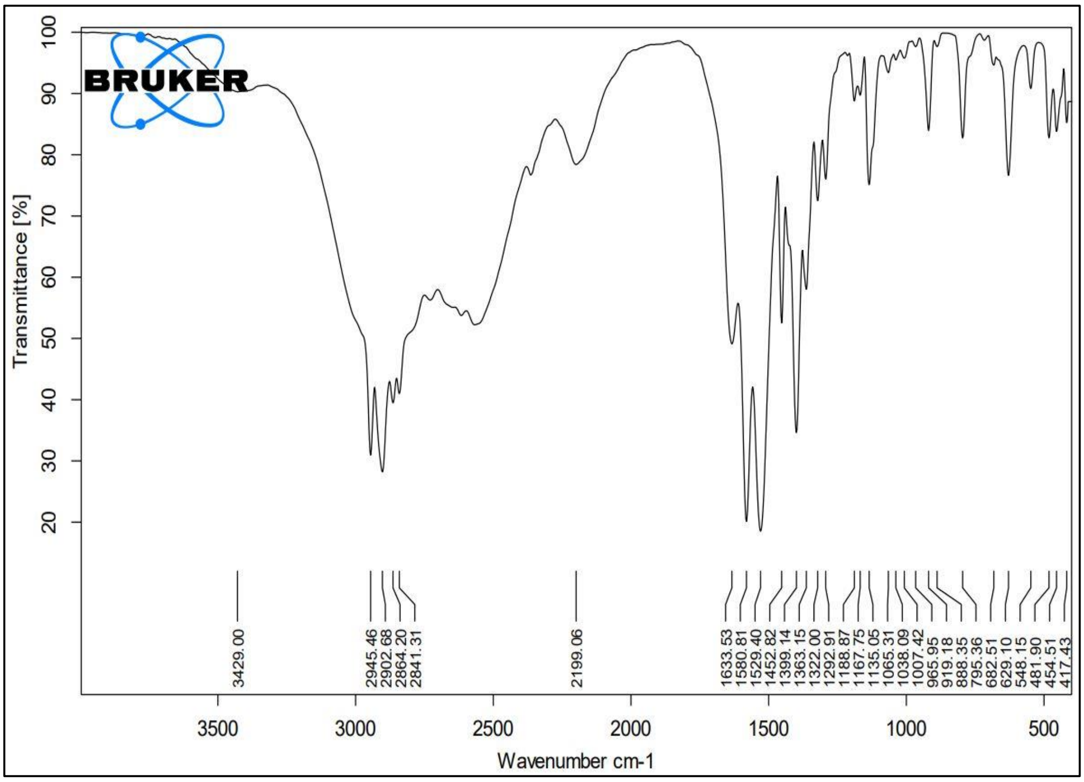
BRUKER
Transmittance [%]
Wavenumber cm-1
3429.00
2945.46
2902.68
2864.20
2841.31
2199.06
1633.53
1580.81
1529.40
1452.82
1399.14
1363.15
1322.00
1292.91
1188.87
1167.75
1135.05
1065.31
1038.09
1007.42
965.95
919.18
888.35
795.36
682.51
629.10
548.15
481.90
454.51
417.43

Salt 1F

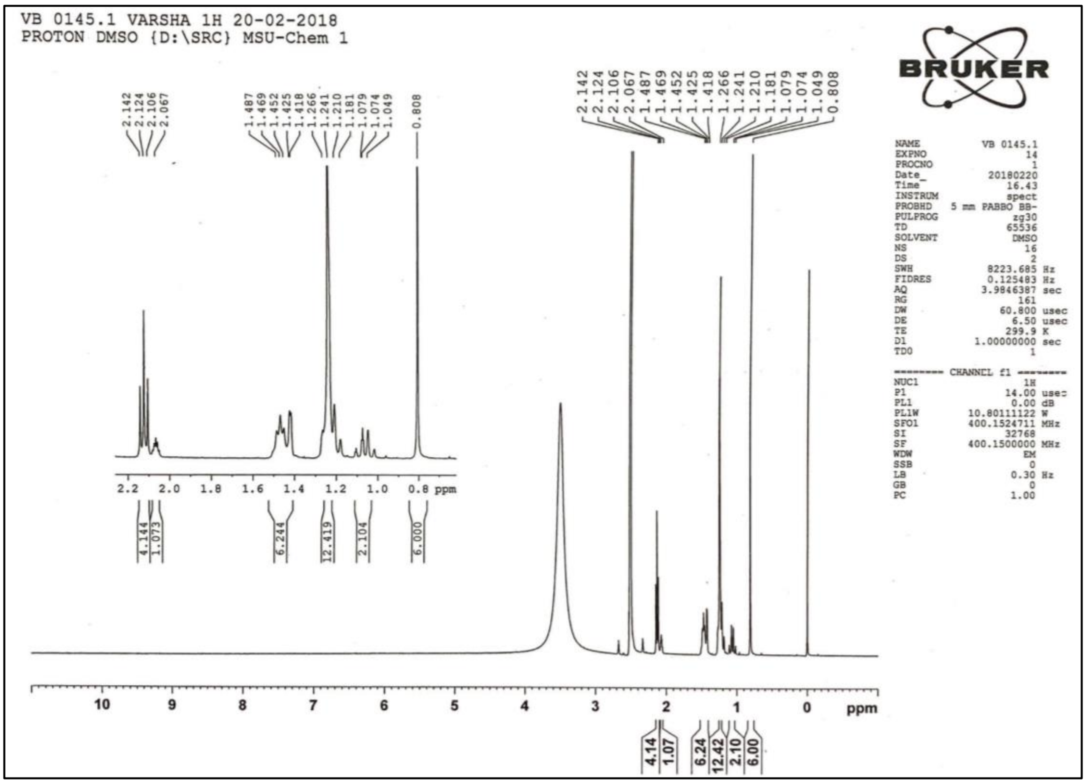
VB 0145.1 VARSHA 1H 20-02-2018
PROTON DMSO {D:\SRC} MSU-Chem 1
BRUKER
2.142
2.124
2.106
2.067
1.487
1.469
1.452
1.425
1.418
1.266
1.241
1.210
1.181
1.079
1.074
1.049
0.808
ppm
4.144
1.073
6.244
12.419
2.104
6.000
NAME VB 0145.1
EXPNO 14
PROCNO 1
Date_ 20180220
Time 16.43
INSTRUM spect
PROBHD 5 mm PABBO BB-
PULPROG zg30
TD 65536
SOLVENT DMSO
NS 16
DS 2
SWH 8223.685 Hz
FIDRES 0.125483 Hz
AQ 3.9846387 sec
RG 161
DW 60.800 usec
DE 6.50 usec
TE 299.9 K
D1 1.00000000 sec
TD0 1
CHANNEL f1
NUC1 1H
P1 14.00 usec
PL1 0.00 dB
PL1W 10.80111122 W
SFO1 400.1524711 MHz
SI 32768
SF 400.1500000 MHz
WDW EM
SSB 0
LB 0.30 Hz
GB 0
PC 1.00
4.14
1.07
6.24
12.42
2.10
6.00

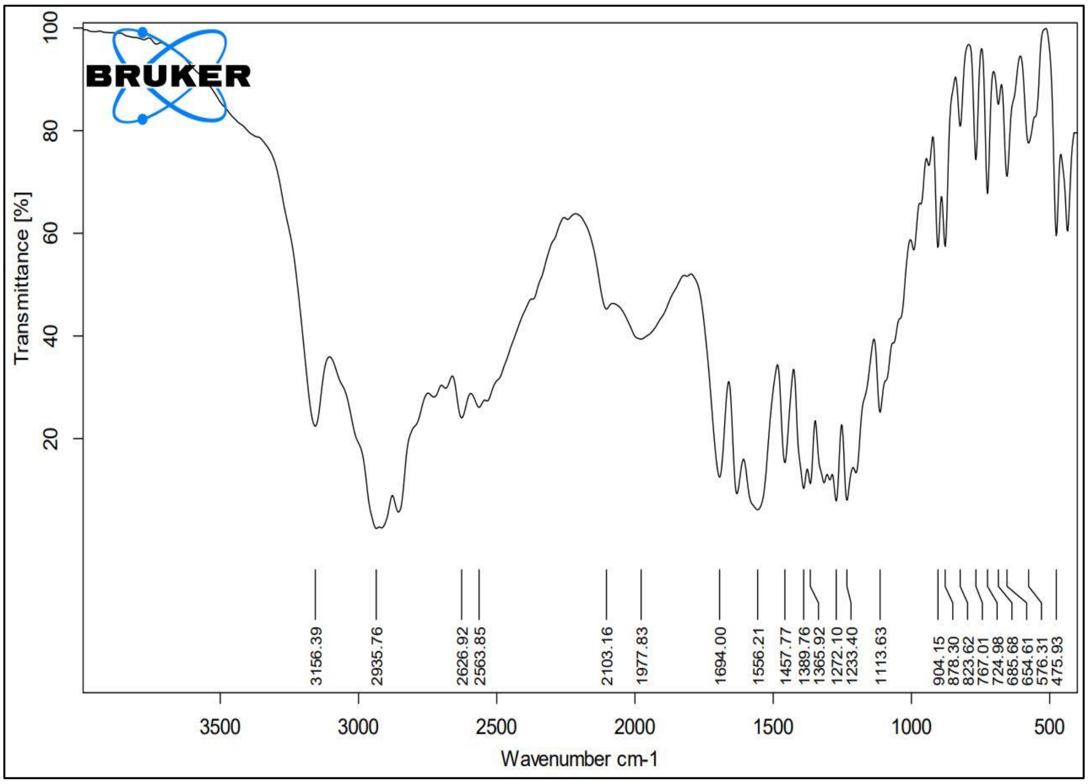
BRUKER
Transmittance [%]
Wavenumber cm-1
3156.39
2935.76
2626.92
2563.85
2103.16
1977.83
1694.00
1556.21
1457.77
1389.76
1365.92
1272.10
1233.40
1113.63
904.15
878.30
823.62
767.01
724.98
685.68
654.61
576.31
475.93

Salt 1G

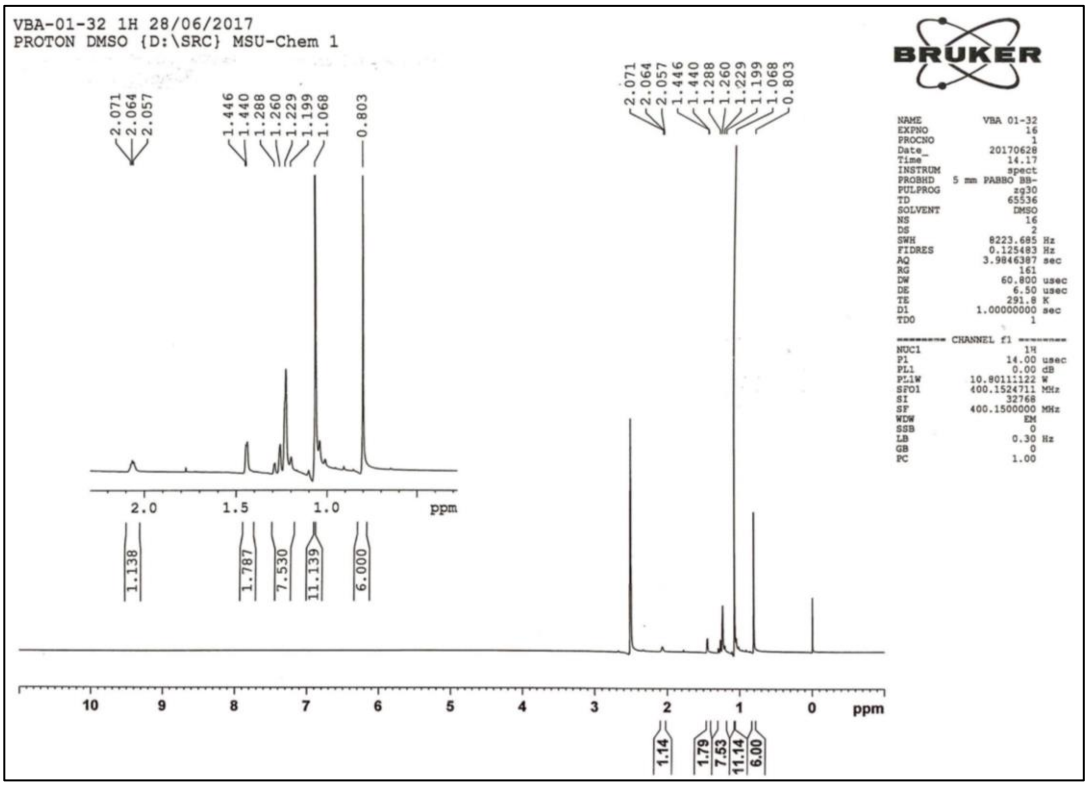
VBA-01-32 1H 28/06/2017
PROTON DMSO {D:\SRC} MSU-Chem 1
2.071
2.064
2.057
1.446
1.440
1.288
1.260
1.229
1.199
1.068
0.803
BRUKER
NAME VBA 01-32
EXPNO 16
PROCNO 1
Date_ 20170628
Time 14.17
INSTRUM spect
PROBHD 5 mm PABBO BB-
PULPROG zg30
TD 65536
SOLVENT DMSO
NS 16
DS 2
SWH 8223.685 Hz
FIDRES 0.125483 Hz
AQ 3.9846387 sec
RG 161
DW 60.800 usec
DE 6.50 usec
TE 291.8 K
D1 1.00000000 sec
TD0 1
======== CHANNEL f1 ========
NUC1 1H
P1 14.00 usec
PL1 0.00 dB
PL1W 10.80111122 W
SFO1 400.1524711 MHz
SI 32768
SF 400.1500000 MHz
WDW EM
SSB 0
LB 0.30 Hz
GB 0
PC 1.00
ppm
1.138
1.787
7.530
11.139
6.000
1.14
1.79
7.53
11.14
6.00

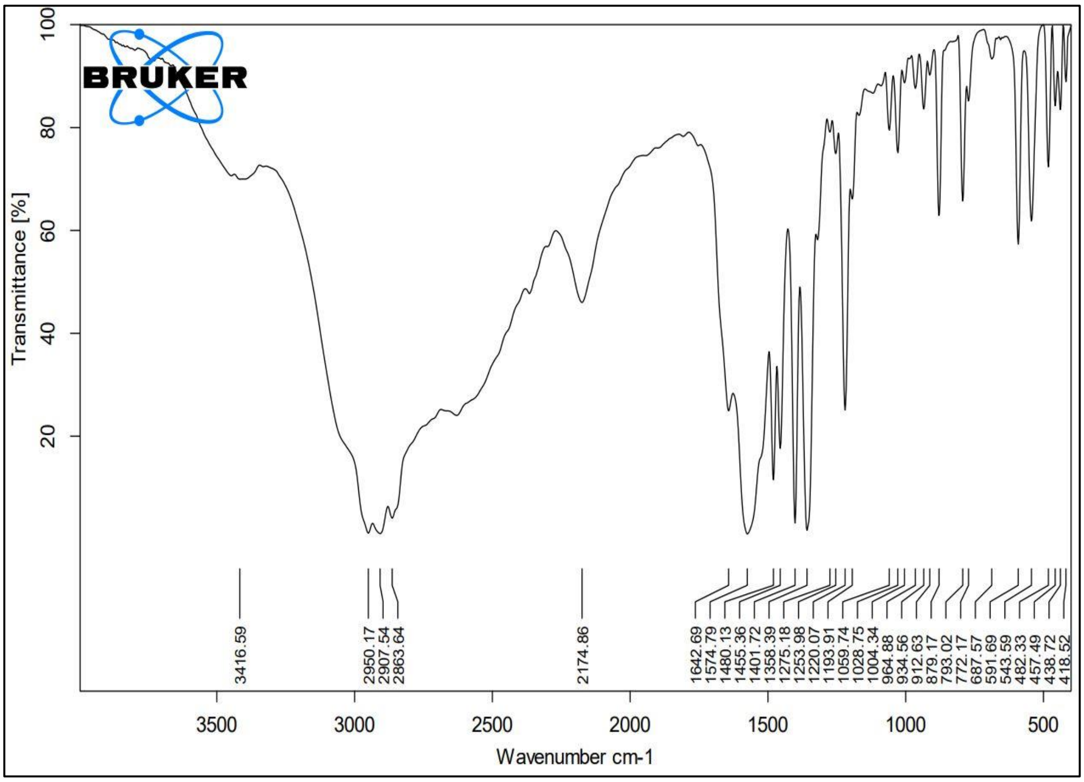
BRUKER
Transmittance [%]
Wavenumber cm-1
3416.59
2950.17
2907.54
2863.64
2174.86
1642.69
1574.79
1480.13
1455.36
1401.72
1358.39
1275.18
1253.98
1220.07
1193.91
1059.74
1028.75
1004.34
964.88
934.56
912.63
879.17
793.02
772.17
687.57
591.69
543.59
482.33
457.49
438.72
418.52

Salt 1H

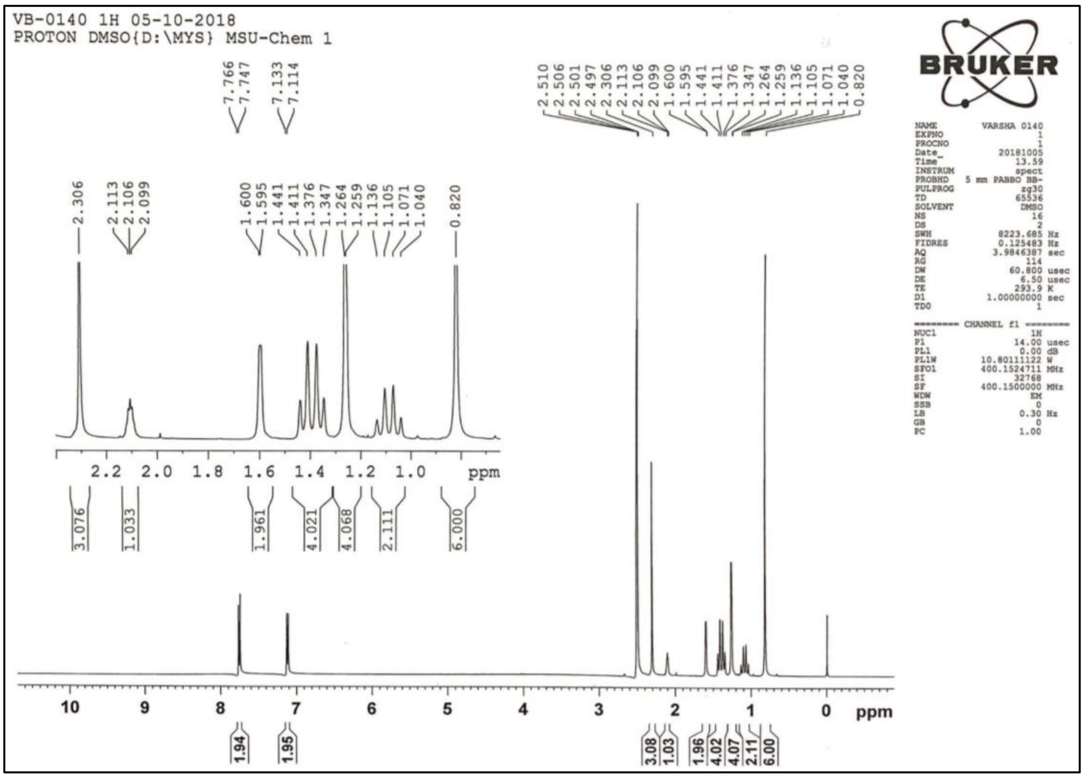
VB-0140 1H 05-10-2018
PROTON DMSO{D:\MYS} MSU-Chem 1
BRUKER
ppm

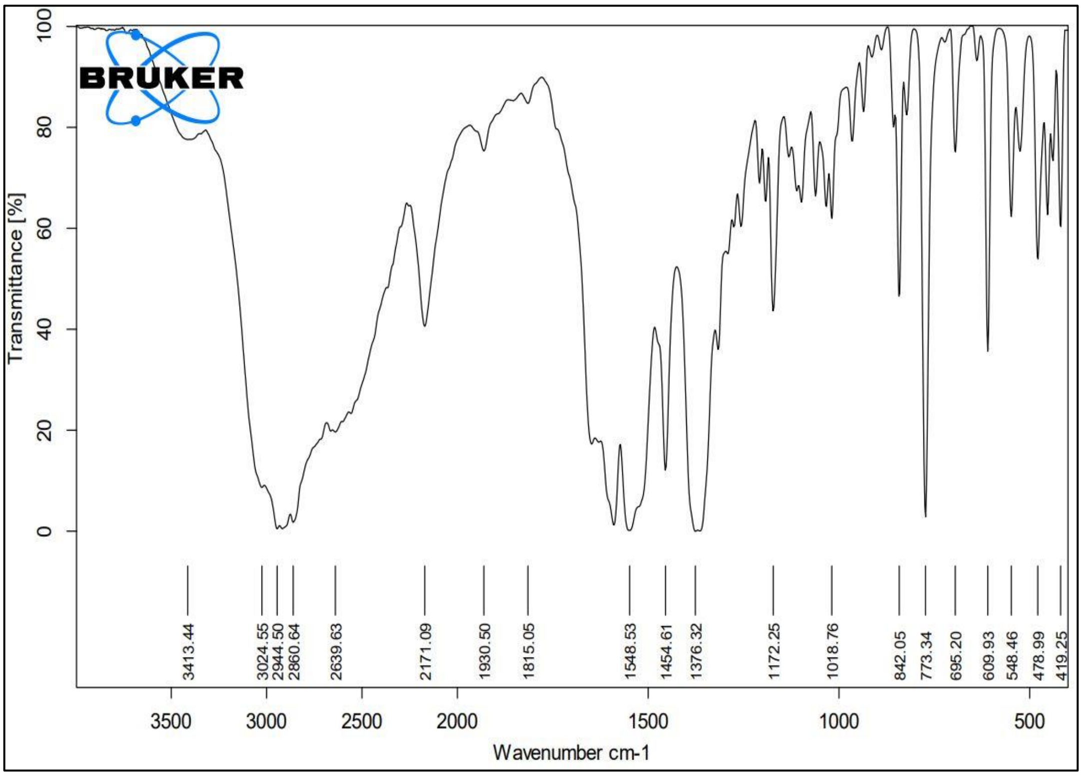
BRUKER
Transmittance [%]
Wavenumber cm-1
3413.44
3024.55
2944.50
2860.64
2639.63
2171.09
1930.50
1815.05
1548.53
1454.61
1376.32
1172.25
1018.76
842.05
773.34
695.20
609.93
548.46
478.99
419.25

Salt 1I

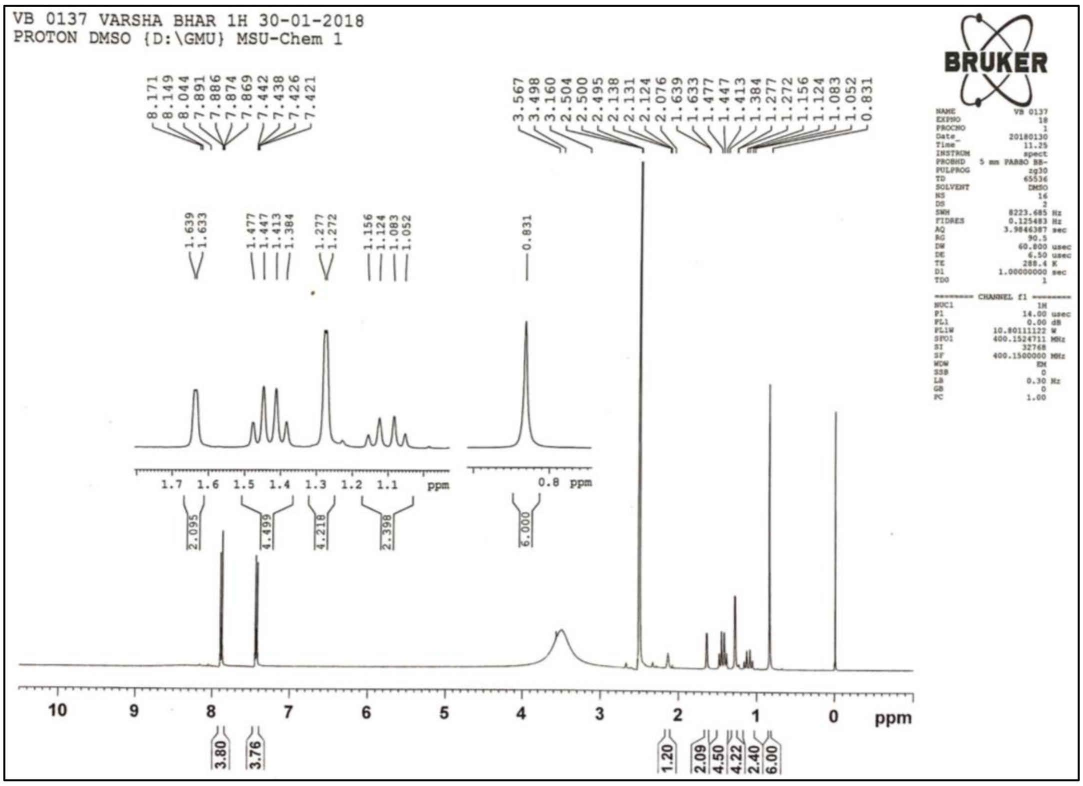
VB 0137 VARSHA BHAR 1H 30-01-2018
PROTON DMSO {D:\GMU} MSU-Chem 1
BRUKER
ppm

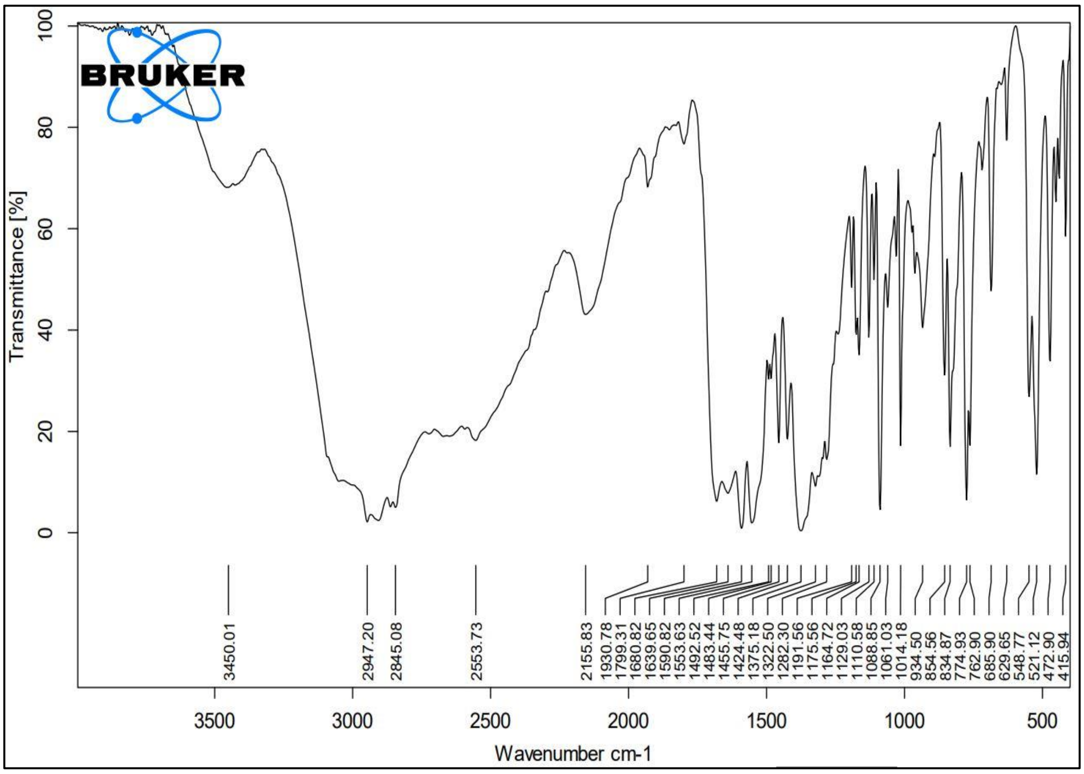
BRUKER
Transmittance [%]
Wavenumber cm-1

Salt 1J

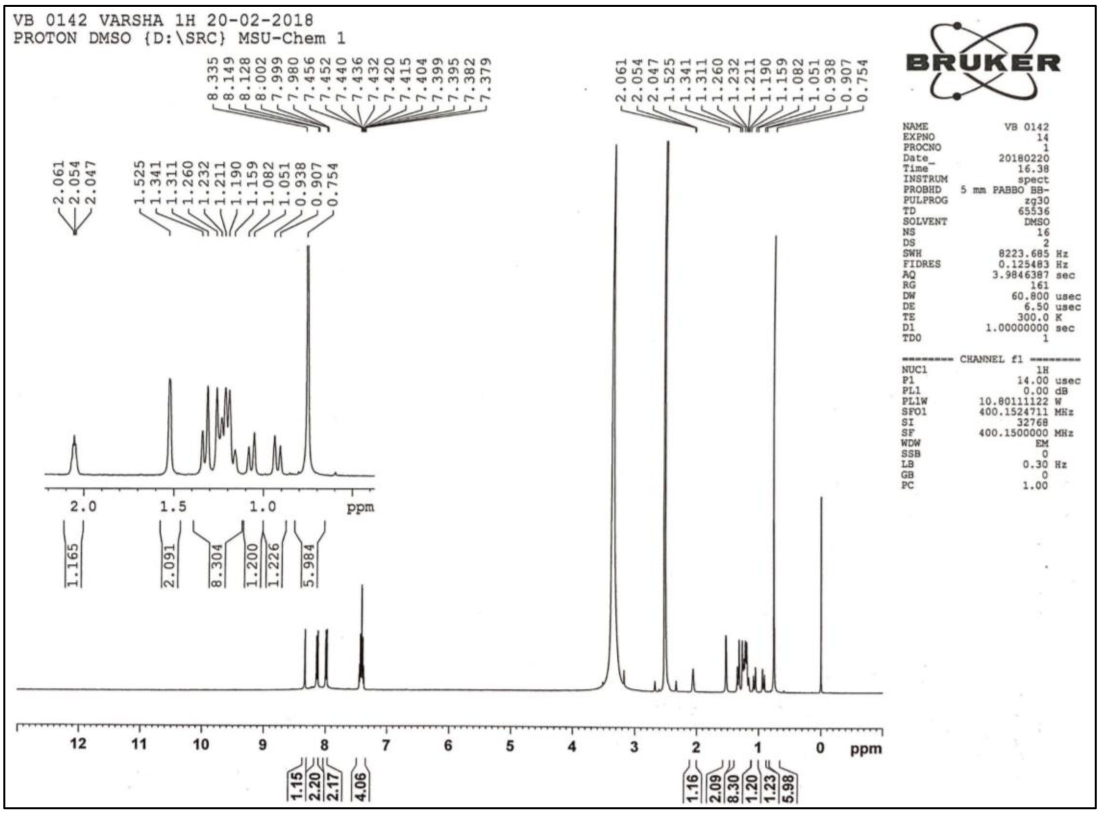
VB 0142 VARSHA 1H 20-02-2018
PROTON DMSO {D:\SRC} MSU-Chem 1
BRUKER
ppm

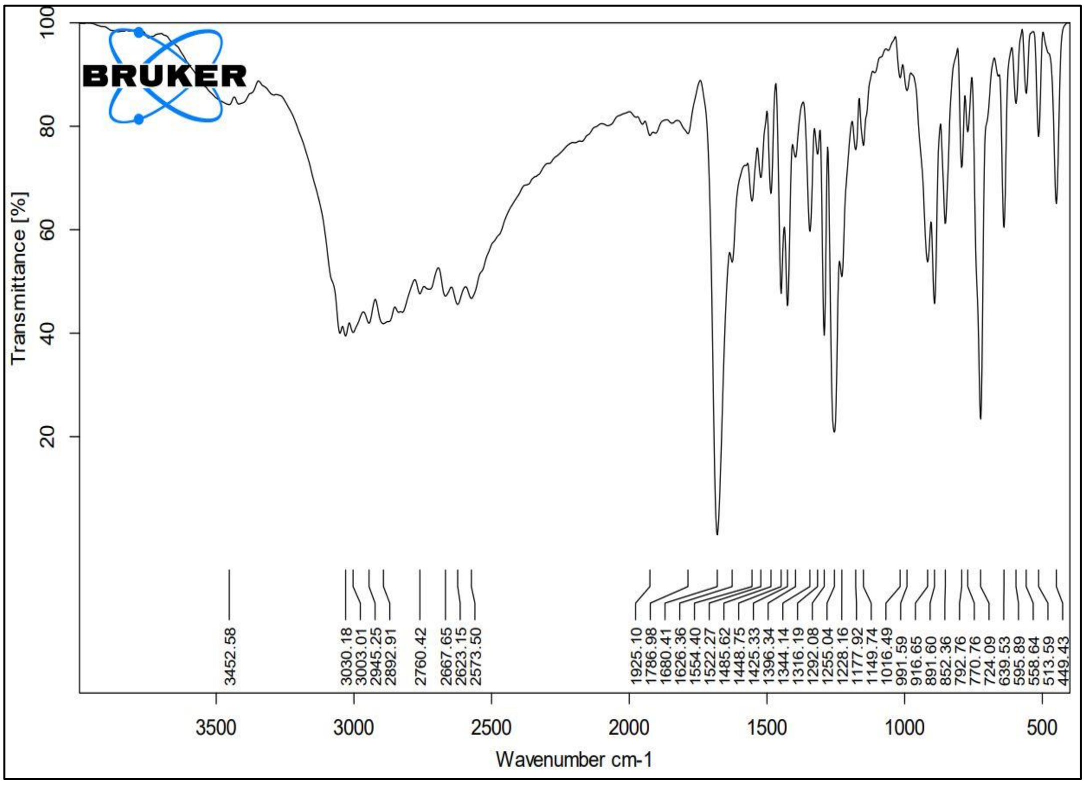
BRUKER
Transmittance [%]
Wavenumber cm-1

Salt 1K

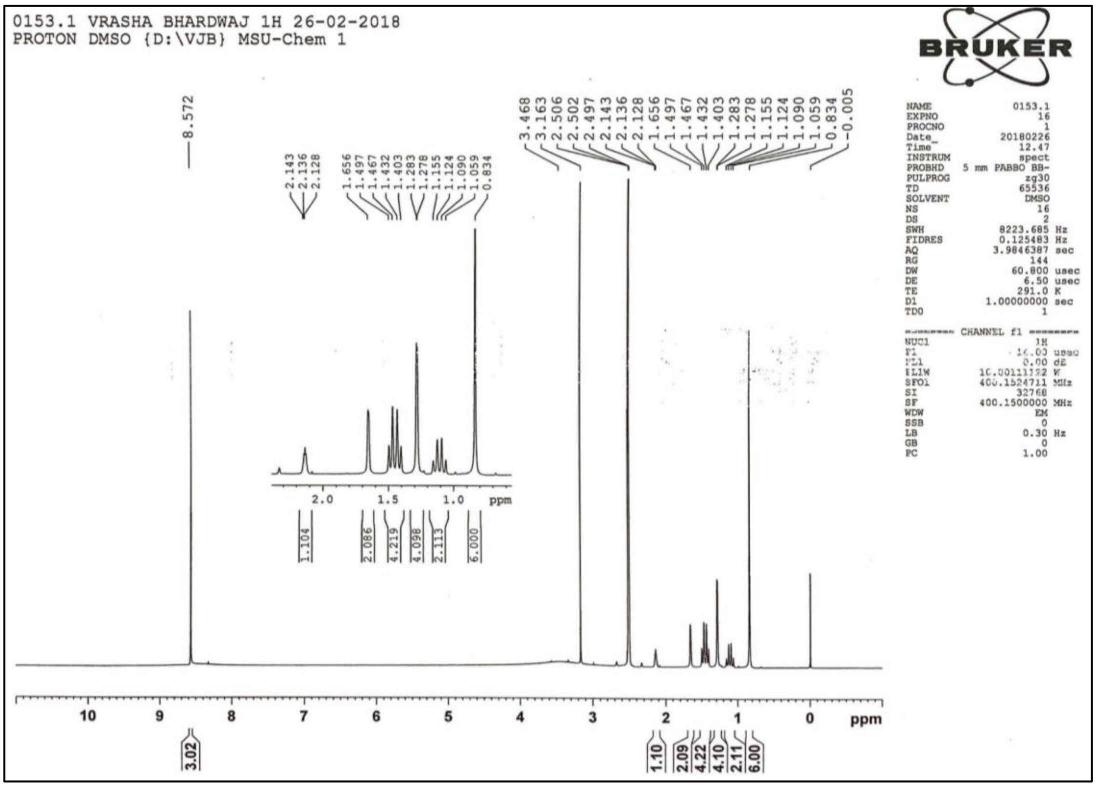
0153.1 VRASHA BHARDWAJ 1H 26-02-2018
PROTON DMSO {D:\VJB} MSU-Chem 1
BRUKER
ppm

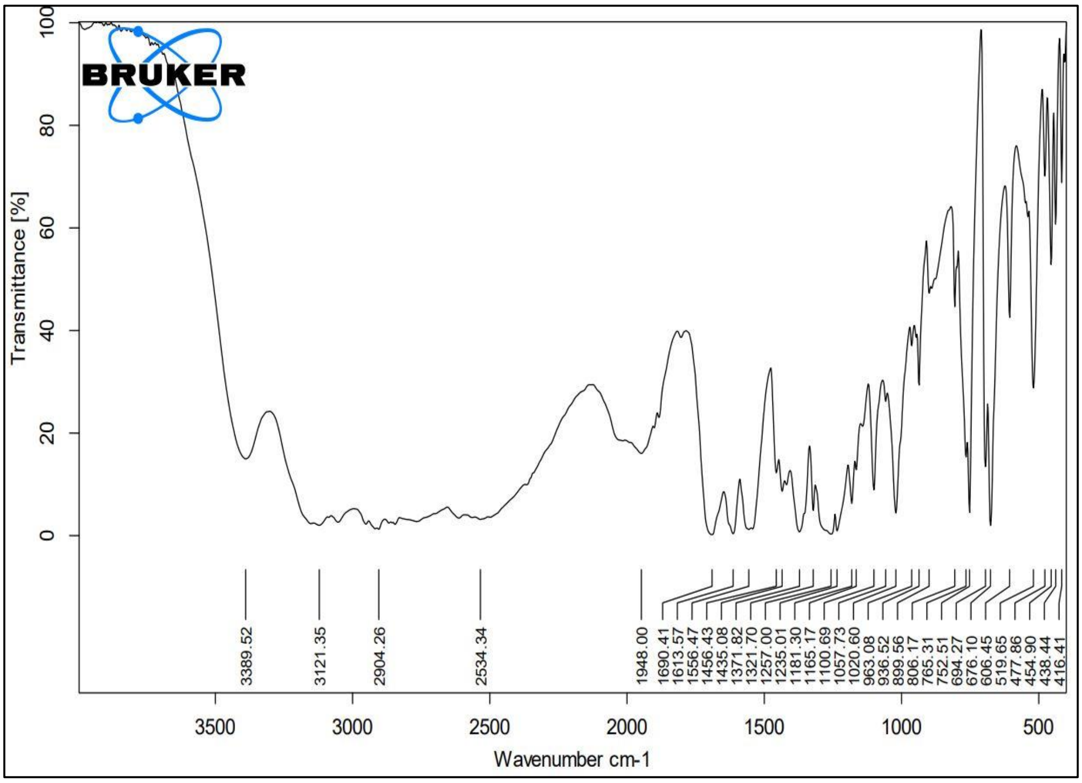
BRUKER
Transmittance [%]
Wavenumber cm-1